İZMİR
KÂTİP ÇELEBİ
ÜNİVERSİTESİ
2010
GRADUATE SCHOOL OF NATURAL
AND APPLIED SCIENCES

Evaluation of Polymeric Composite Material Alternatives for Metal Fulcrum Ring Part Used in Dry Friction Clutches

Submitted to the Graduate School of Natural and Applied Sciences
in partial fulfillment of the requirements for the degree of

Master of Science

in Materials Science and Engineering

by

Ibrahim Can KAYMAZ

ORCID 0000-0001-5340-9844

December, 2022

This is to certify that we have read the **Evaluation of Polymeric Composite Material Alternatives for Metal Fulcrum Ring Part Used in Dry Friction Clutches** submitted by **Ibrahim Can KAYMAZ**, and it has been judged to be successful, in scope and in quality, at the defense exam and accepted by our jury as a MASTER'S THESIS.

APPROVED BY:

Advisor: **Prof. Dr. Mehmet Özgür SEYDİBEYOĞLU**
İzmir Kâtip Çelebi University

Committee Members:

                                  Assoc. Prof. Dr. Hüseyin Ata KARAVANA
Ege University

                                  Assist. Prof. Dr. İsmail Doğan KÜLCÜ
İzmir Kâtip Çelebi University

Date of Defense: January 30, 2023

Declaration of Authorship

I, **Ibrahim Can KAYMAZ**, declare that this thesis titled **Evaluation of Polymeric Composite Material Alternatives for Metal Fulcrum Ring Part Used in Dry Friction Clutches** and the work presented in it are my own. I confirm that:

- This work was done wholly or mainly while in candidature for the Master's / Doctoral degree at this university.

- Where any part of this thesis has previously been submitted for a degree or any other qualification at this university or any other institution, this has been clearly stated.

- Where I have consulted the published work of others, this is always clearly attributed.

- Where I have quoted from the work of others, the source is always given. This thesis is entirely my own work, with the exception of such quotations.

- I have acknowledged all major sources of assistance.

- Where the thesis is based on work done by myself jointly with others, I have made clear exactly what was done by others and what I have contributed myself.

Signature: _____

Date: 30.01.2023

_____

Evaluation for Polymeric Composite Material Alternatives for Metal Fulcrum Ring Part Used in Dry Friction Clutches

Abstract

As same as in other industries, the automotive industry is one of the industries that expects continuous improvements. In this context, it is very important to integrate new technologies into the industry and to use new, alternative materials for industrial products. With the increase of these studies, cost and weight reduction are improved while serious advantages are obtained by maintaining the product's performance. The suitability of production with additive manufacturing of the fulcrum ring, which is a sub-component of the clutch cover assembly in the dry friction clutch system, acts as a support point. It has a very important role in system performance. Additionally, the system was simulated using finite element methodology in a working environment, and it was discovered that the compressive loads are the main loads operating on the system. The behavior of the materials against these loads was tested respectively. According to test data, %20 fiber addition makes the material closer to the metal replacement. It was observed that the strain rates dropped by %59,61 in PA6-%20CF, making this material suitable for prototyping. In order to examine the behavior of the materials under compressive load, their compatibility with the nine different macro scale material models. Finally, the fulcrum rings were produced with the FFF method and tested in the clutch cover assembly performance test device. It was seen that the composite alternative worked adequately. Even if the clamp load dropped %2, this load can work properly due to its tolerance limits. It is aimed this study will help studies such as increasing the industrial applications of alternative materials, studying new production methods and advancing material modeling studies.

Keywords: Dry friction clutches, fulcrum ring, polymeric composites, fued deposition modeling

Kuru Sürtünmeli Kavramalarda Kullanılan Metal Fulcrum Ring Parçasının Polimerik Kompozit Alternatiflerinin Değerlendirilmesi

Öz

Otomotiv endüstrisinde, diğer endüstrilerde olduğu gibi sürekli iyileştirme hedefleri bulunmaktadır. Bu kapsamda yeni teknolojilerin endüstriye entegre edilmesi, yeni, alternatif malzemelerin farklı ürünlerde kullanılması oldukça önemlidir. Bu çalışmaların artması ile birlikte maliyet, ağırlık gibi konular iyileştirilirken, mukavemet ve ürün performansı korunarak ciddi avantajlar elde edilmektedir. Kuru sürtünmeli debriyaj sisteminde bulunan debriyaj baskı kompleksinin bir alt komponenti olan, mesnet noktası görevi gören ve sistem performansı için oldukça önemli bir role sahip olan fulcrum ringlerin alternatif malzeme ve eklemeli imalat tekniği ile üretilebilirliği araştırılmıştır. Bu kapsamda, sistem çalışma koşulları sonlu elemanlar analizi ile simüle edilmiş ve bası yüklerinin en etkin yük olduğu görülmüştür. Altenratif malzemelerin bası yüküne karşı gösterdiği davranış test edilmiş, metal ile karşılaştırılarak uygunlukları değerlendirilmiştir. Test verileri incelendiğinde, %20 elyaf oranının malzemeyi metal ikamesine daha da yaklaştırdığı görülmüştür. Tüm alternatif malzemeler arasında PA6-%20CF malzemesinde %59,61 oranında gerinim düşüşü gözlemlenmiş ve bası yükü altında metal davranışına en yakın davranış olması sebebiyle prototip malzemesi olarak seçilmiştir. Bununla birlikte, malzemelerin bası yüküne karşı gösterdiği davranışın incelenmesi için dokuz farklı makro malzeme modelleri ile uyumu çalışılmıştır. Son olarak gerçek ölçekli ürün eklemeli imalat yöntemi ile üretilmiş ve performans ölçümleri alınmıştır. Baskı kuvveti metal parçaya göre %2 düşmüş ancak tolerans limitlerinde olduğu saptanmıştır. Yapılan bu çalışmanın alternatif malzemelerin endüstriyel uygulamalarının arttırılması, yeni üretim yöntemlerinin çalışılması ve malzeme modelleme çalışmalarının ilerletilmesi gibi çalışmalara yardımcı olması hedeflenmiştir.

Anahtar Kelimeler: Kuru sürtünmeli kavrama, fulcrum ring, polimerik kompozitler, erimiş filaman ekstrüzyonu

to my family.

Acknowledgment

First of all, I want to express my gratitude to Prof. Dr. M. Özgür Seydibeyoğlu, my thesis supervisor, for his deep knowledge, excellent assistance, and support during the completion of my master's thesis. His insightful remarks advanced the study.

I would like to thank Alperen Doğru for supplying filaments, expertise in additive manufacturing, and for his great help. Also, I would like to thank Asst. Prof. Dr. İsmail Doğan Külcü for his help and guidance in numerical modeling. I would like to thank İbrahim Yozgatlı for his valuable comments on finite element simulations. Also, I want to thank Dönmez Clutch Company for their great support for this study. Their support was one of the key factors for the success of this study.

I also want to extend my gratitude to everyone else who contributed to the study.

Table of Contents

List of Figures

List of Tables

List of Abbreviations

WEO	World Energy Outlook
AM	Additive Manufacturing
CAD	Computer Aided Design
CA	Cover Assembly
DDA	Driven Disc Assembly
RBA	Release Bearing Assembly
ME	Material Extrusion
MJ	Material Jetting
BJ	Binder Jetting
SL	Sheet Lamination
VP	Vat Photopolymerization
PBF	Powder Bed Fusion
DED	Directed Energy Deposition
FFF	Fused Filament Fabrication
FDM	Fused Deposition Modeling
PA	Polyamide
CF	Carbon Fiber
CF	Glass Fiber

List of Symbols

D_e	Outer Diameter [mm]
D_i	Inner Diameter [mm]
D_o	Diameter of Center of Rotation [mm]
E	Young's modulus [N/mm2]
l_o	Height of unloaded spring [mm]
t	Thickness of the spring [mm]
$h_0 = l_0 - t$	Cone height of an unloaded single spring, calculated as [mm]
$\delta = D_e/D_i$	Diameter ratio [-]
s	Deflection of a single spring [mm]
μ	Poisson's ratio (for spring steel = 0.3)
K_1, K_4	Spring Constant
C_1, C_2	K4 Parameters
F	Spring Force [N]
P_1^{UT}	Uniaxial Tensile/Compressive Stress
$\mu_k^{UT}, \alpha_k^{UT}$	Ogden Model Parameters
μ^{UT}	Neo-Hooke Model Parameter
c_{10}^{UT}, c_{01}^{UT}	Mooney Rivlin Model Parameters
$c_{10}^{UT}, c_{20}^{UT}, c_{01}^{UT}$	Isihara Model Parameters
c_1^{UT}, c_2^{UT}	Gent-Thomas Model Parameters
$A_i, B_j, \alpha_i\ \beta_j$	Swanson Model Parameters
C_1, C_2, C_3	Yeoh Model Parameters
μ_k^{UT}, C_k, N^{UT}	Arruda – Boyce Model Parameters
μ^{UT}, J_m^{UT}	Gent (1996) Model Parameters
λ	Stretch

Chapter 1

1. Introduction

As the demand for a cleaner planet increases, the world faces various major concerns. One of the most crucial topics of the global warming debate is the rise in carbon emissions and how they relate to energy use and economic expansion [1]. Among the most significant problems that must be solved for the next generations is emission pollution. The global energy crisis the world is experiencing is at an incredible level and the reduction of emissions can only be succeeded by using energy efficiently [2], [3].

According to World Energy Outlook (WEO) 2022, The global energy crisis has harmed businesses, homes, and entire economies around the world while it has affected the emission badly [2]. Emission from sectors where items made of steel, cement, plastic, paper, and aluminum abound is reported that need to be reduced by at least 50% by 2050 [3, 4]. The main causes of this pollution are generally heavier designs of products, the use of non-recyclable materials, and inefficient production methods (over usage of energy). By lowering demand, such as through product life extension, material replacement, or "light-weighting," the emissions target might be reached. Furthermore, component reuse and ground-breaking process innovations could also result in positive outcomes [5].

Burning fossil fuels produces the majority of energy [6]. The significance of adopting cleaner power sources is being highlighted by recent research. There are a few non-fossil fuel sources available worldwide, but they aren't very widely available. That is why a bigger focus is required on optimizing our product's weight [7]. It is important to keep a part's strengths the same as those of its previous design while decreasing weight [8]. The optimization process needs to solve a variety of complexity in structural systems subject to different failure modes in each of several load conditions and design constraints [9]. It is challenging to ensure the persistence of a topologically optimal design's manufacturability [10]. Material selection is the key that helps to

lever design to the next level at this point. The selection should be done by considering manufacturability first. All materials have different properties which determine the product behavior in working conditions. Consequently, it is essential to choose the right materials for a specific design. Material selection has a power that can increase a product's preferability [11, 12]. Moreover, the manufacturing method has crucial importance on the emission problem. Avoiding energy waste through efficient production methods is one of the most important things to cope with challenging emission problems [13].

The transportation sector is one of the most significant industries that contribute to emission pollution [14]. In 2020, the transportation sector accounted for 25% of all final energy consumption [15]. In 2021, road transportation (the automotive industry) generated the greatest revenue share at more than 55.0% [16]. Reducing the weight of the vehicle can lower registration expenses, tire and brake wear, vibrational strain, and freight costs. Added to these advantages weight reduction increases fuel economy [17]. According to assessments, fuel economy increases by 7% for every 10% reduction in a vehicle's overall weight [18]. This industry is made up of several sub-systems, and each of these systems offers a great deal of potential for applications involving the use of new materials, enhanced production methods, and weight reduction.

The application of composite materials in the automotive industry has grown significantly due to their high strength/weight ratios, good corrosion resistance, thermal properties, high stiffness, impact resistance, and fatigue properties [19]. Even if automotive sector players thoughts that materials and manufacturing techniques used to make automobiles are close to being ideal. As the industry grows, the lead time of projects is becoming shorter day by day [20]. Enhancing the processing techniques for further weight reduction, developing new production methods, and application of new materials (becoming more cost-friendly), increasing recycling technology to manage production wastes, and accelerating the application of new processes, and materials are required [21]. Additive manufacturing (AM) is a modern method used to build three-dimensional prototypes from computer aided design (CAD) models. The methodology is based on adding or bonding layers to form objects. AM allows producing complex designs, is available in a short time, uses materials efficiently, and doesn't require any extra support fixtures [20, 22]. In terms of quick responses to

2

market demands, additive manufacturing might be the most promising option for future applications [20]. All of the mentioned applications can lead to a notable decrease in emission pollution.

1.1 History of Clutches

The powertrain group typically accounts for %28 of the mass of the vehicle and contains various sub-sections [23]. The clutch is one of the parts of the powertrain that engages or disengages the drivelines and engine. Hydraulic, electromagnetic, safety, and dry-friction clutches are just a couple of the clutch systems that industrial sectors have been successfully implementing in their machines for decades.

Internal combustion engines had competed with steam and electricity-based automotive power alternatives and were not able to suppress until the end of the 20th century. In those days, vehicles powered by steam and electricity have offered great advantages including not needing a clutch or transmission, having fewer errors, and having torque characteristics that are nearly ideal while internal combustion engines require a system that connects the engine with the driveline [24]. Karl Benz introduced the clutch to the automotive industry in 1885 with his patented Motorwagon (Figure 1.1) [25, 26]. He has inspired by the principles of the mechanized factories of early modern industry and preferred to use transmission belts in his invention. The belt is tensioned by a roller which provides transmitting torque to the transmission gears and allows it to slip through when loosened (disengaging) [24].
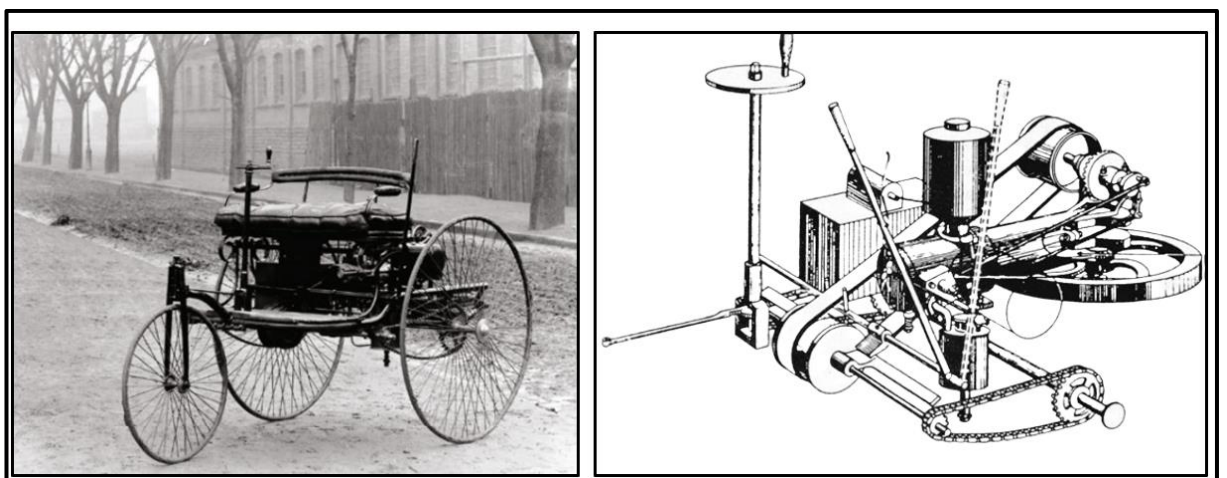
Figure 1.1: The Benz Patent-Motorwagen [24, 25].

Karl Benz also added an idler pulley for preventing wear out and reduced the wear problems of belts. Even if the wear issue was reduced, the demands were increasing rapidly. These systems could not be an answer to new requirements due to their low performance in rainy conditions and nonadaptable to variable speed transmissions. Engineers were compelled to look for alternative methods of transferring engine power through the transmission as a result of this issue [24]. All the alternatives are based on friction principles and are pioneers of current clutch technologies. The main idea is to reach the same rotational speed on both sides of the engagement. Until power transfer is achieved, the driving disc accelerates the driven disc and during this movement, heat is generated [24, 27]. Cone types of clutches were widely used for both passenger cars and trucks during the beginning of clutch history (Figure 1.2) [27]. Some of the early transmissions' shifting issues were associated with cone clutches. Gear crashing was also a result of inadequate steel selection, improper gear construction, and incorrect gear tooth engagement angles [28]. Through the 1920s, the cone-type clutch has undergone numerous revisions to eliminate of its drawbacks, which helped it keep popularity [24, 29].
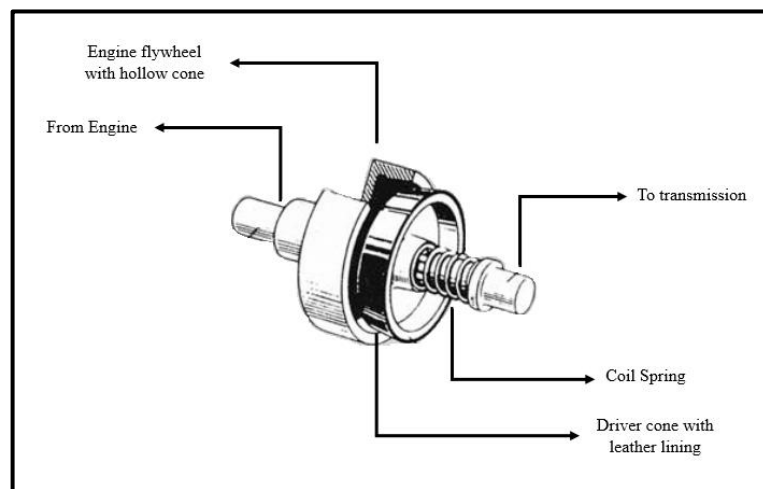
Figure 1.2: Cone clutch design [24].

Engineers found that if an angle of a cone increases, the required spring load to carry a given load will decrease. This knowledge came up with the double cone clutch design which is able to carry all of the load without slipping (Figure 1.3). Almost all cone clutch facings were constructed of leather, which frequently hardens and occasionally glazes as a result of slippage during the engagement. As a result, the clutch failed. The cone-type clutches were stigmatized by this form of inconvenience, which encouraged the development of other types. [30].
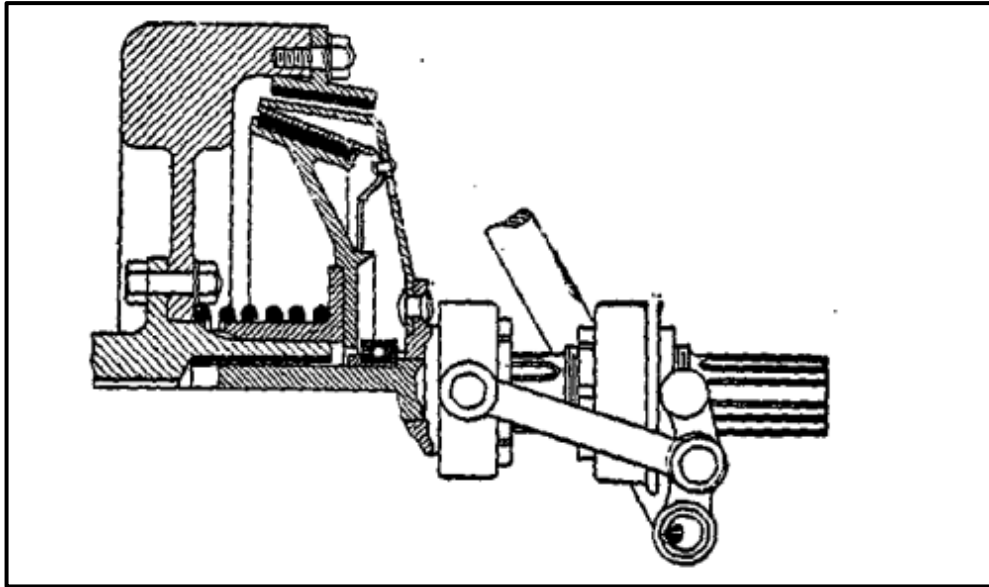
Figure 1.3: Double-Cone clutch design [30].

Around the same period, Professor Hele-Shaw from England began testing a multi-plate clutch that can be seen as the forerunner to the common single-disc dry clutch used today [24]. The following four conditions are listed as appearing to be connected to the friction clutch problem:

1. It must have enough clutching force.
2. The surfaces must not be exposed to excessive wear.
3. In situations where there is a lot of slipping contact in the clutch, a cooling system must be in place to remove the heat.
4. Motion should be transmitted to the driven shaft softly (avoiding shock effects) [31].

All of these clutches can be modified in great detail in a variety of ways, but their countless ideas focus on how to create the necessary pressure between the friction surfaces. The clutch offered by Hele-Shaw offered a number of noteworthy advantages, including a bigger friction surface area that could transmit more torque and installation space savings (Figure 1.4) [24, 29, 31].
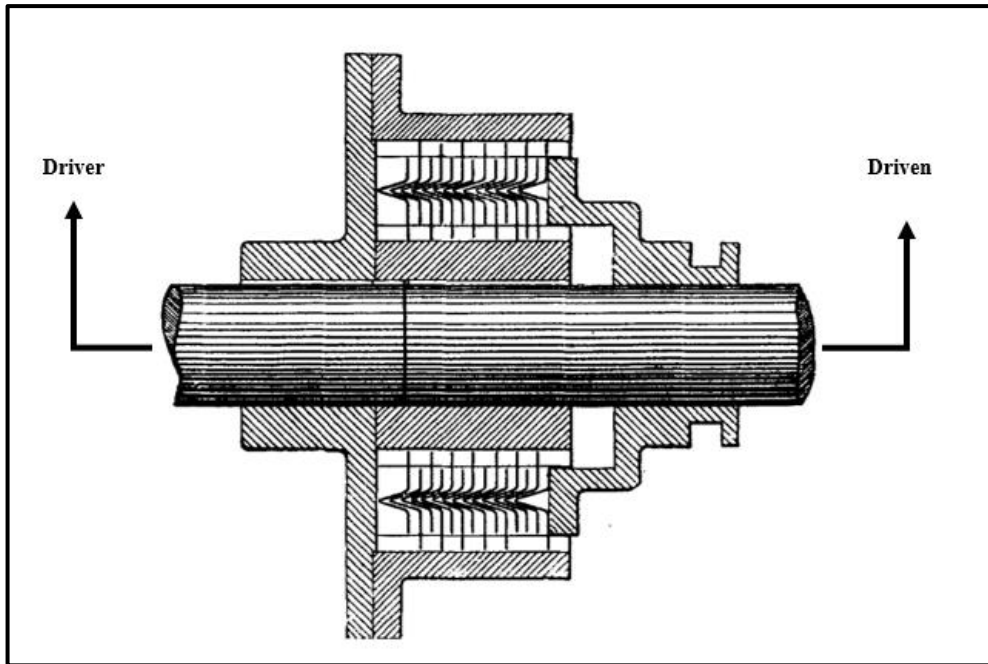
Figure 1.4: The first experiment with multi-plate clutches offered by Professor Hele-Shaw [31].

The single-plate clutch idea was established by De Dion & Bouton in 1904 but it was complicated when compared to the other types (Figure 1.5) [24].
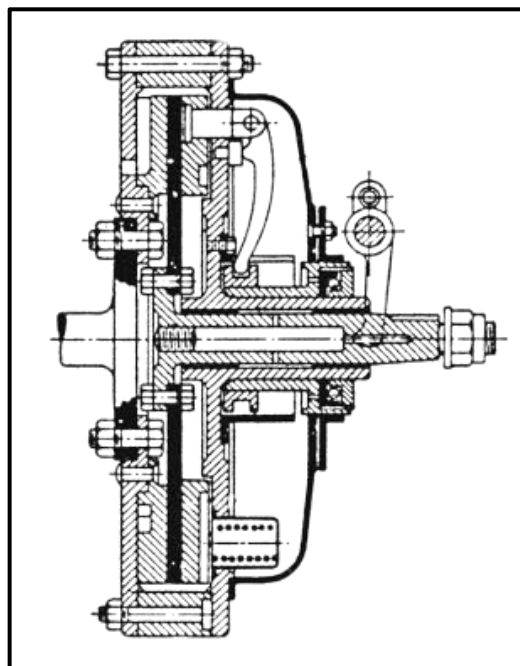
Figure 1.5: De Dion & Bouton's first single- plate clutch design [24].

Cone and multi-plate clutches were replaced by single-plate clutches, especially once asbestos linings were developed. Despite their somewhat complex construction, single-plate clutches provided several benefits over the other kinds of clutches that

were readily available at the time [24, 29]. Shifting gears were made considerably simpler by the single-plate dry clutch's reduced mass, which also allowed it to come to rest quickly when released [24]. Engineers concentrated on single-plate clutch research and development at that time. The development of coil springs was boosted; the force of compressed coil springs was used to create the clamp load needed to transmit torque by using a releasing bearing and the levers compress the coil springs. The use of coil springs had the drawback of pushing the springs outward into the spring housing as a result of centrifugal force. Even if the friction created by this scenario between the springs and housings, results in the clamp load change (Figure 1.6) [24, 29].
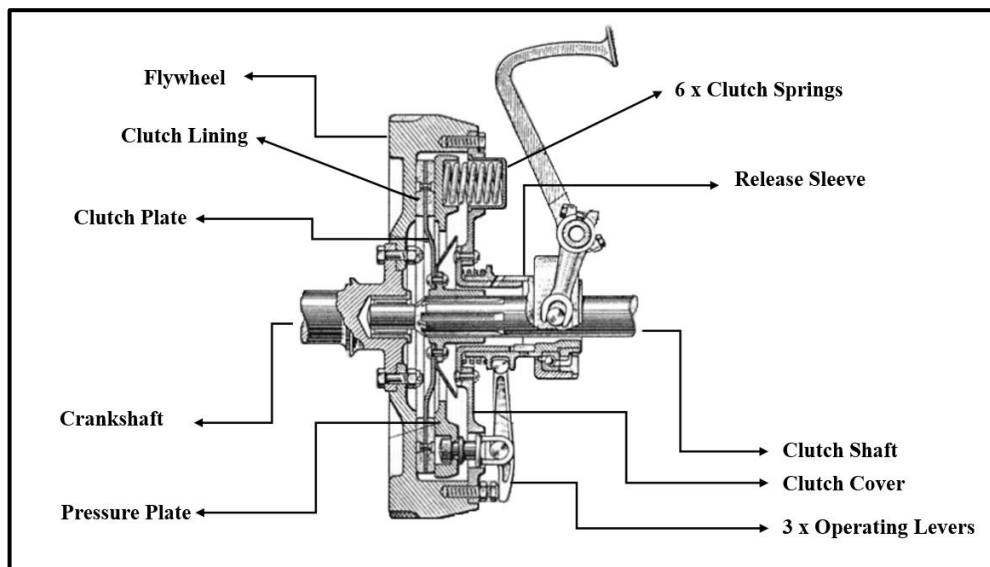
Figure 1.6: Coil spring clutch [24].

The diaphragm spring clutch was created to address these systemic problems. The diaphragm spring is speed-insensitive because it is rotationally symmetric. Nearly all manufacturers had switched to diaphragm spring clutches by the end of the 1960s (Figure 1.7) [24, 29]
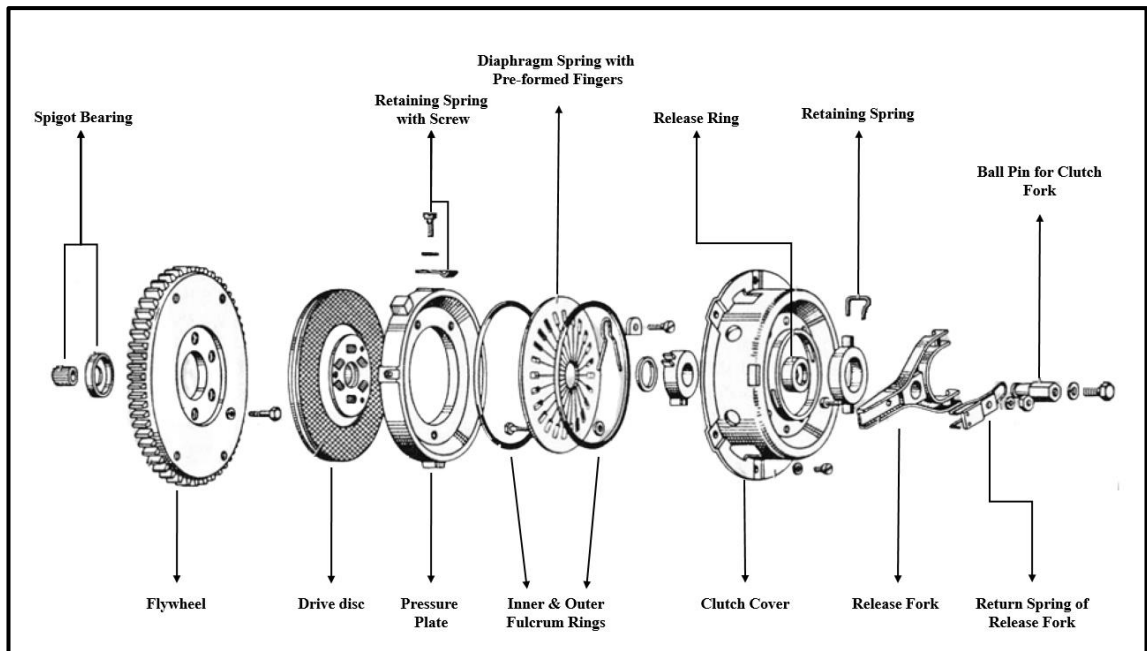
Figure 1.7: The multi-plate clutch developed by Chevrolet, the coil springs were replaced by a diaphragm spring [24].

1.2   Clutch System

Regarding their excellent performance and reasonable pricing, dry-friction clutches are frequently used in the industry.

1.2.1   Working Principles of Dry Friction Clutches

An automotive system called a clutch is used to smoothly engage two shafts in relative motion, while one of them remaining stationary, and to release them either rapidly or slowly as desired (Figure 1.8) [32, 33]. The following requirements should be met in order for a clutch to be installed between a motor and transmission;

1. The system should be able to gentle and non-vibration starting
2. It must provide swift gear shifting.
3. It must maintain the avoidance of the engine's torsional vibrations to protect the transmission as much as possible.
4. The system should transmit the torque through the drivetrain.
5. It should match the speed of both sides by regulating the transmitting torque [24 , 29, 32].
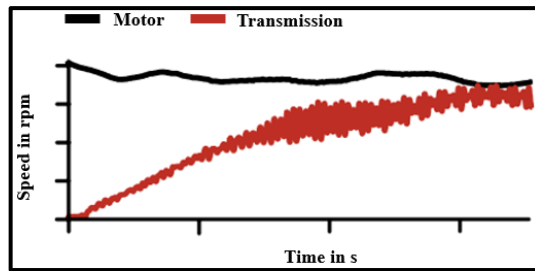
Figure 1.8: The engine and transmission alignment in terms of speed (Engagement process) [33].

These systems are controlled with a pedal supported by two hydraulic cylinders. When the pedal is pushed, the clutch fork pushes/pulls (depending on the clutch type) the release bearing which activates the clutch mechanism. Once the diaphragm spring force is removed, the pressure plate is lifted-off with the help of strap plates. This move provides disengagement of the pressure plate from the disc surface and allows to free disc (transmission becomes free for the shifting process). After the shifting process is done the pedal is released, and the diaphragm spring forces back of its original position and applies pressure on the clutch disc's facings again. Speeds of t both sides are different during this process. The Clutch provides an alignment for both engine and transmission speed. As a result of this movement, the engagement and torque transfer can be provided between the engine and transmission. [24, 29, 34]. The clutch system is demonstrated in Figure 1.9 [35, 36]
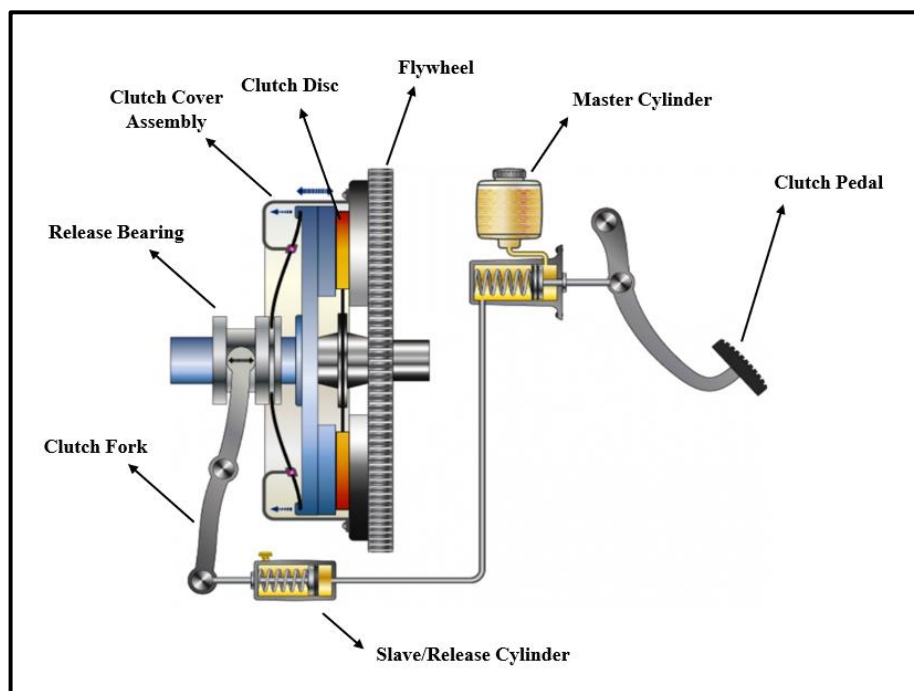
Figure 1.9: Clutch Actuation Scheme [35], [36]

9

1.2.2   Dry Friction Clutch Types

Today's clutches are mainly separated into two distinct groups which are push and pull types (Figure 1.10 and Figure 1.11). Clutch type preferences are made by the requirements of the vehicle. The most typical clutches are push types, although it's crucial to note that certain cars also have pull types. Between the two designs, there are no noticeable, overall advantages and disadvantages, as it is necessary to take into account not only the clutch assembly but also the actuation mechanism and installation space [37].
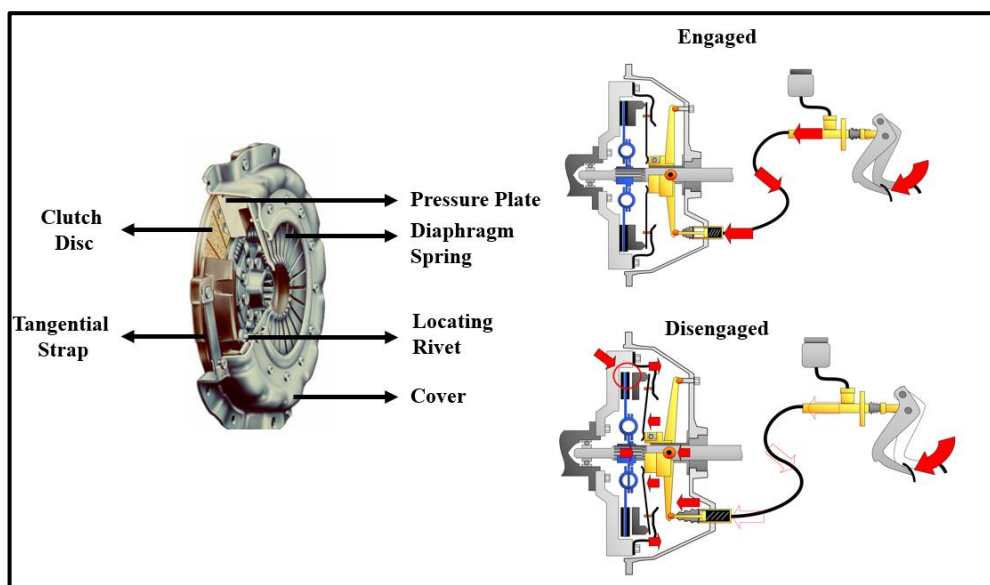
Figure 1.10: Push type clutch and its working principles [38].

The release bearing of push type clutches pushes the diaphragm spring when the driver moves the clutch pedal. They are preferred in designs with limited spaces due to their lower lever ratios [29, 37]. In pull type clutches, the release bearing moves the opposite way for providing engagement/disengagement when compared with the push type (Figure 1.11) [34].
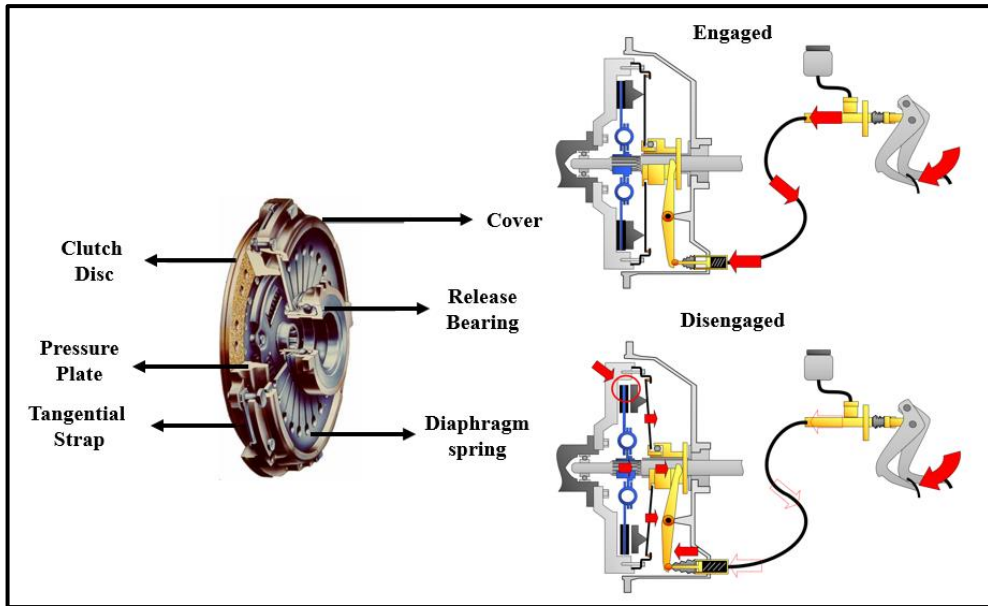
Figure 1.11: Pull type clutch and its working principles [38].

It is a fact that a pull type clutch has a larger lever ratio, hence providing lower forces for actuation/deactuation (good for pedal load) while it requires more stroke (Figure 1.12) [37]. Pull type clutches are commonly used in vehicles with higher engine torque. While they are having low pedal loads, their heat absorption abilities are better than the push types (due to their allowance for the use of larger pressure plates) [29, 34].
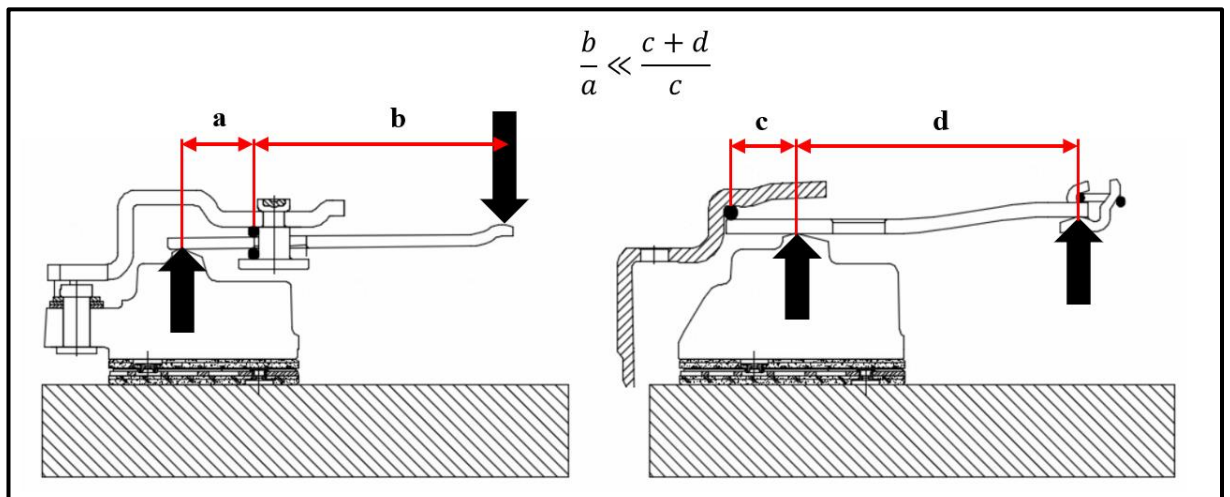
Figure 1.12: Lever ratios of both push and pull type clutches.

1.2.3   Clutch System Elements

Clutch systems are requiring a long service life, and a comfortable torque transition, especially in heavy-duty vehicles [24]. Clutch systems are requiring a long service life, and a comfortable torque transition, especially in heavy-duty vehicles. The three primary parts of dry friction clutches are cover assembly (CA), driven disc assembly (DDA), and release bearing assembly (RBA) (Figure 1.13).
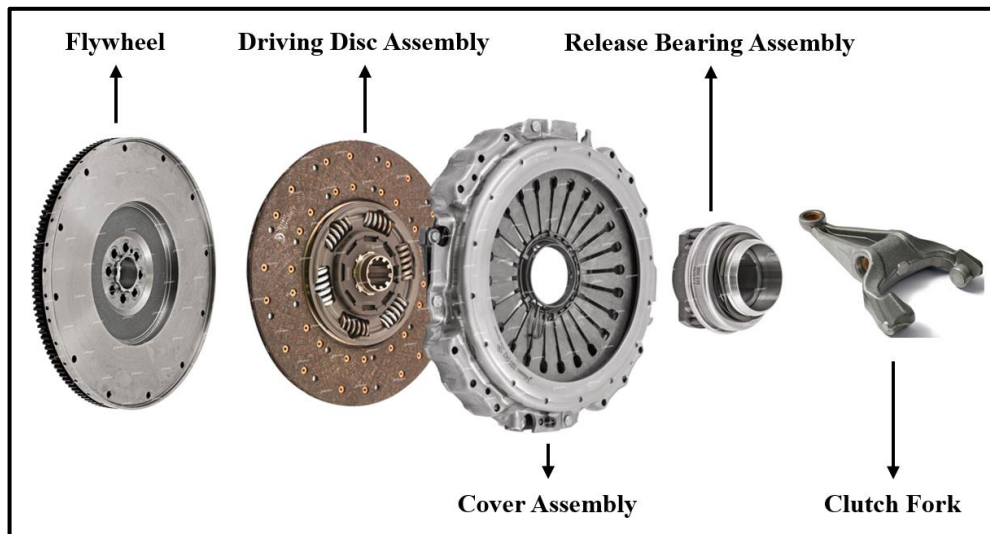
Figure 1.13: Clutch system elements [39, 40].

When compared to passenger vehicle clutch systems, these components are very complex and heavy. In addition to their complexity, they are frequently built of metals and cast materials, which are produced using old, ineffective production methods. By incorporating modern production techniques and materials into their systems, these issues could be resolved.

1.2.3.1.   Clutch Cover Assembly (CA)

Several crucial components make up the clutch cover assembly, including a steel cover, a pressure plate, a diaphragm spring, fulcrum rings, tangential straps, and rivets. Figure 1.14 shows a typical push-type clutch cover assembly that will be used in this study.
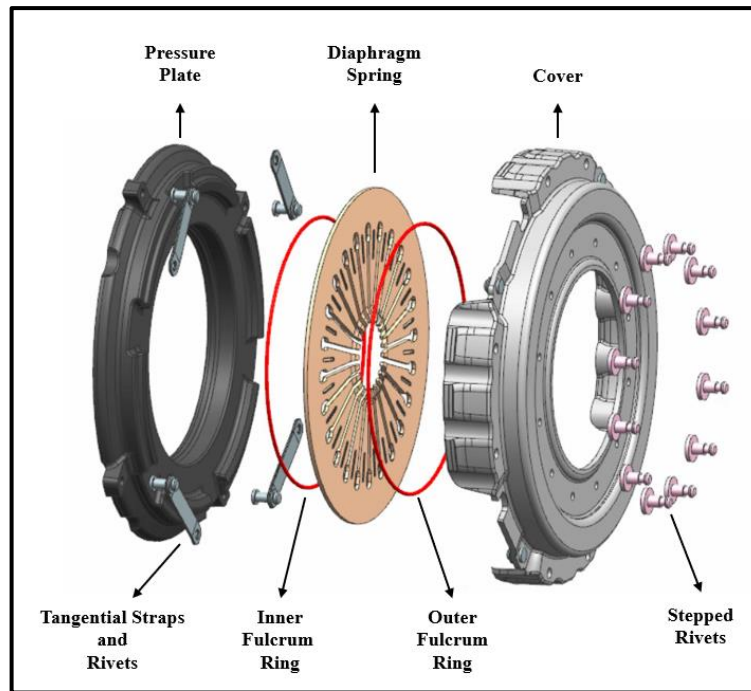
Figure 1.14: Clutch cover assembly.

The clutch cover assembly receives its drive from the crankshaft through the flywheel and cover connection. As the pressure plate is connected to the cover via tangential straps and the plate has a connection surface with the disc, the torque can be transmitted from the engine through the transmission input shaft during the engagement in this way. Tangential straps have an important role in the cover assembly. They are responsible for moving the pressure plate during the engage/disengage process and providing the centering at the same time [24, 29].

As the cover is mounted to the flywheel through the bolt holes, the diaphragm spring (belleville spring) makes a displacement which resulted in tension. The pressure plate transfers this tension as an axial force, which is also called clamp load. It pushes the driven disc assembly to the flywheel surface to provide engagement. This tension which occurs while the mounting process is the biggest component of the clamp load in the clutch mechanism [29, 41]. By pushing the clutch pedal, the release fork and release bearing assembly connected to it travel towards the clutch cover assembly, where they press the fingers (inner diameter) of the diaphragm spring by acting against them. As more pressure is applied, the load of the diaphragm is relieved, and tangential straps back away the pressure plate from the driven disc assembly [24, 29]. Friction forces created on both contact surfaces (flywheel-disc assembly and pressure plate-disc assembly) are proportional to the coefficient of friction and normal forces.

Moreover, the maximum friction force is developed when the clutch is fully engaged. Such connections produce heat during the engagement/disengagement which makes material selection a very important part of designing [29, 37]. During an unpleasant clutch engagement, the pressure plate is one of the important parts for cover assembly that may be exposed to considerable slippage, and kinetic energy can produce heat, eventually leading to high peak temperatures. Even though the temperature may be at a critical value, the part should be able to cool itself off by having an optimum mass and good thermal conductivity [29, 42]. To compensate for the above arduous situations pressure plates are made of grey cast iron due to their good mechanical and thermal properties [29, 34].
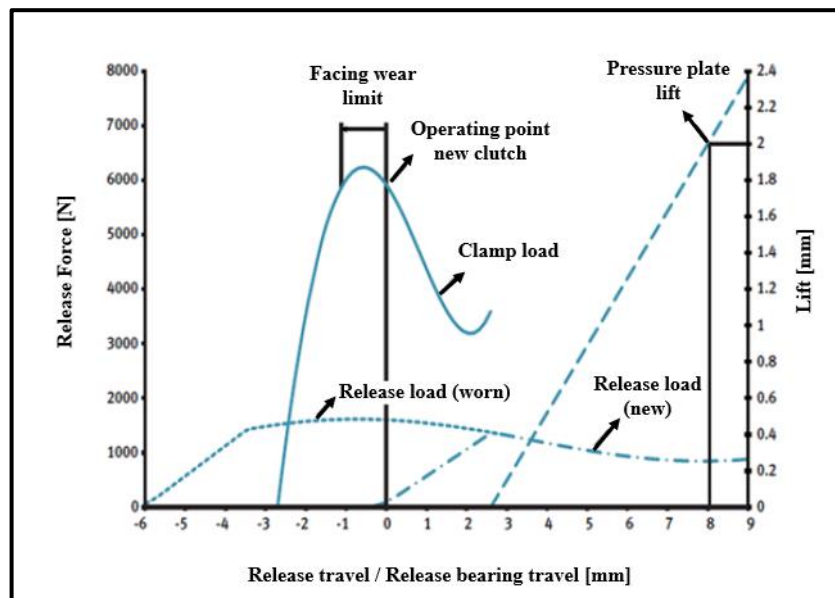
Figure 1.15: Clutch characteristic curves [29].

The diaphragm is a crucial element for the cover assembly which carries the required load for engagement/disengagement. These springs are supported by fulcrum rings and pressure plate forms. High-quality spring steels are mostly preferred for diaphragm springs to carry the required load in cyclic loading conditions [29]. Clutch springs experience significant thermal loading in addition to intense and cycling mechanical loading. Heat is quickly transported from the contact surfaces of the clutch, where temperatures can exceed 400 C, to the spring. High temperatures generate a significant additional stress that often causes the spring force to decrease. Because of this, the clutch and spring system's design, production, and materials must be carefully chosen and appropriate for the tasks that are intended. Higher thermal loads often ask for lower mechanical spring (pre) load and strains, which demands for a larger clutch diameter

[37]. Their biggest advantage comes with disadvantages. It is a fact that they are preferred due to their smaller pedal forces. Even if they have a preferable load at the beginning, their pedal loads increase by the effects of the wear in the driven disc assembly (cf. principle of belleville springs) [41]. A variety of clutch characteristic curves are shown in Figure 1.15. The left and right y-axes indicate the load and the lift of the pressure plate, respectively, while the x-axis denotes the release travel. The release load curve, which represents the load on the release bearing to trigger the clutch, is shown by the dotted line. As it can be seen that the release load increases with the increasing clutch lining wear [29].
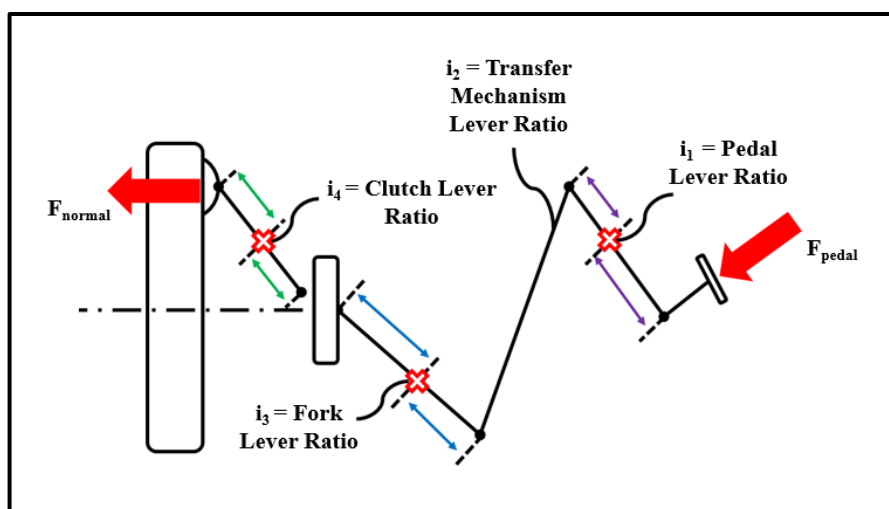
Figure 1.16: Clutch System Lever ratios [37, 41].

The clutch mechanism is based on terms of the diaphragm spring characteristic. While the lower side of the spring connects with the pressure plate, the other side provides a connection with the release bearing when the pedal is depressed. Three forces are important for this mechanism (pedal load, diaphragm load, and release bearing load). The pedal force that applies by the driver effects as a release bearing load after the implication of the three lever ratios (i_1, i_2, i_3). The pedal force F_{pedal} must be greater than the normal force F_{normal} after implication of the last lever ratio i_4 for the disengagement process (Figure 1.16). When there is no force on the pedal, the clutch is already in an engaged position to transfer engine torque [37, 41]. The only way for the driver to disengage the clutch is that the moment that will be created by pressing the clutch pedal is greater than the resultant moments of the other forces [41]. This situation can be explained by moment conservation equations for the mechanism shown in Figure 1.17 [43].
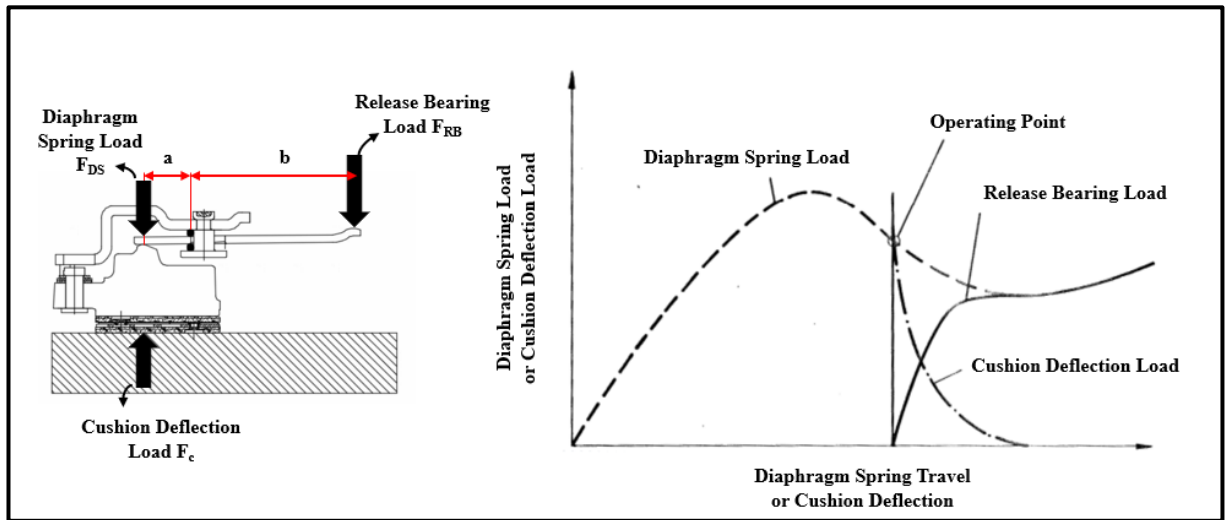
Figure 1.17: Loads applied on clutch mechanisms and their effect on the operating point [43].

$$(F_{DS} - F_c) \times a - F_{RB} \times b = F_{Clamp} \times a \qquad (1.2.3.1.1)$$

A key component of the clutch that is vital to producing torque is the diaphragm spring. Due to their large load capacity, they are beneficial for short operating distances. The majority of the time, rivets or fulcrum rings mounted on the cover are preferred to support these springs. The diaphragm has no international standard form. The majority of companies continue their R&D efforts in order to find the best form for their needs [34, 37]. Almen and László stated that these springs are moving around their center of rotation in 1936 [44]. DIN 2092 and DIN 2093 standards were created by referencing these statements [34, 41]. The following formulas (Table 1) are used to compute the diaphragm spring (Figure 1.18) characteristic under some assumptions. It has been stated that the material's elastic modulus remains linear throughout these calculations. Sharp corners and a rectangular cross-section characterize the spring. During the spring's manufacturing process and subsequent heat-treatment procedures, residual stresses are disregarded [45].

16
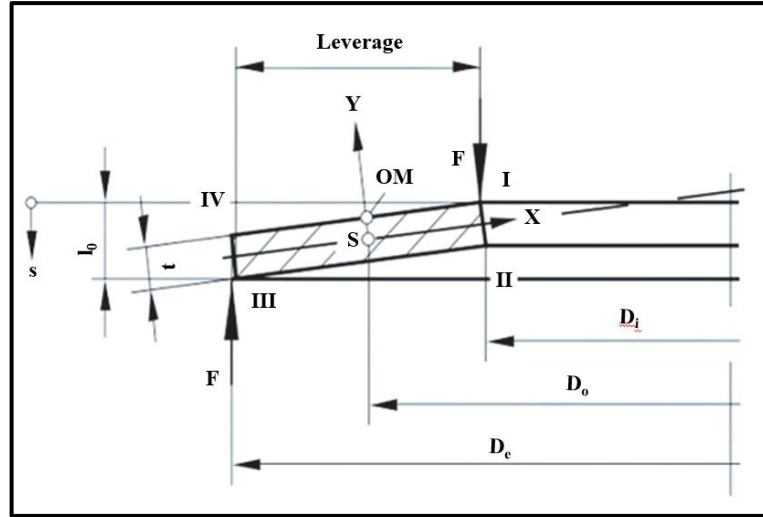
Symbols	Identification	Symbols	Identification
D_e	Outer Diameter [mm]	t	Thickness of the spring [mm]
D_i	Inner Diameter [mm]	$h_0 = l_0 - t$	Cone height of an unloaded single spring, calculated as [mm]
D_o	Diameter of Center of Rotation [mm]	$\delta = D_e/D_i$	Diameter ratio [-]
E	Young's modulus [N/mm^2]	s	Deflection of a single spring [mm]
l_o	Height of unloaded spring [mm]	μ	Poisson's ratio (for spring steel = 0.3)

Figure 1.18: The cross section of the diaphragm spring [45].

Table 1.1: Diaphragm spring calculation formulas [45].

Formula	Identification
$$K_1 = \frac{1}{\pi} \times \frac{\left(\frac{\delta-1}{\delta}\right)^2}{\left(\frac{\delta+1}{\delta-1} - \frac{2}{ln\delta}\right)}$$	Spring Constant
$$K_4 = \sqrt{-\frac{C_1}{2} + \sqrt{\left(\frac{C_1}{2}\right)^2 + C_2}}$$	Spring Constant
$$C_1 = \frac{\left(\frac{t'}{t}\right)^2}{\left(\frac{l_0}{4t} - \frac{t'}{t} + \frac{3}{4}\right)\left(\frac{5l_0}{8t} - \frac{t'}{t} + \frac{3}{8}\right)}$$	Parameter for K$_4$
$$C_2 = \frac{C_1}{\left(\frac{t'}{t}\right)^3}\left[\frac{5}{32}\left(\frac{l_0}{t} - 1\right)^2 + 1\right]$$	Parameter for K$_4$
$$F = \frac{4E}{1-\mu^2}\frac{t^4}{K_1 D_e^2}K_4^2\frac{s}{t}\left[K_4^2\left(\frac{h_0}{t} - \frac{s}{t}\right)\left(\frac{h_0}{t} - \frac{s}{2t}\right) + 1\right]$$	Spring Force

When displacement is applied, the diaphragm spring force never increases linearly; it is always curved. The force begins to drop over a particular displacement amount, and the shape of this force curve depends on the h_0/t ratio (Figure 1.18) [45]. By installing the cover to the flywheel and tightening the bolts by 6,963 mm, a 6,963 mm pre-stress is applied to the pressure plate, and as a result, to the lower support point of the diaphragm spring. As the diaphragm spring force can be calculated with the formulas written in Table 1 In our study, the diaphragm force is calculated as FDs = 20740 N

1.2.3.2.   Driving Disc Assembly (DDA)

By virtue of the friction forces produced at its surfaces, the friction disc (Figure 1.19) is clearly a key element in torque creation. These forces creates torque (moment) on the disc axis, which is transferred through the hub and its spline to the gearbox input shaft [37]. Even though the main function of a disc is transmitting the torque, it should provide a smooth startup, fast gear changing, and keeping the engine vibrations away from the transmission to avoid transmission noise. If the disc blocks the vibrations from the engine, it means that it helps to prolong the life of synchromesh gears [29, 34, 46]. When transferring power, the clutch disc makes direct contact with both of the engine's flywheel and pressure plate. For providing smooth engagement characteristics, It is made up of an axial cushion in the middle and frictional material on both sides. [37, 47].
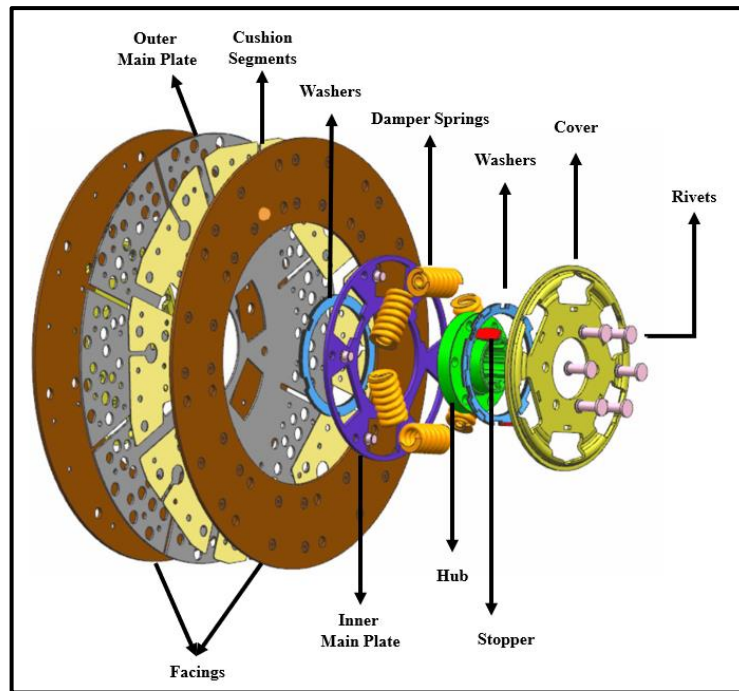
Figure 1.19: Clutch driven disc assembly.

Heat energy is produced in the friction surfaces at the interfaces when the friction clutch starts to engage because slippage takes place between the contact surfaces (pressure plate, clutch disc, and flywheel). The frictional heat produced at high relative sliding velocities causes the clutch disc surfaces to heat up rapidly, which can result in thermomechanical errors [48]. Estimating temperature fluctuation and how it varies depending on operating factors such as load, convective cooling intensity, material qualities, and friction element dimensions is crucial to prevent clutch system failure [49]. The torque transmission characteristics and major load types during the engagement can be illustrated in Figure 1.20 [48]. The important parts of the facing material used in clutches include matrix resin, fiber enhancers (fiberglass etc.), fillers, and friction performance regulators [50, 51]. The facings' temperature may quickly rise to extremely high values when friction is significantly high, which specifically happens during clutch engagement. The base material is very likely to sustain damage in this scenario due to the considerable fall in the coefficient of friction. When surface friction approaches 300°C in the majority of applications using organic facing, the clutch begins to fade and material damage increases exponentially [29].
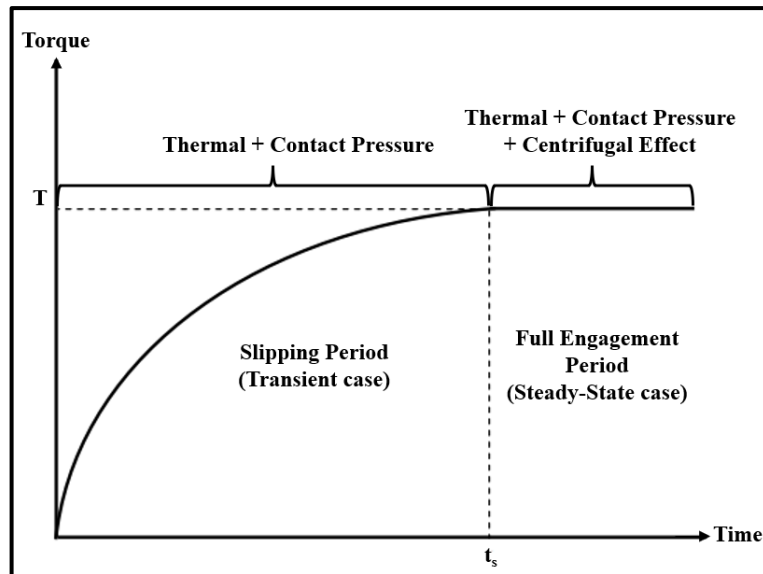
Figure 1.20: The torque transmission characteristics [48].

A clutch disk often features two different types of dampers: a main damper for driving conditions and a pre-damper for idle conditions. Depending on the application requirements, each mechanism consists of single-stage or multi-stage ordered spring sets to transmit various torque amplitudes and offer various damping effects on the driveline (Figure 1.21) [52, 53]. Modern drivetrains with combustion engines can almost entirely be optimized for torsional vibration and fuel economy by using a closed clutch. The torsional vibration damper clearly defines the interaction between the engine and transmission [54].
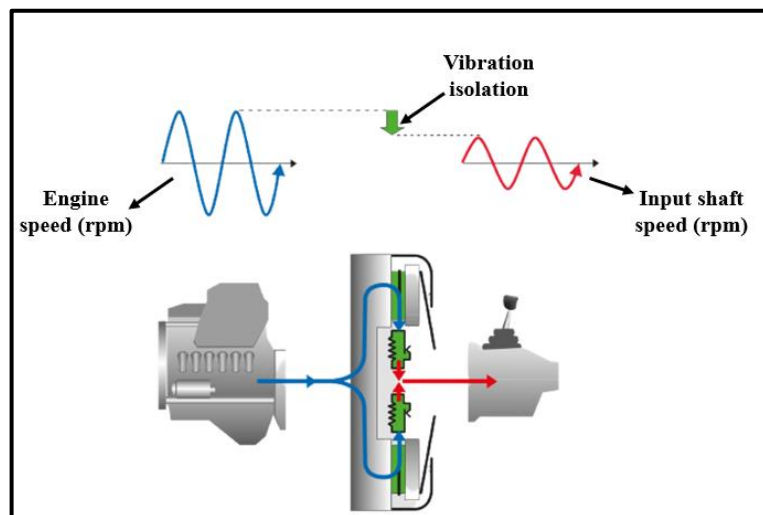
Figure 1.21: Vibration characteristic of clutch [52].

The cushion segments are located between the facing materials (connected to the outer main plate with rivets). They make sure the clutch is engaged smoothly. The pressure plate must initially push the clutch disc against the flywheel while working against the cushion segments' spring load. The flexing of the segments allows for a delay in adjusting the transmission speed to the engine speed as this load builds up gradually and prolongs the engagement procedure. In addition to a smooth takeoff, the cushion segments' benefits include good wear resistance, a smoother wear pattern, and also a more even distribution of heat [24]. The cushion segment placement and its force reaction can be shown in Figure 1.22 [55, 56].
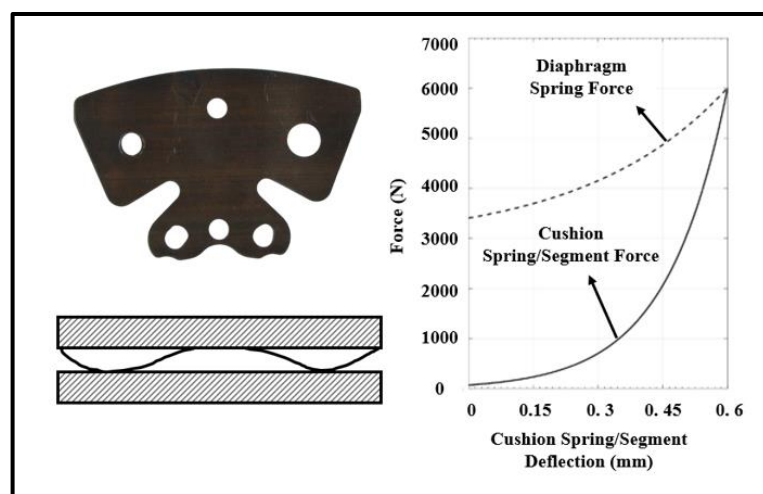
Figure 1.22: Cushion Segment and Force reaction [55, 56].

1.2.3.3. Release Bearing Assembly (RBA)

Automobile clutch release bearings are required to have good strength and toughness, impact resistance, abrasion resistance, and excellent contact fatigue performance under situations of high speed, strong vibration, high temperature, humidity, and pollution [57]. They are starter elements of clutch mechanism which is activating by pushing or pulling the clutch cover assembly's diaphragm spring to produce disengagement [58]. Types of the release bearing assemblies can be shown in Figure 1.23 [59, 60].
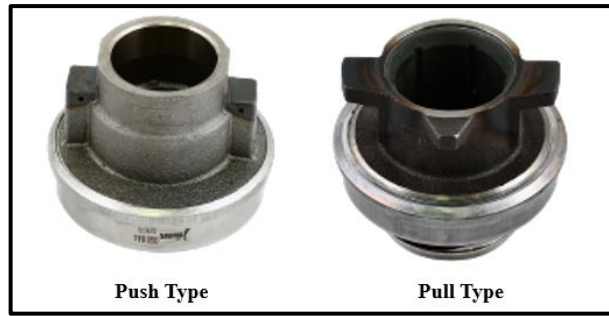
Figure 1.23: Release bearing assembly types [59, 60].

1.2.3.4. Flywheel and Clutch Fork

An ancient method of storing energy and minimizing energy losses is the flywheel. The spinning wheel and the potter's wheel are two instances of flywheels being used in the past [57]. It spins with the engine speed and is linked to the crankshaft. It looks like a big metallic disc and is typically composed of cast iron (Figure 1.24). It squeezed the clutch disc between the pressure plate and a friction surface [29].

Figure 1.24: Single Flywheel design [61].

A flywheel mass plays a key role in restricting speed fluctuations by containing a certain amount of inertia, or mass moment of inertia. Furthermore, It prevents vibrations and relaxes the torsional excitation of the crankshaft [62]. Rotational vibrations affect durability of the drive train components and create gear rattle, body boom and tip-in/back-out. The use of torsion damper in disc assemblies aims to keep engine-induced torsional vibrations as far away from the rest of the drivetrain as possible. However, a compromise must be made while tuning the torsion damper. Because of the attainable torsion damper spring rates, a conventional system can only meet this requirement at high engine speeds, where the natural frequencies are always within the permissible driving range. To solve this unpleasant issue, the Dual Mass Flywheel torsion damper concept was developed (Figure 1.25) [63, 64]. Due to the

inertial, stiffness, and damping specifications of the dual mass flywheel, this vibration has recently been reduced. When a DMF is fitted, the transmission input shaft inertia is increased, allowing for improved vibration insulation in both idle and drive rattling conditions as opposed to employing a single flywheel inertia coupled to the crankshaft [63].
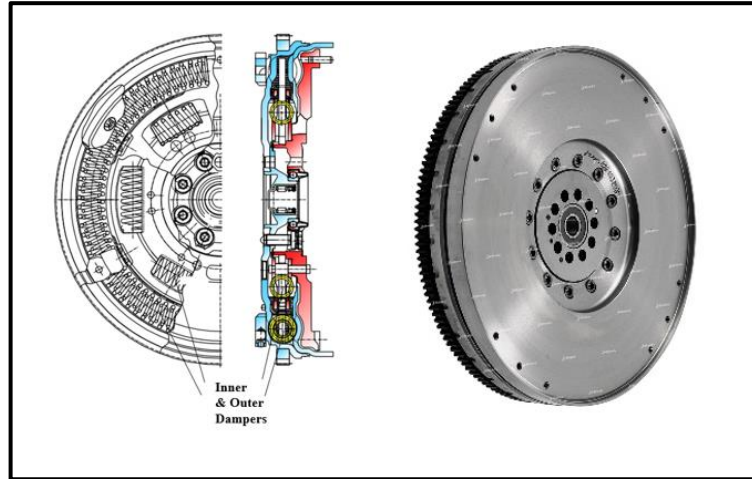
Figure 1.25: Dual Mass Flywheel designs [63, 64].

One of the automotive clutch's key components that transform the clutch pedal's motion to the back-and-forth motion of the clutch throw-out bearing is the clutch fork. It works as a lever where the pivot point is halfway between the input and output ends [65]. The fork is prone to wear and tear by nature because of the constant load it bears. Because of this, a release fork's top material and processing quality are crucial [66].

Chapter 2

2. Replacement of Metallic Parts by Polymers & Composites

Population growth, consumerism, and changes in the way that people live today have all contributed to an increase in the need for novel materials during the past few decades [67]. JJ Berzelius proposed polymer materials as one of the materials for the first time in 1833 [68]. Performance enhancement, weight reduction, and price reduction are the driving forces behind material development. Depending on the application, the major priorities can include, among other things, mechanical qualities, weight, volatility, thermal stability, chemical reactivity, and, most importantly, durability [69]. The need to establish a sustainable chemical industry has gained acceptance among scientists in recent decades. Due to this increased awareness, the prospect for a renewable future is currently positive, with active research fields including the synthesis of sustainable thermosets, thermoplastics, and vitrimers made from biorenewable molecules [70]. Polymers are common components of rubber and plastics. On the basis of hydrogen, carbon, and other non-metallic components, they are primarily organic molecules. The dominant molecular structure of a polymer affects how it responds to mechanical stresses at high temperatures. In fact, one system for categorizing these materials is based on how they respond to temperature increases [71].

The two subcategories are thermoplastics (also known as "linear" polymers) and thermosets (also known as "cross-linked" polymers). Thermoplastics undergo completely reversible, repeatable processes of softening when heated (and eventually liquefying) and hardening when cooled while thermosetting polymers become permanently hard during their formation, and do not soften upon heating again [71, 72]. Different thermoplastic kinds, such as crystalline thermoplastics and amorphous or semi-crystalline thermoplastics, have distinctive physical, thermal, and electrical qualities that make them suitable for a variety of industrial applications [73].

24

Contrarily, thermosets are heavily cross-linked three-dimensional materials that do not melt or soften when heated repeatedly [74, 75]. Furthermore, the material maintains its shape even at high temperatures. Examples of widely used thermosets are vulcanized rubber, polyurethane foams, unsaturated polyester and epoxy, and phenolic resins [73, 76]. Thermoplastics, which are mostly utilized as packaging or textile fibers, make up about 80% of all consumed plastics. Most of them—about 50%—are single-use disposable applications such as packaging, agricultural films and disposable consumer items [77, 78]. Between 20 and 25 percent are employed in long-term infrastructures like pipes, cable coverings, and structural materials while the rest are employed in long-lasting consumer applications with a medium lifespan, such as electronic devices, furniture, and automobiles [77]. Contrarily, thermosets are typically utilized in long-lasting applications, electrical and thermal insulation materials, adhesives, and especially where high strength and modulus including as structural elements, wind-turbine blades, and composites used in the automotive and aerospace sectors [72, 73]. Because they are lightweight, inexpensive, and easy to produce, polymeric materials have already displaced traditional materials like metals and ceramics [79]. Additionally, polymers have excellent corrosion resistance and positive mechanical qualities (ductility) [80]. Despite the fact that numerous new materials have been created to fulfill the demands of technology. It might not always be possible to use a single type of material to satisfy the demanding property requirements. As a result, the idea of combining different materials emerged, leading to composite materials [81]. Polymer composites were created by strengthening the matrix with a variety of filler components. The polymer matrix can be supplemented with a variety of fillers (particles, fibers, or platelets, synthetic or natural, organic or inorganic), at any scale, depending on the desired performance of the final material (macro, micro, or nano) [80].Compared to metallic materials, composites offer much higher strength-to-weight and stiffness-to-weight ratios; as a result, they have been widely used to replace metals in recent years [82]. Particularly, it is discovered that the reinforcing of fiber upon polymeric matrix results in significant improvements in the mechanical behaviors of polymeric hosts [83]. The strength and other properties of fiber-reinforced composites are significantly influenced by the distribution, concentration, and arrangement of the fibers in relation to one another [71].
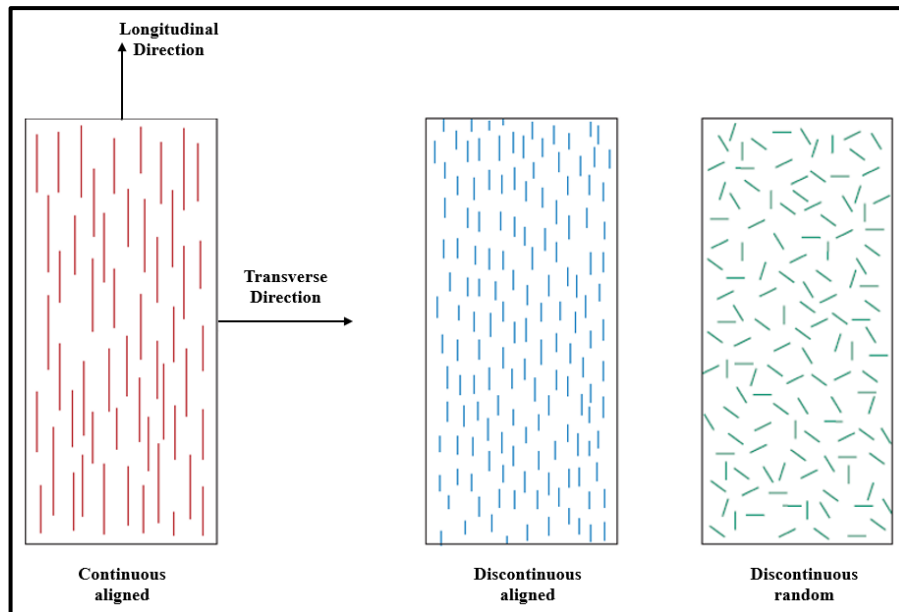
Figure 2.1: Schematic representations of fiber-reinforced composites [71].

Two things are possible in terms of orientation: a completely random alignment and a parallel alignment of the fibers' longitudinal axes in a single direction. While discontinuous fibers might be randomly oriented, partially oriented, or aligned, continuous fibers are typically aligned (Figure 2.1) [71]. The pie chart (Figure 2.2) below provides an in-depth analysis of market shares for fiber reinforced plastics across a range of application fields [83].
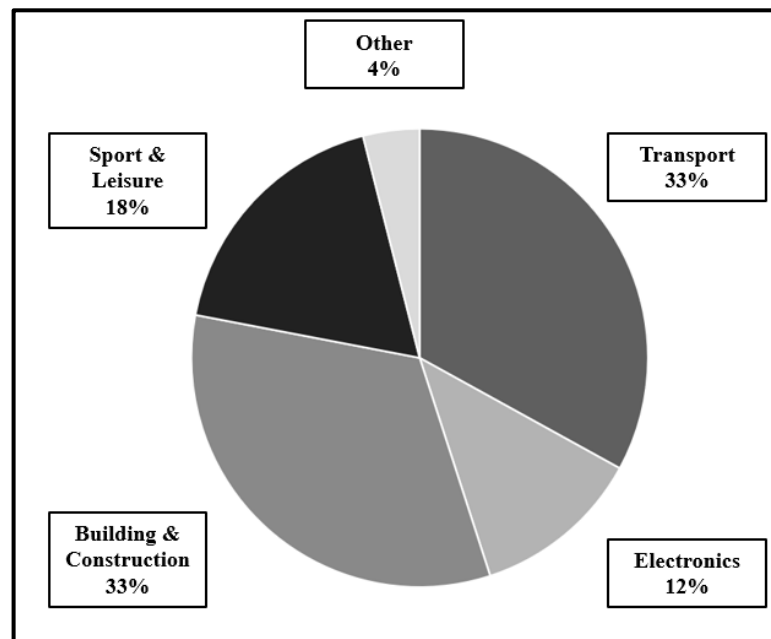
Figure 2.2: Market shares of fiber-reinforced composites [83].

Numerous projects that successfully substitute composite materials for metals can be found in the literature. A. A. Baker, et al. have described a cost-effective method for replacing metallic honeycomb panels with stiffened graphite/epoxy composite panels that are more durable [84]. In a work published by Kawabe H. et al., biomimetics is used to develop an innovative and effective composite airframe structural design. As a composite wing (dragonfly wing) was used in place of the traditional metal construction, it allowed for a significant weight reduction when compared to the corresponding metallic structure [85]. A. Sellitto et al. stated that the wind turbine system becomes one of the industries that is incredibly significant in customizing its strength and durability, taking into account the intended production costs. Their study shows that the development of novel design and manufacturing procedures, able to fully utilize the potential of modern composite materials by introducing lightweight structural concepts linked with the reduction of production times and costs is very crucial for this sector [86]. According to DuPont Automotive, the company is working on new high-performance composite materials and engineering polymers that will boost function in automotive applications while weighing 30 to 40% less than metal components. Moreover, DuPont claims that the materials' integration of different components into modules can result in cost reductions of 30–50% [87]. In order to produce components for motorcycle oil pumps, S.D. Mancini et al. investigated the viability of replacing glass-fiber-reinforced polyphthalamide with metallic materials (steel and aluminum). Results indicate that composite materials can be used to build motorcycle oil pump parts [88].

Chapter 3

3. Additive Manufacturing

Rapid prototyping, which was created in the 1980s for making models and prototype parts, was the first method of building a three-dimensional object layer by layer using computer-aided design. Engineers developed this technology to aid in the execution of their ideas. One of the earliest additive manufacturing techniques is rapid prototyping. Not just models but also printed items can be made with it. Time and cost savings increased human connection, and a shorter product development cycle is just a few of the significant improvements this process brought to product development [89]. According to the latest developments, the phrase "Rapid prototyping technology" was no longer appropriate and was not adequately reflecting the latest applications of the technology, as users have come to understand. There was now a much closer connection between the output of these machines and the finished product thanks to improvements in output quality. In actuality, a lot of parts are now produced directly in these machines, therefore it was not a good choice to categorize them as "prototypes" [90]. The fundamental idea behind this technology is the direct fabrication of a model after it has been created utilizing a three-dimensional computer-aided design system without the requirement for process planning [89], [90]. The complete process can be summarized as shown in Figure 3.1 [91].
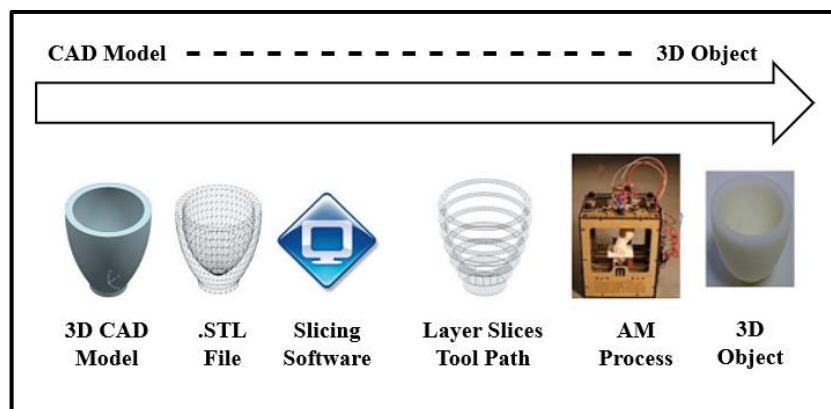
Figure 3.1: Additive Manufacturing Process [91]

With the aid of additive manufacturing techniques, actual items can be created from digital data piece by piece, line by line, surface by surface, or layer by layer [92]. The International Standards Organization/American Society for Testing and Materials Standards (ISO/ASTM 52900:2021) categorize additive manufacturing methods based on their operating principle, kind of material utilized, and energy type. There are seven different types of AM processes, according to this standard, including material extrusion (ME), material jetting (MJ), binder jetting (BJ), sheet lamination (SL), vat photopolymerization (VP), powder bed fusion (PBF), and directed energy deposition (DED) [93]. One of the most common AM techniques is called fused filament fabrication (FFF), sometimes known as fused deposition modeling (FDM) (Figure 3.1) [94]. The melted polymer is extruded onto a build stage to create a thin layer that is specified in thickness. The layer is then further solidified and binds with neighboring layers to create a part [95].
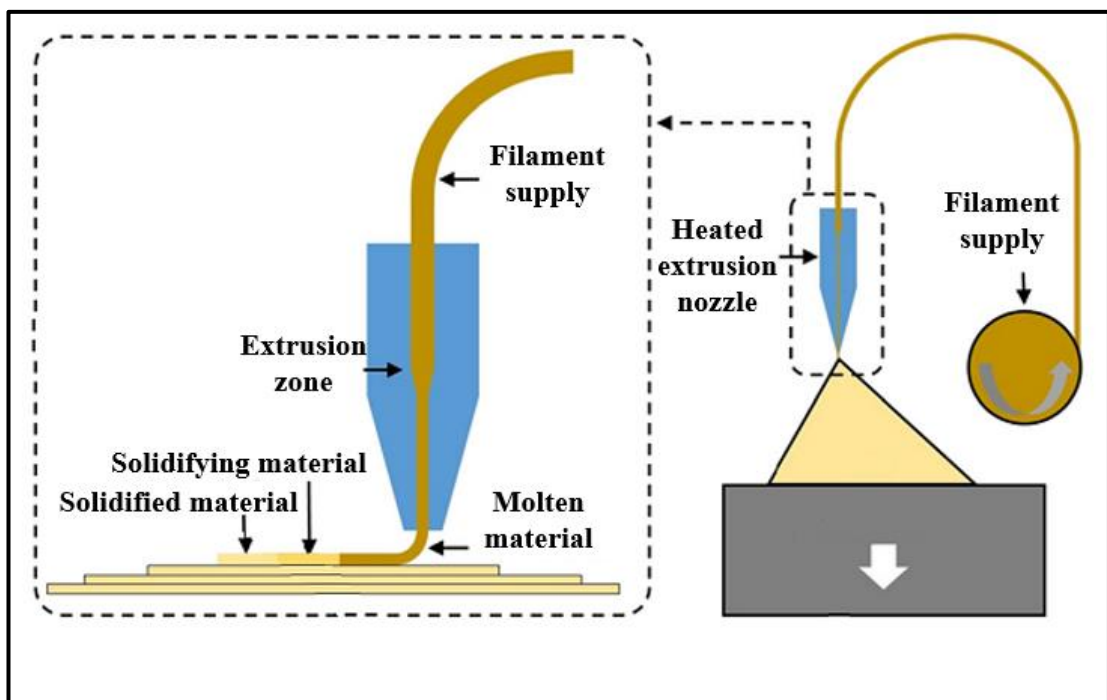
Figure 3.2: Fused filament fabrication process principle [96]

Literature and recent commercial developments in Additive Manufacturing are showing that the FFF method can be used in several sectors efficiently. Melnikova R et. al. showed that the FFF method enables the creation of unique building techniques and pattern designs for clothing and related fields, enabling the creation of new designs and functionalities that are not possible with standard textile production methods [97].

A similar technique was utilized by Romero P.E. et al to replace metal mold parts with polymers in the automotive industry. Even though the process of demolding is made more difficult by the poor surface finish of these 3D-printed molds. They did a polish operation on the materials and looked at the results to overcome this disadvantage [98]. Additionally, Garmabi M.M. et al. investigated improving 3D printing parameters to address weak layer bonding characteristics. By utilizing response surface methodology, they were able to optimize the effects of the nozzle temperature, chamber temperature, and layer height on the interlayer bond quality for polyphenylene sulfide in the FFF method and successfully create an inlet coolant tube for the automobile sector [99]. The usage of manufacturing aids, such as jigs, fixtures, templates, and gages, is one basic but crucial use in automotive quality and production that is ready for change. To increase revenues and product quality, producers need to be able to deliver goods consistently, reliably, and affordably. Jigs and fixtures made via additive manufacturing can have shorter lead times and cost less money to make because less material is used and the designs are better. According to this study, Lead times are 40-90% faster than conventional fabrication in additive manufacturing. The same study also mentioned that BMW use additive manufacturing to build lighter fixtures with design complexities and the seat manufacturer shaved 31% in costs and 90% in weight with a 3D-printed check fixture [100]. Additionally, 3D-printed components are being used more and more frequently in structural elements for automobiles. Riccio A. et. al. have managed to create an upper roof shock absorber that improves the head injury criteria in this study. They said that the best production alternative to reduce costs, produce variously shaped absorbers tailored to particular vehicle locations, and reduce vehicle weight has been additive manufacturing [101]. S. Çakmak et. al. studied the replacement of metallic parts in clutch mechanisms with 3D-printed polymeric alternatives and managed to replace stoppers. According to their study, these materials and FFF processes are a promising way for further studies [102]. The aviation sector can likewise follow the same scenario. Every year, well-known manufacturing firms like Boeing, Airbus, SpaceX, Blue Origin, Rocket Lab, and others add more 3D-printed components to their product designs [103]. Since the development of composite and high-temperature polymer materials for 3D printing, FFF technology has become widely used in the manufacture of parts and assemblies for aircraft and unmanned aerial vehicles [104].

In this thesis, the study was carried out to gain the ability to produce thermoplastic matrix composites with the FFF method and to investigate the possibility of usage in heavy commercial vehicles. For this purpose, a push-type clutch mechanism was modeled in Unigraphics 8.0 and analyzed by using the finite element method in ANSYS Workbench 2022 R2 to find mechanical loads on specific parts (fulcrum rings) during the engagement/disengagement movement. In order to identify the required load for material testing, finite element results were examined carefully. Five materials (Pure PA6, PA6-%10Glass-fiber, PA6-%20Glass-fiber, PA6-%10Carbon-fiber, PA6-%20Carbon-fiber) were tested in this manner and compared with their metallic counterpart. To be more efficient and specific, test specimens were prepared in the form of the product and tested for each material combination. The same test was applied on both filaments and 3D print specimens to see the effects of additive manufacturing on mechanical strength. Moreover, numerical modeling of material characteristics is very crucial to avoid unnecessary material usage. A good prediction of the material behavior enables the save costs and time. The uniaxial compression test results were used in numerical modeling studies.

Chapter 4

4. Experiments and Simulations

4.1. Modeling of Clutch Cover Assembly Mechanism

The pushed-type clutch cover assembly is modeled using Unigraphics 8.0 to investigate the stress distribution of the fulcrum ring during the mechanism's operation. The 3D model of the cover assembly can be shown in Figure 4.1.
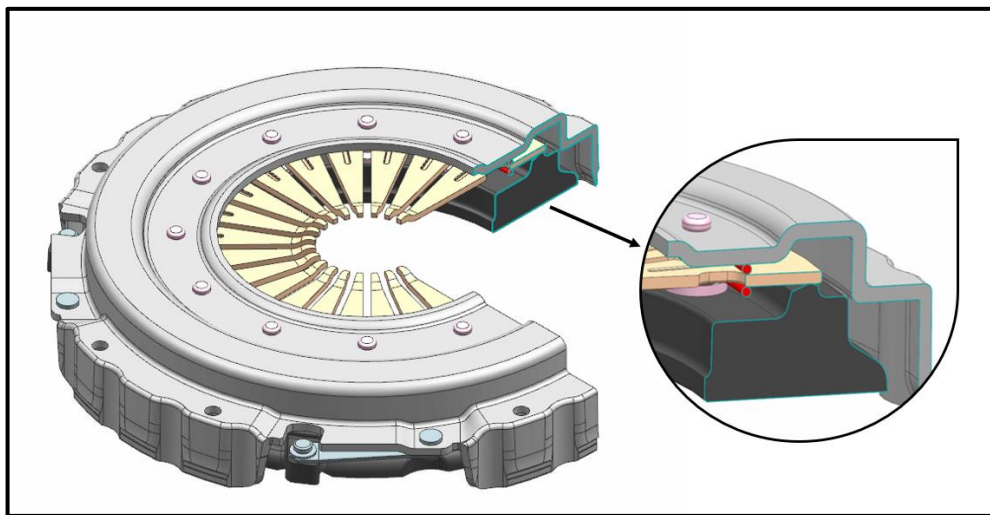
Figure 4.1: The pushed-type clutch cover assembly mechanism.

Fulcrum ring operating conditions will be investigated by using finite element methodology. As the previous (Figure 4.1) model involves too many small faces, rounded edges, and sharp vertices, the right simulation will require too much effort to get (contact relations, meshing, solution time, etc.) results. The finite element analysis is a powerful method for solving real-life simulations of complex structures. It breaks down geometry into tiny elements and tries to figure out design behavior by considering material properties. If the complexity grows, the method will require more time to get results. Figure 4.1 involves repeated components that require a large number of calculations to get finite element analysis results. Instead of using this complex geometry, it can be simplified with the help of circular symmetry as shown

in Figure 4.2. This simplification will help reduce solution time considerably while maintaining the result accuracy.
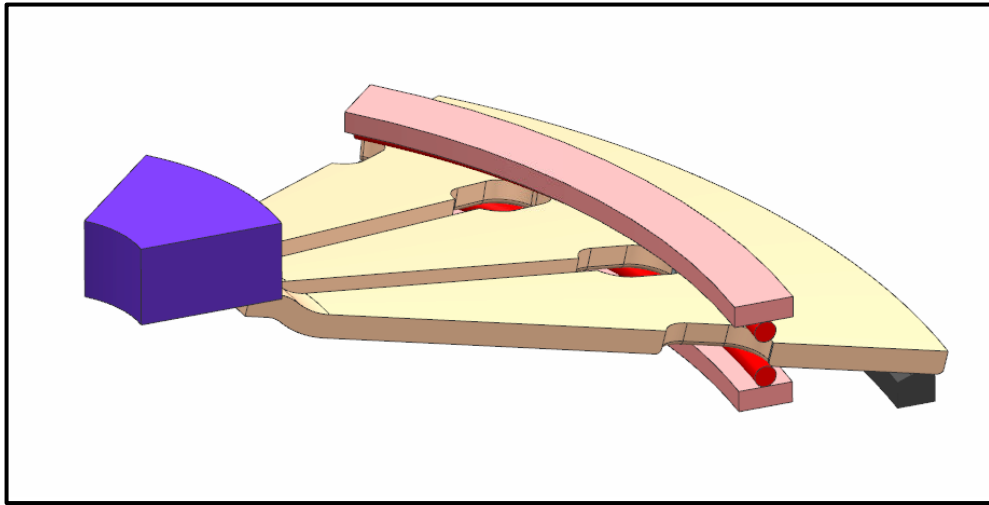
Figure 4.2: The simple model of pushed-type clutch cover assembly mechanism.

4.2. Materials

Materials are playing an important role in every design project [105]. They must be able to support loads and endure frequently unfavorable conditions without causing environmental harm or incurring excessive costs [106] Unfortunately, materials are often considered after the design process is complete. It is a fact that the performance of the products depends on the material searching procedure. This search focuses on comparing a limited number of material groups and selecting the most suitable one. Designing is a complex study which involves requirements, working principals, different concept, and materials (Figure 4.3). Since some of the materials may directly contribute to the accomplishment of some of the necessary functions, they could need to be determined their properties in early stages [105].
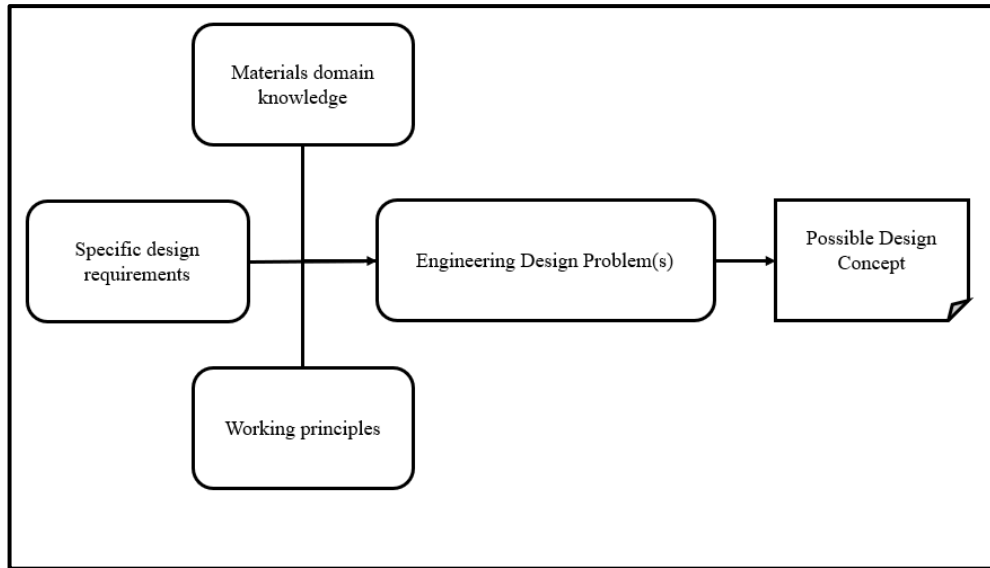
Figure 4.3: High level problem solving during early design. Adapted with permission from [105].

4.2.1. Polyamide (PA) 6

A growing number of industrial applications, including those in the chemical, automotive, electronics, and aerospace sectors, utilize the thermoplastic material polyamide 6 (PA6), often known as nylon 6, and its composites. This is due to the fact that these materials offer a high strength-to-weight ratio when compared to conventional materials, as well as self-lubricating and damping properties, corrosion resistance, immunity to UV and gamma radiation, and very straightforward and affordable manufacturing methods [107–109]. Due to all of these factors, PA6 material was chosen as the primary source for the thesis research. The BASF company's Ultramid B40LN product is the PA6 polymer used in the thesis study. The relative viscosity of this substance is 4, and its density is 1.13g/cm^3 (Figure 4.4).

Figure 4.4: Ultramid B40LN PA6 Pellet

4.2.2.   Carbon Fiber (CF) and Glass Fiber (GF) Reinforcements

Glass fiber, carbon fiber, and other inorganic reinforcements have been used to successfully reinforce polyamides for the past few decades [110]. Due to their outstanding characteristics, such as high strength, high modulus, high temperature resistance, corrosion resistance, fatigue resistance, and creep resistance, carbon fibers (CF) have been used extensively as structural and functional materials in the fields of aerospace, sports and leisure products, automobiles, wind power blades, and other industrial fields [111–113]. Dowaksa's AC4102 chopped fiber product was utilized as carbon fiber reinforcement in this study (Figure 4.5).

Figure 4.5: Dowaksa AC4102 Short Carbon Fiber

The Sisecam company's PA2 e-glass product was employed as glass fiber reinforcement. When compared to other glass kinds, its electrical insulation is exceptionally good because of its low alkaline ratio. It has a good amount of strength.

Figure 4.6: Sisecam PA2short e-glass fiber

4.2.3. Short Fiber Reinforced Polyamide 6 Composites

The mechanical characteristics, dimensional stability, and thermal distortion temperature of thermoplastics can all be enhanced by fiber reinforcing [114]. To examine how fiber addition affect the mechanical characteristics of products made using the FFF technique, four different combinations which are PA6-%10GF, PA6-%20GF, PA6-%10CF, PA6-%20CF were studied.

4.3. FFF Production with Short Fiber Reinforced PA6 Composites

In this study, 3D printing polymeric composite opportunities will be investigated as an alternative to TS EN 10270 steel fulcrum rings. Fulcrum rings are support points for pushed-type clutch cover assembly mechanisms. It is a fact that the compression loads constitute the majority of the loads acting on the material. Before putting 3D printing materials into practice, all of the materials should be tested under these loads and identified respectively. For being more specific on this scenario, test specimens were modeled with respect to the fulcrum ring geometry which can be seen in Figure 4.4.
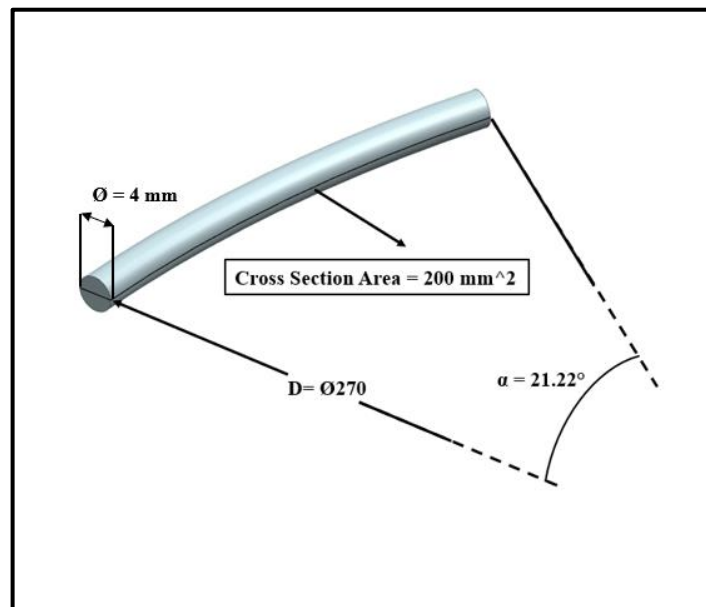
Figure 4.7: Compression test specimen dimensions.

Five different filaments were used to create the test specimens using the FFF technique. The CURA CAM was used to do the parameters and part positioning

necessary to construct the drawn parts in the FFF device shown in Figure 4.8 (The Ultimaker 3 device in the Ege University Aviation Vocational School Composite Laboratory). As the specimen has non-ideal geometry, the required compression load should be determined for the material testing stage considering loads applied on fulcrum rings during the engagement/disengagement analysis.
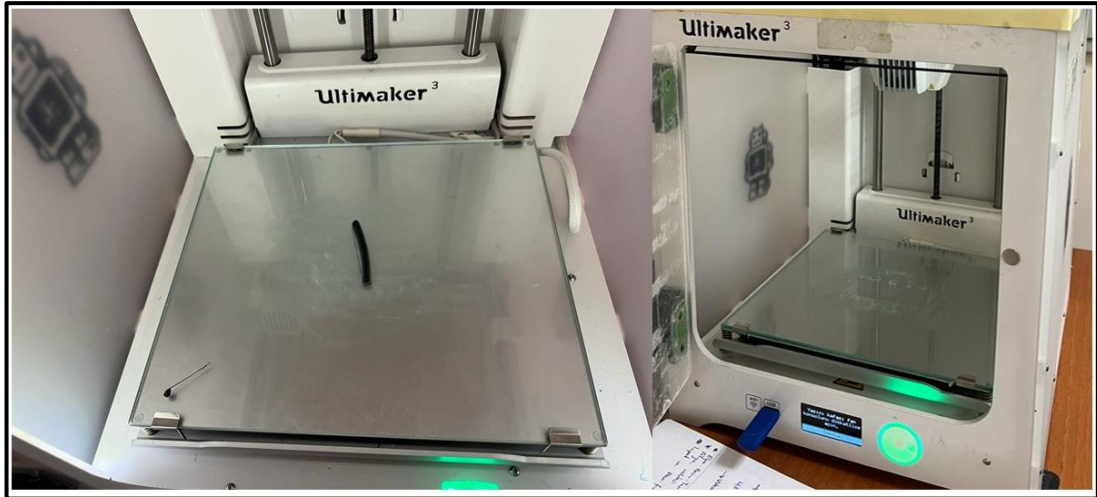
Figure 4.8: Ultimaker 3 FFF Device and Compression test specimen.

The ultimaker CC printcore was used to create each specimen on a sapphire tip of 0.6 mm in diameter, as seen in Figure 4.9. It is preferable to use a specific nozzle with a sapphire tip since carbon and glass fibers have abrasive properties.

Figure 4.9: Ultimaker CC Red Printcore nozule

Table 4.1: 3D Printing Parameters.

Infill Percentage	%100
Infill Pattern	0° - 90°
Print Speed	50mm/s
Flow Rate	%100
Bed Temparature	80°C

Specimens were created by using FFF method to compare the compression characteristics under working conditions (Figure 4.10).
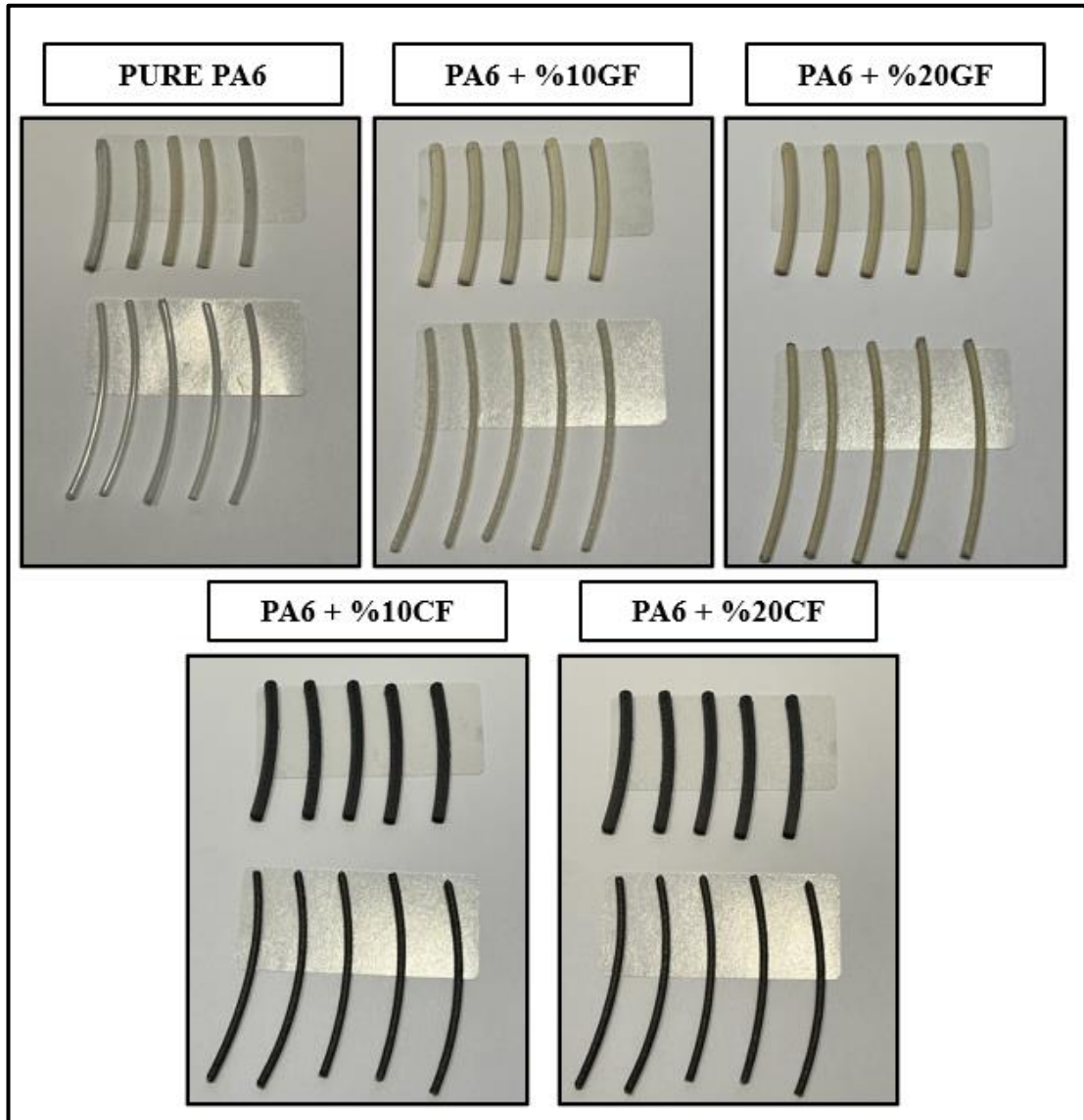
Figure 4.10: Compression Test Specimens

4.3.1. Engagement/Disengagement Analysis of Clutch Mechanism

The finite element study was conducted using Ansys Workbench 2022 R2 to determine the necessary load for the compression test. The diaphragm spring design consists of 24 identical fingers that are cylindrically placed at an angle of 15° along the same axis. The model was simplified as 1:8 in Figure 4.2 to take advantage of the solution time. This ratio should be taken into account while analyzing the outcomes of simulations.
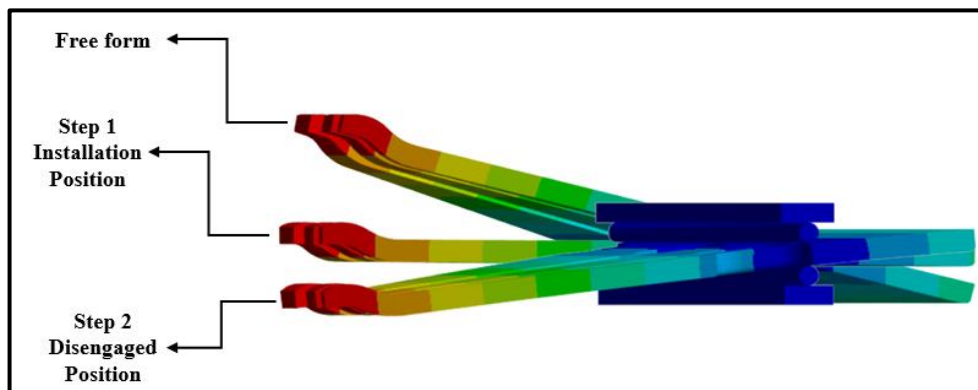
Figure 4.11: Finite element analysis steps for the mechanism.

As the mechanism involves two steps (installation and disengagement), the analysis was also separated into two stages. The first step represents the installation of the clutch mechanism into the vehicle. The cover is attached to the flywheel and the bolts are tightened by 6.963 mm. This prestresses the pressure plate and, as a result, the lower support point of the diaphragm spring. In the second part of the analysis, the release bearing part pushes the diaphragm fingers until a specific distance to separate the diaphragm spring–pressure plate connection. Once the connection is lost, the disc becomes free and the driver can shift gears (Figure 4.9). The analysis setup can be seen in Figur 4.10.
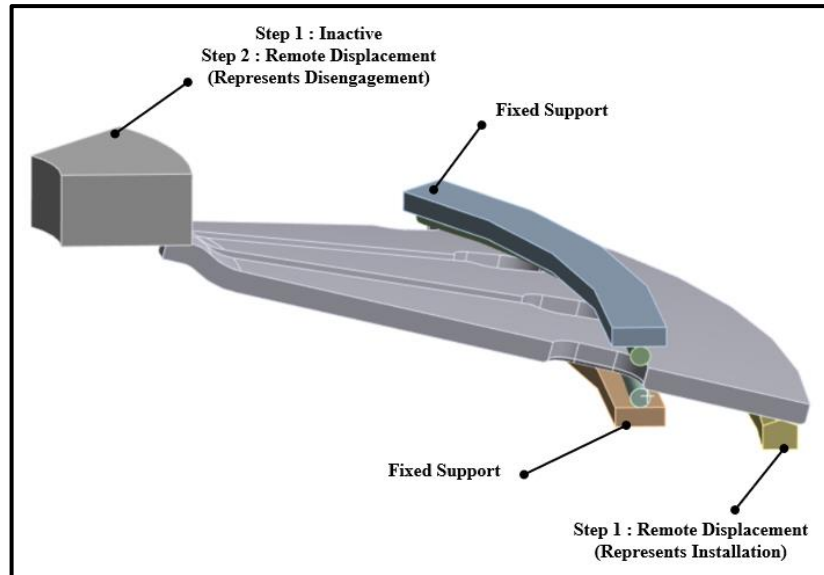
Figure 4.12: Finite element analysis setup for the mechanism.

4.4. Uniaxial Compression Test

A 100kN load sensor in a SHIMADZU AG-IC testing device was used in compression testing at the mechanical engineering lab of the Izmir Katip Celebi University (Figure 4.13). The experiments were run at a constant displacement speed of 2 mm/min. The samples were tested up to a load of 15 kN, which was determined from the findings of the finite element analysis.

Figure 4.13: SHIMADZU AG-IC testing device

4.5. Macro Scale Material Modeling

In its most basic form, material constitutive models define the relationship between material stress and strain and depict the behavior of materials at the point or "element" level. The ideas of yielding and plasticity are incorporated into numerous constitutive models used in engineering mechanics [115]. The demand for technologies that facilitate the efficient design of complicated devices for various loading circumstances is particularly on the rise [116]. The macro models are founded on the idea of a continuum of matter, where the densities of mass, momentum, and energy exist in the mathematical meaning of the continuum [117]. In this study, nine different macro-scale material models (Ogden (4.5.1) [118], Neo-Hooke (4.5.2) [119], Mooney Rivlin (4.5.3)[120–123], Isihara (4.5.4) [124], Gent-Thomas (4.5.5) [125], Swanson (4.5.6) [126], [127], Yeoh (4.5.7) [128], [129], Arruda Boyce (4.5.8) [130] and Gent(1996) (4.5.9) [131]) were utilized to predict material behavior under compressive loads by using Matlab R2021b.

$$P^{UT} = \sum \mu_k^{UT} \left[\lambda^{\alpha_k^{UT}-1} - \lambda^{-\frac{1}{2}\alpha_k^{UT}-1} \right] \tag{4.5.1}$$

$$P_1^{UT} = \mu^{UT}[\lambda - \lambda^{-2}] \tag{4.5.2}$$

$$P_1^{UT} = c_{10}^{UT}[2\lambda - 2\lambda^{-2}] + c_{01}^{UT}[2 - 2\lambda^{-3}] \tag{4.5.3}$$

$$P_1^{UT} = [2c_{10}^{UT} + 4c_{20}^{UT}c_{01}^{UT}[I_1^{UT} - 3][I_2^{UT} - 3] + c_{20}^{UT}c_{01}^{UT}\lambda^{-1}[I_1^{UT} - 3]^2][\lambda - \lambda^{-2}] \tag{4.5.4}$$

$$P_1^{UT} = \frac{2c_1^{UT}[\lambda^3 - 1]}{\lambda^2} + \frac{2c_2^{UT}[\lambda^3 - 1]}{2\lambda^4 + \lambda} \tag{4.5.5}$$

$$\left[\sum_{i=1}^{n} A_i \left[\frac{I_1^{UT}}{3} \right]^{\alpha_i} + \sum_{j=1}^{n} \frac{B_j}{\lambda} \left[\frac{I_2^{UT}}{3} \right]^{\beta_j} \right] \left[\lambda - \frac{1}{\lambda^2} \right] \tag{4.5.6}$$

$$P_1^{UT} = [2c_1 + 4c_2[I_1^{UT} - 3] + 6c_3[I_1^{UT} - 3]^2][\lambda - \lambda^{-2}] \tag{4.5.7}$$

$$P_1^{UT} = \left[\sum_{k=1}^{K} \frac{2\mu_k^{UT}C_k}{[N^{UT}]^{k-1}} [I_1^{UT}]^{k-1} \right] [\lambda - \lambda^{-2}] \tag{4.5.8}$$

$$P_1^{UT} = \frac{\mu^{UT}J_m^{UT}[\lambda^3 - 1]}{\lambda[\lambda J_m^{UT} - \lambda^3 + 3\lambda - 2]} \tag{4.5.9}$$

4.6. Optical Microscopy Analysis

For a better understanding of the effects of reinforcing elements and 3D printing techniques, an optical microscope was used. Studies were conducted at the Izmir Katip Celebi University Laboratory utilizing the Nikon ECLIPSE LV150N device (Figure 4.14).

Figure 4.14: Nikon ECLIPSE LV150N

4.7. Scanning Electron Microscope (SEM)

The scanning electron microscope (SEM) was used to investigate the effects of reinforcing elements and 3D printing processes on microstructure. At the Izmir Katip Celebi University Central Research Laboratory, microstructure studies were carried out using the Carl Zeiss 300VP SEM device (Figure 4.15).

Figure 4.15: Carl Zeiss 300VP SEM device

For each material combination and geometry, imaging of damaged surfaces was conducted following the uniaxial compression test. All specimens were coated with 10 nm gold by QUORUM Q150 RES before being put in the microscope chamber, and they were all secured on stubs with double-sided carbon tape (Figure 4.16).

Figure 4.16: QUORUM Q150 RES

Chapter 5

5. Results and Discussion

The mechanical test results are shown in this section. For each studied material, the impacts of the FFF process on compressive strength were investigated and shared. In order to find these effects mechanical tests were applied on both 3D-printed specimens and their filaments. The outcomes of the mechanical tests were also contrasted with those of the metal component to examine the potential material replacement options. Nine alternative macro scale material models were studied and presented for compliance to predict uniaxial compression behavior in addition to these experiments. Following that, the true scale prototypes were produced from the most suitable material option to test performance metrics. Three distinct approaches were used to identify and compare the clutch mechanism's performance characteristics. These performance indicators were computed based on theoretical information, examined using finite element analysis, and put to the test on a real test rig.

5.1.   Finite Element Analysis Results

The finite element analysis was conducted to define the maximum loads applied to each component. Afterward, the required load for the uniaxial compression test was calculated through the analysis results. Results showed that the load was applied on the inner fulcrum ring at the second step of the analysis while the outer fulcrum ring at the first stage. The Figure 5.1 shows the equivalent stresses on both metal outer and inner fulcrum rings. In order to define the majority of loads, principal stresses were evaluated. When the results are considered, it was shown that the minimum principal stresses constitute the majority of the loads applied on both fulcrum rings during the analysis. These stresses can be shown in Figure 5.2.
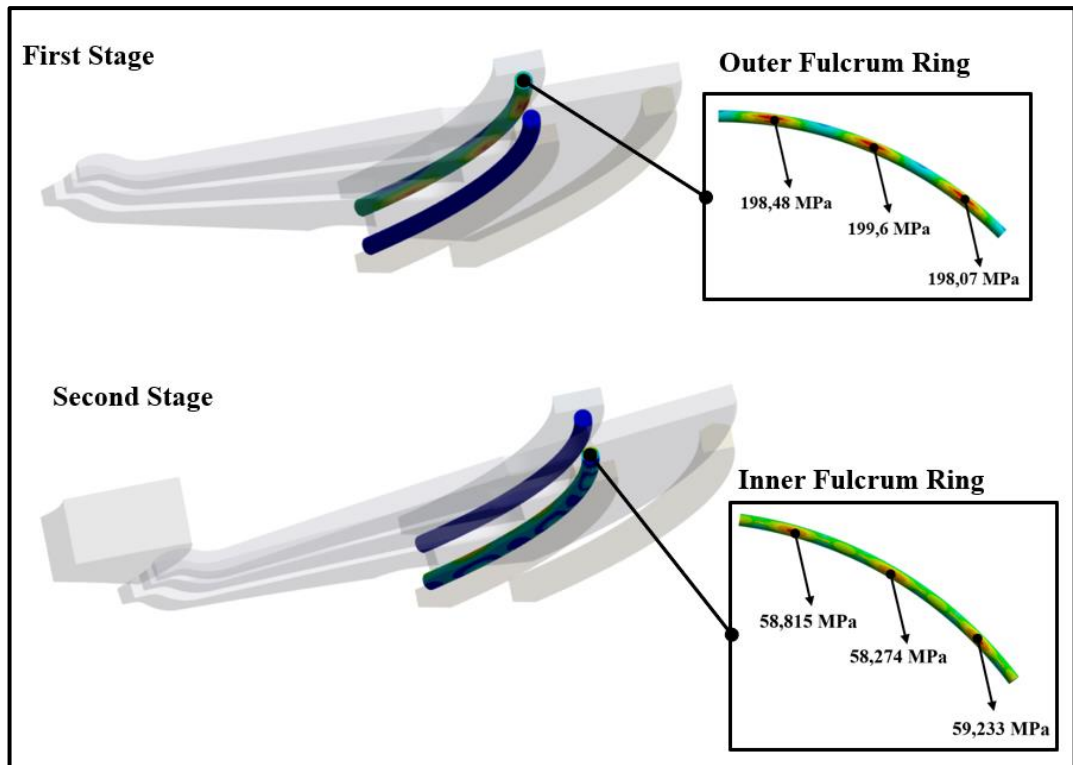
Figure 5.1: The equivalent stresses on both outer and inner fulcrum rings.
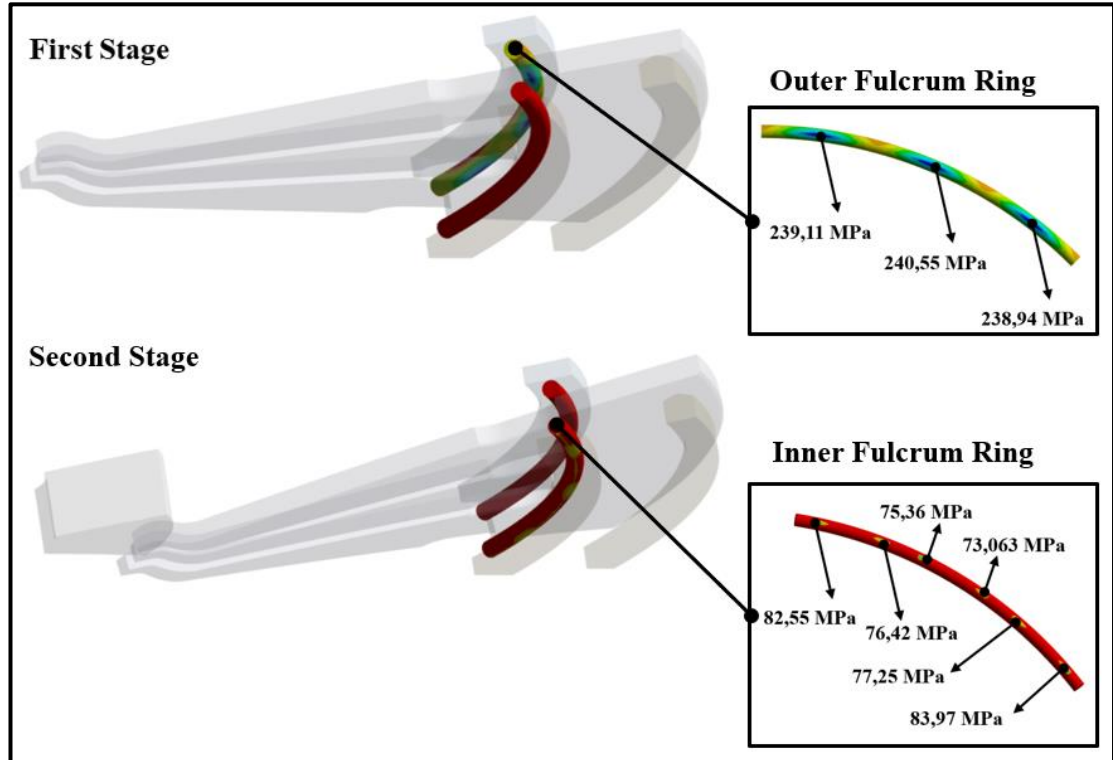
Figure 5.2: The minimum principal stresses on both outer and inner fulcrum rings.

The biggest stress was found in the outer fulcrum ring as 240,55MPa. After finding the critical stresses on the system, the required load found for the uniaxial compression test. An area assumption was made to determine this load, as illustrated in Figure 5.3. Since 132,32 mm^2 was subjected to the maximum stress of 240,55 MPa. The maximum load applied on 62,45 mm^2 can therefore be calculated as 15022,35 N using a simple formula for stress. This load will be applied to the compression test specimen in the uniaxial compression test.
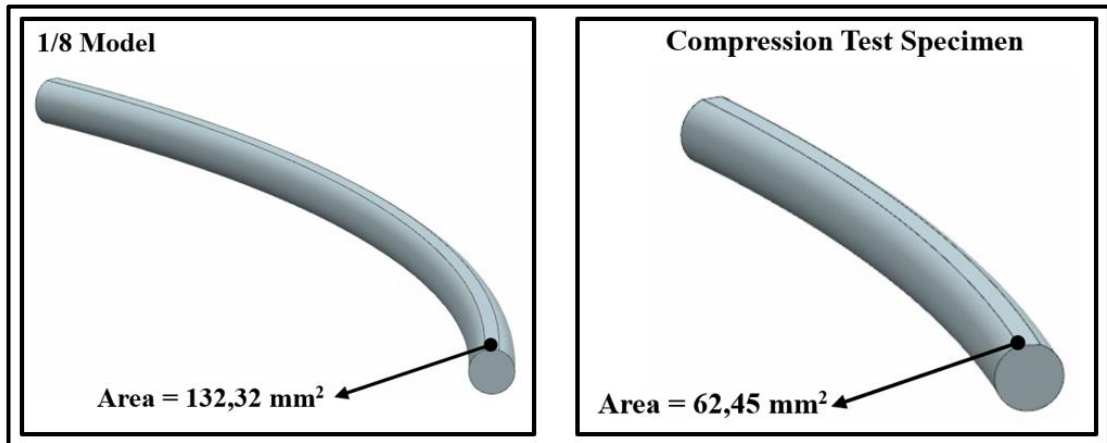
Figure 5.3: Area assumption for the compression load calculation.

5.2. Uniaxial Compression Test

In this research, FFF was used to create test specimens for uniaxial compression that had a particular geometry. Five materials and two geometry configurations of specimens prepared for this mechanical test (3D print and filament). The test was performed with the SHIMADZU AG-IC testing device and the load that was found in finite element analysis was applied to the specimens. The results are shown in Figure 5.4 for pure PA6, Figure 5.5 for PA6-%10 GF, Figure 5.6 for PA6-%10 CF, Figure 5.7 for PA6-%20 GF, and Figure 5.8 for PA6-%20 CF.
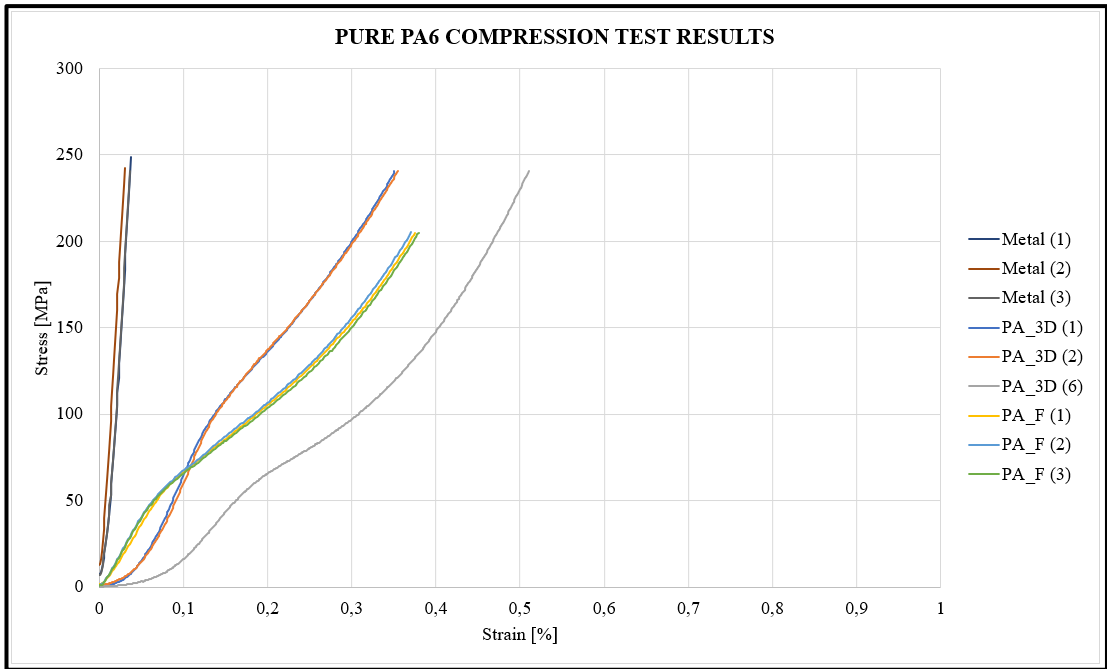
Figure 5.4: Uniaxial compression test results of Pure PA6
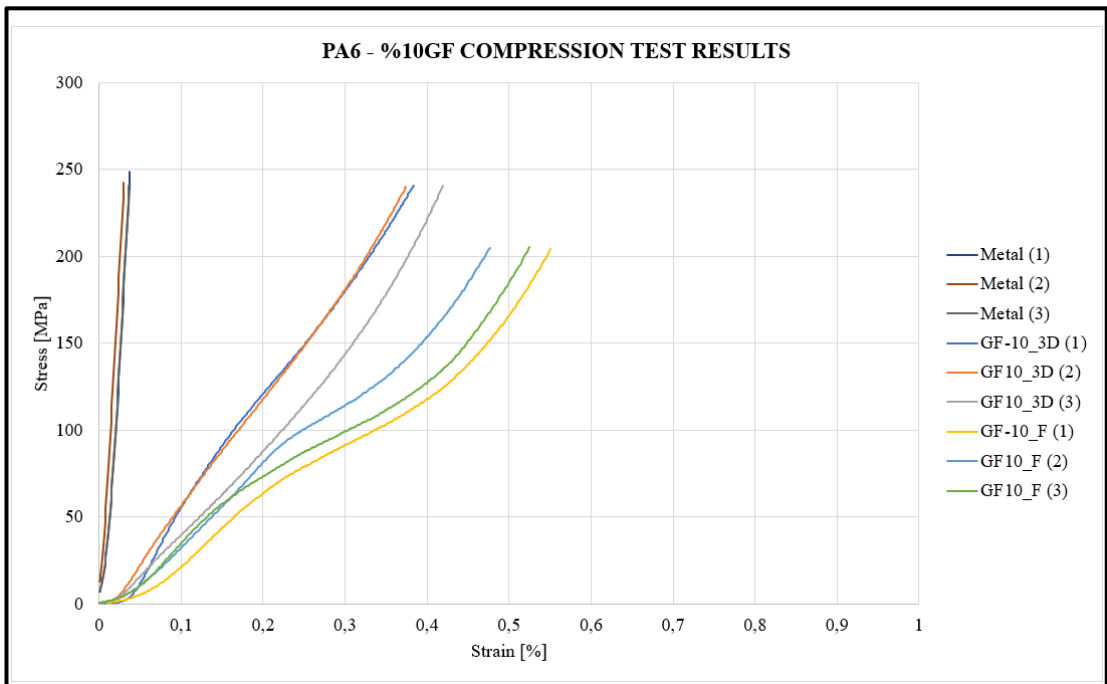
Figure 5.5: Uniaxial compression test results of PA6 - %10 GF.
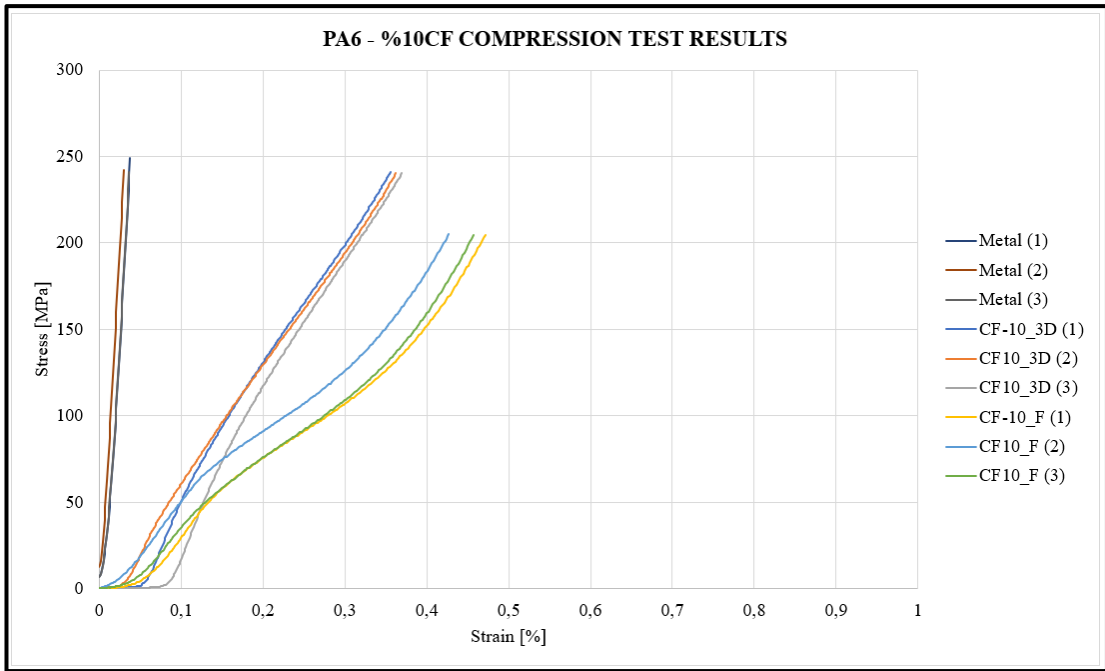
Figure 5.6: Uniaxial compression test results of PA6 - %10 CF.
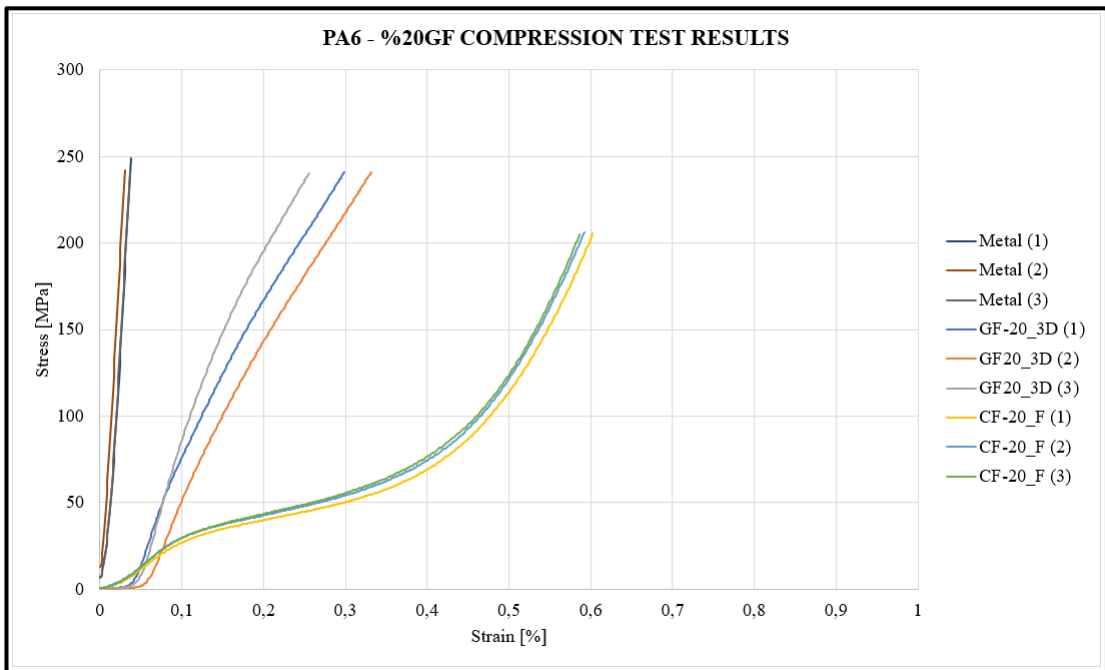
Figure 5.7: Uniaxial compression test results of PA6 - %20 GF.
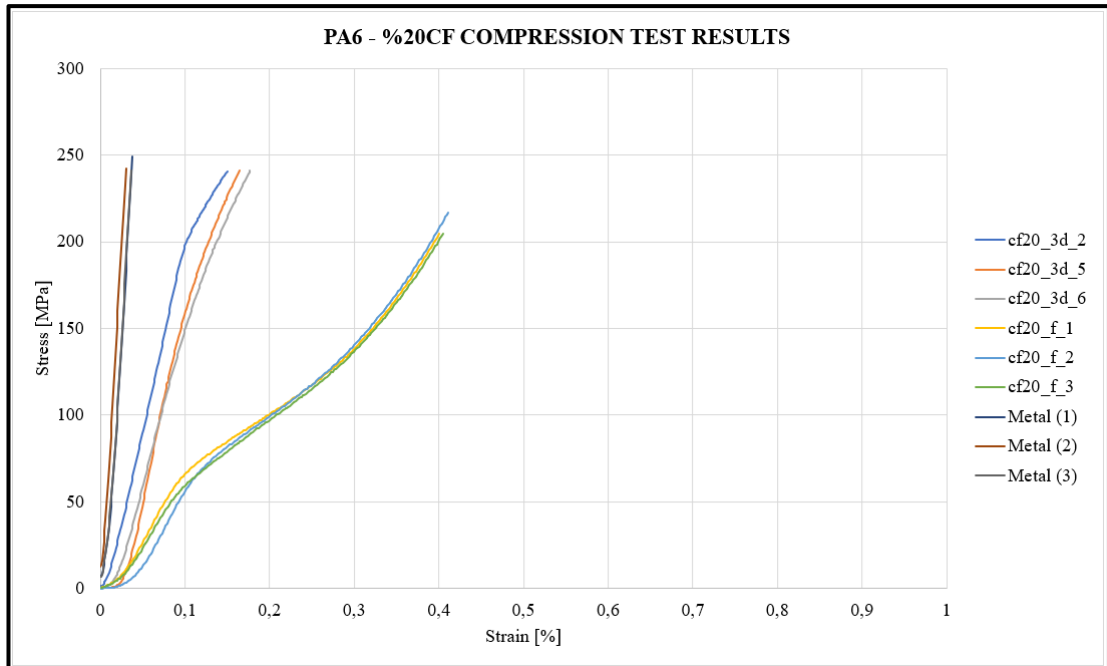
Figure 5.8: Uniaxial compression test results of PA6 - %20 CF.

When the effects of FFF methodology, fiber addition, and different fiber addition rates on specific compression specimens are investigated;

It was observed that by adding fibers to the polyamide 6 matrix, compression strength and strain were reduced. Figure 5.4 illustrates that compared to their 3D printed counterparts, Pure PA6 filaments have a more flexible structure under compressive forces. It was found that using the FFF approach caused the strain values to drop by 7% (PA-3D (6) is not included due to its unlike tendancy). The same drop was observed in PA6-%10 GF by %24,2 (Figure5.5) while PA6-%10CF is %19,76 (Figure 5.6). When it comes to the %20 fiber addition ratios, It was observed that the mechanical behavior of the specimens became closer to the metal counterpart. The results showed that the strain rates dropped by %50,31 in PA6-%20GF (Figure 5.7) while it dropped by %59,61 in PA6-%20CF (Figure 5.8). Compared to the pure PA6, the compressive strength of fiber added composites was closer to the metal counterpart. The strain values were decreased under compressive load in %20 fiber addition. The increase of compressive strength with the addition of short fiber reinforcements is consistent with the findings obtained by E.C. Botelho et al [132], M.A. Albadrani [133] and J. Pratama et al [134]. They have observed the effects of the additive manufacturing process on compressive strength and mechanical property improvement methods like fiber reinforcements. E.C. Botelho et al were also

investigated the effects of the fiber volume fraction and the matrix on mechanical properties through tensile, interlaminar shear and compressive tests. They stated that their results had shown an increase of the composite elastic modulus, tensile and compressive strength with the increase of carbon fiber content [132]. J.Justo et al showed that nylon's mechanical properties could be significantly improved by reinforcing materials. They compared the stiffness of the glass-fiber-reinforced nylon with the pure one and observed that reinforcement improved properties dramatically. Moreover, they stated that the FDM method was a very promising method for producing reinforced composites [135].

5.3.   Macro Scale Material Modeling

Macro-scale material modeling studies were carried out to predict each material behavior under uniaxial compressive loads. To obtain the compatibility of the material behavior to the models, curve fitting was also applied to the models. As a result, The material parameters were found for each material group and can be seen in tables from 5.1 to 5.9. As the PA6 - %20 CF has the closest behavior of the metal counterpart, these models were applied to the compression test results of PA6 - %20 CF and their suitability can be shown in Figure 5.9 for 3D printed PA-%20 CF and Figure 5.10 for filament PA-%20 CF.

When the suitability of the macro models with the uniaxial test results are considered; It was observed that Ogden, Swanson and Yeoh models are reflecting the behavior closer than the other macro models for 3D printed test specimen. When it comes to the filament specimen, besides these three models Gent-Thomas model was also shown a close tendancy with the experimental data.
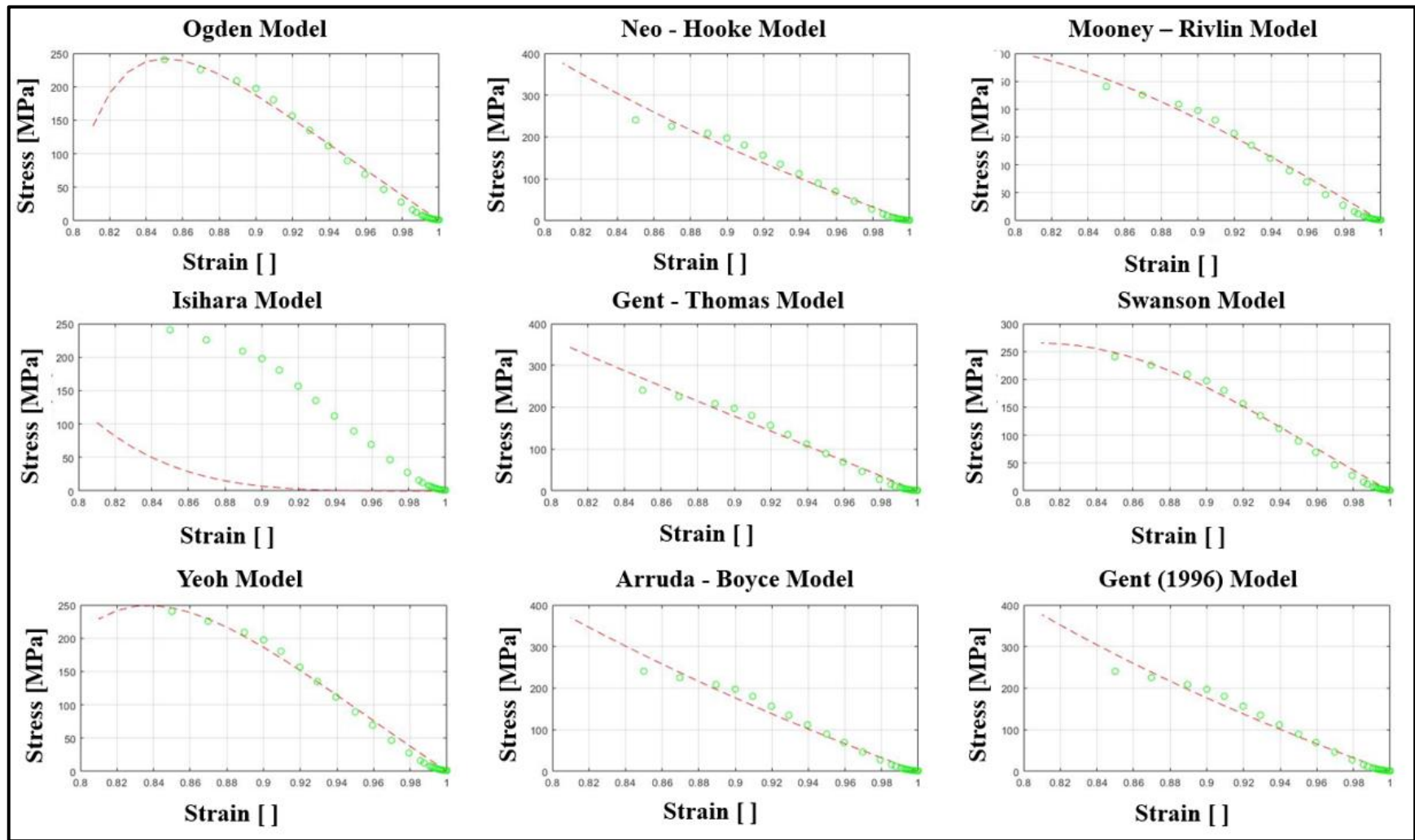
Figure 5.9: Macro-scale material model suitability for 3D printed PA6 - %20 CF
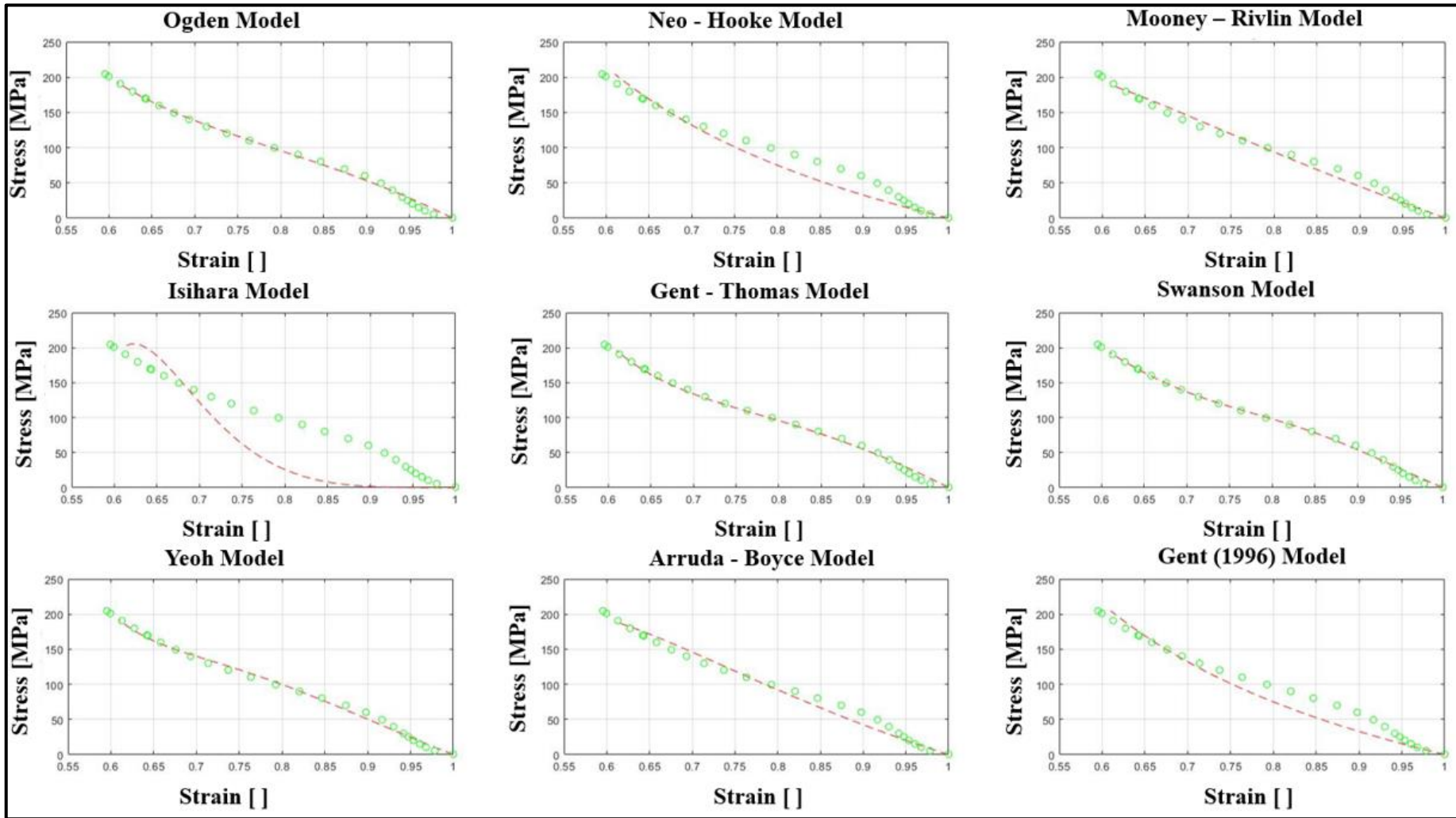
Figure 5.10: Macro-scale material model suitability for filament PA6 - %20 CF

Table 5.1: Ogden model parameters (n=3)

Material Parameters	μ_1^{UT}	μ_2^{UT}	μ_3^{UT}	α_1^{UT}	α_2^{UT}	α_3^{UT}
Pure PA6 (3D)	81,9393	24,4018	81,9333	3,1259	-3,9716	3,0668
Pure PA6 (F)	74,694	83,3491	94,6768	0,9281	-4,8984	9,5413
PA6-%10GF (3D)	83,2768	26,615	83,276	2,6411	-3,337	2,6176
PA6-%10GF (F)	57,6868	71,632	49,1266	2,9739	-2,8752	6,3085
PA6-%10CF (3D)	93,8693	25,8129	93,8692	2,5254	-3,6008	2,5064
PA6-%10CF (F)	29,0574	-7,2541	29,064	2,4768	-0,228	2,6732
PA6-%20GF (3D)	97,3604	117,1282	115,3752	-2,141	2,9832	3,0491
PA6-%20GF (F)	62,2516	61,0352	53,1917	8,2155	-0,3566	-4,233
PA6-%20CF (3D)	155,8074	1,0199	155,7985	4,0872	-25,863	4,0872
PA6-%20CF (F)	69,1210	101,8023	74,9458	6,9972	-3,0916	3,2376

Table 5.2: Neo-Hooke model parameters

Material Parameters	μ^{UT}
Pure PA6 (3D)	-125,647
Pure PA6 (F)	-114,4668
PA6-%10GF (3D)	-132,1528
PA6-%10GF (F)	-55,6305
PA6-%10CF (3D)	-146,2968
PA6-%10CF (F)	-75,2473
PA6-%20GF (3D)	-200,8000
PA6-%20GF (F)	-36,1213
PA6-%20CF (3D)	-527,2038
PA6-%20CF (F)	-98,5005

Table 5.3: Mooney-Rivlin model parameters

Material Parameters	c_{10}^{UT}	c_{01}^{UT}
Pure PA6 (3D)	-168,49	65,2678
Pure PA6 (F)	-143,1479	58,0295
PA6-%10GF (3D)	-134,8206	46,7195
PA6-%10GF (F)	-58,5463	16,1985
PA6-%10CF (3D)	-152,1314	55,2999
PA6-%10CF (F)	-66,2765	17,2812
PA6-%20GF (3D)	-184,6091	64,0675
PA6-%20GF (F)	-17,6926	-0,1676
PA6-%20CF (3D)	-869,9867	537,5135
PA6-%20CF (F)	-113,2231	41,3332

Table 5.4: Isihara model parameters

Material Parameters	c_{10}^{UT}	c_{01}^{UT}	c_{20}^{UT}
Pure PA6 (3D)	-1000	36,899	36,899
Pure PA6 (F)	-655,5258	31,0242	31,0242
PA6-%10GF (3D)	-702,7808	32,7329	32,7329
PA6-%10GF (F)	48,3305	6,5689	6,5689
PA6-%10CF (3D)	-1000	36,8205	36,8205
PA6-%10CF (F)	15,0599	12,9616	12,9639
PA6-%20GF (3D)	-1000	40,8103	40,8103
PA6-%20GF (F)	26,3039	30,2217	0,2771
PA6-%20CF (3D)	-10	-70	25
PA6-%20CF (F)	-210,8212	22,0811	22,1043

Table 5.5: Gent-Thomas model parameters

Material Parameters	c_1^{UT}	c_2^{UT}
Pure PA6 (3D)	-305,4597	558,34
Pure PA6 (F)	-369,3396	752,9144
PA6-%10GF (3D)	-260,3480	469,8808
PA6-%10GF (F)	-6,5591	-52,6225
PA6-%10CF (3D)	-275,4060	491,5668
PA6-%10CF (F)	-151,6765	275,0927
PA6-%20GF (3D)	-233,9112	332,2133
PA6-%20GF (F)	-27,6131	25,0624
PA6-%20CF (3D)	-633,4466	1000
PA6-%20CF (F)	-319,6936	649,7315

Table 5.6: Swanson model parameters (n=2)

Material Parameters	A_1	B_1	α_1	β_1	A_2	B_2	α_2	β_2
Pure PA6 (3D)	-25,13	-115,09	0,12	-30,30	237,89	-114,32	-132,88	-2,26
Pure PA6 (F)	-57,50	-43,34	1,58	-53,07	-92,52	-43,34	-6,40	-53,07
PA6-%10GF (3D)	-3,06	-73,30	9,77	-4,21	-3,02	-73,30	9,76	-4,21
PA6-%10GF (F)	-24,83	-27,25	0,08	-8,48	-24,83	-27,25	0,10	-8,48
PA6-%10CF (3D)	54,14	-89,81	-60,72	-14,40	-16,34	-90,09	1,28	-1,30
PA6-%10CF (F)	41,48	-61,02	-35,82	-1,15	47,16	-102,14	-52,70	-21,06
PA6-%20GF (3D)	-17,41	-88,14	-1,26	-3,84	-17,41	-88,14	-1,26	-3,65
PA6-%20GF (F)	-69,36	30,23	-20,23	-661,86	-30,68	28,97	0,36	-659,03
PA6-%20CF (3D)	-92,22	209,63	-10,89	-15,86	-92,22	-209,64	-10,89	-14,63
PA6-%20CF (F)	-49,88	-35,62	-0,40	-20,17	-49,88	-35,62	-0,39	-20,16

Table 5.7: Yeoh model parameters

Material Parameters	c_1	c_2	c_3
Pure PA6 (3D)	-99,3727	46,5277	-20,8583
Pure PA6 (F)	-93,4062	82,0592	-55,144
PA6-%10GF (3D)	-85,1642	31,0337	-11,2808
PA6-%10GF (F)	-49,7785	19,498	-5,3063
PA6-%10CF (3D)	-92,3132	33,7311	-11,1863
PA6-%10CF (F)	-52,3806	19,7677	-7,8502
PA6-%20GF (3D)	-105,7972	-30,617	110,3895
PA6-%20GF (F)	-23,8414	4,815	-1,1745
PA6-%20CF (3D)	-307,4962	400,0067	1000
PA6-%20CF (F)	-78,5700	53,0127	-28,7565

Table 5.8: Arruda Boyce model parameters (K=3)

Material Parameters	μ_1^{UT}	μ_2^{UT}	μ_3^{UT}	N^{UT}
Pure PA6 (3D)	-490,5486	1000	208,8707	2,1750
Pure PA6 (F)	-537,8422	949,1423	-253,8629	1,1515
PA6-%10GF (3D)	-526,0383	949,2711	-287,8421	1,1981
PA6-%10GF (F)	-264,5291	1000	-735,6336	2,2825
PA6-%10CF (3D)	-517,8559	972,5004	-207,4513	1,4924
PA6-%10CF (F)	-320,2965	858,5303	-462,6111	1,5149
PA6-%20GF (3D)	-531,9724	993,2942	173,4574	2,0924
PA6-%20GF (F)	-168,8835	819,2921	-794,7874	2,6626
PA6-%20CF (3D)	-853,0464	253,4115	82,4376	0,6870
PA6-%20CF (F)	-559,7065	942,1923	-285,9513	0,9016

Table 5.9: Gent (1996) model parameters

Material Parameters	μ^{UT}	J_m^{UT}
Pure PA6 (3D)	-153,5932	1000
Pure PA6 (F)	-114,4159	1000
PA6-%10GF (3D)	-132,0956	1000
PA6-%10GF (F)	-55,5682	1000
PA6-%10CF (3D)	-146,2423	1000
PA6-%10CF (F)	-75,1938	1000
PA6-%20GF (3D)	-200,7550	1000
PA6-%20GF (F)	-35,2598	67,5417
PA6-%20CF (3D)	-527,1788	1000
PA6-%20CF (F)	-98,4472	1000

5.4. Optical Microscopy Images

The structure of both filaments and 3D printed specimens was investigated after uniaxial compression test by using the optical microscope. When the Nikon ECLIPSE LV150 figure 5.11 is magnified 200 times, it is simple to observe the filament structures. The same investigation was also carried out for 3D printed specimens with a 100 times amplification, and fiber formations can be seen in both reinforced specimens (Figure 5.12).
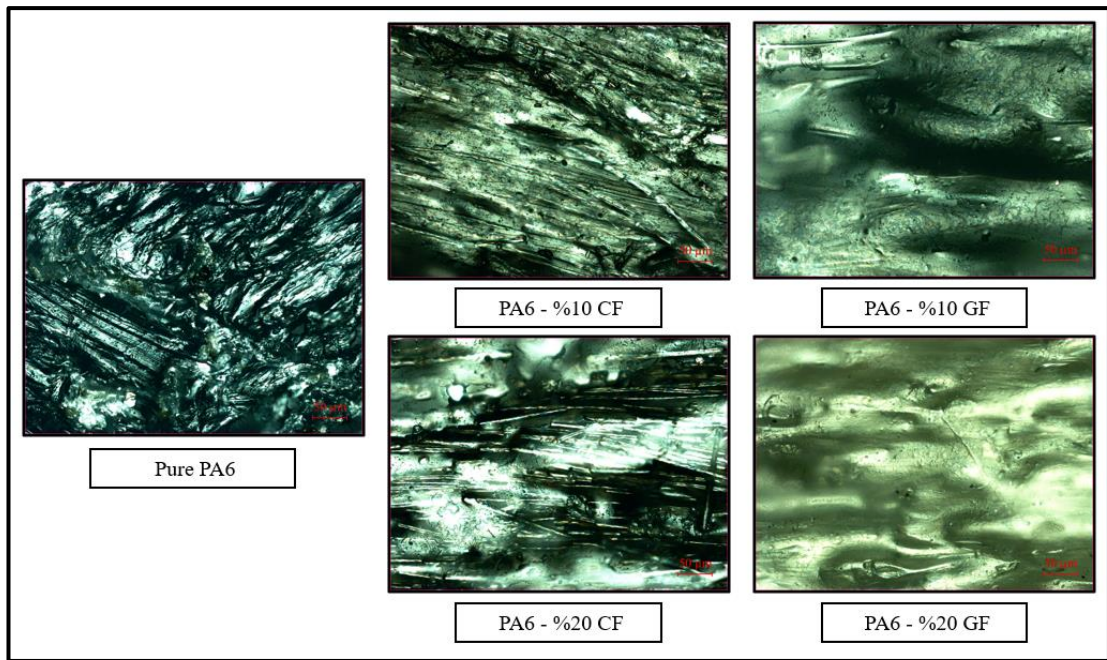
Figure 5.11: Photographic of filaments amplified 200 times by Nikon ECLIPSE LV150.
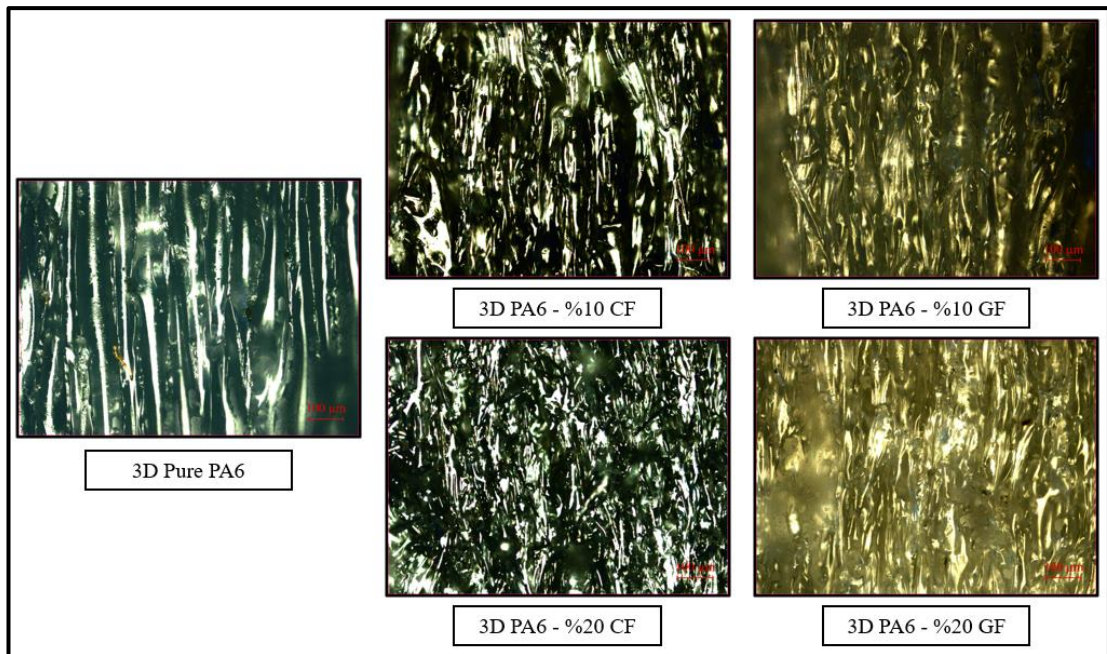
Figure 5.12: Photographic of 3D printed specimens amplified 100 times by Nikon ECLIPSE LV150.

57

5.5. Scanning Electron Microscope (SEM)

After the uniaxial compression test, the impacts of reinforcing materials and 3D printing techniques on microstructure were examined using the scanning electron microscope (SEM). Figure 5.13 shows the microstructure of the filaments.
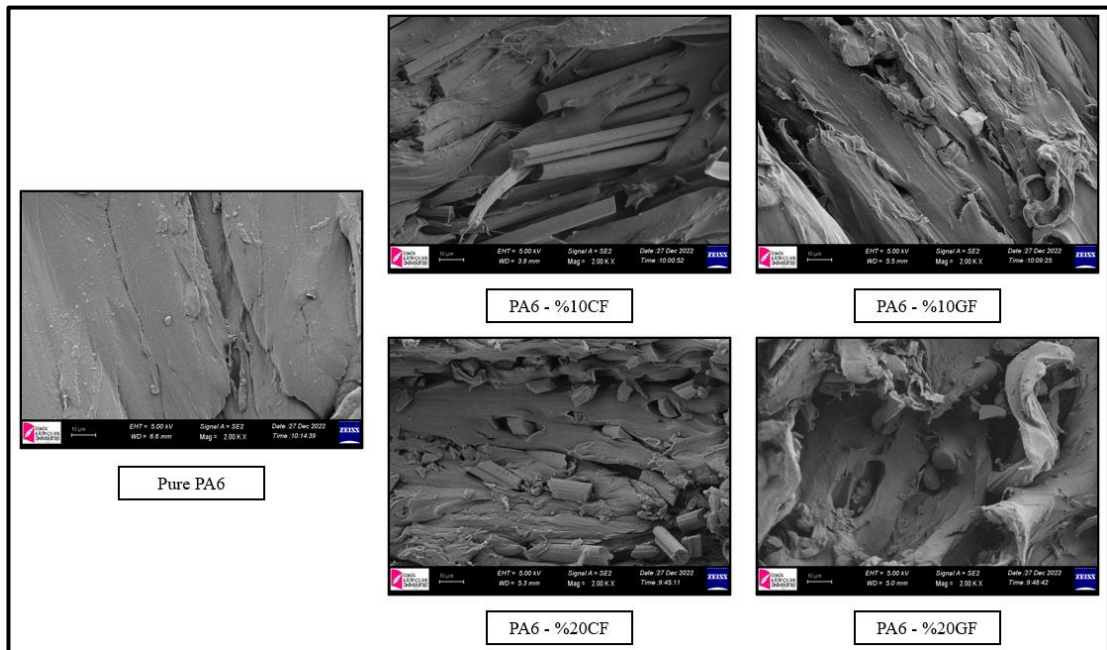
Figure 5.13: SEM images of the filaments
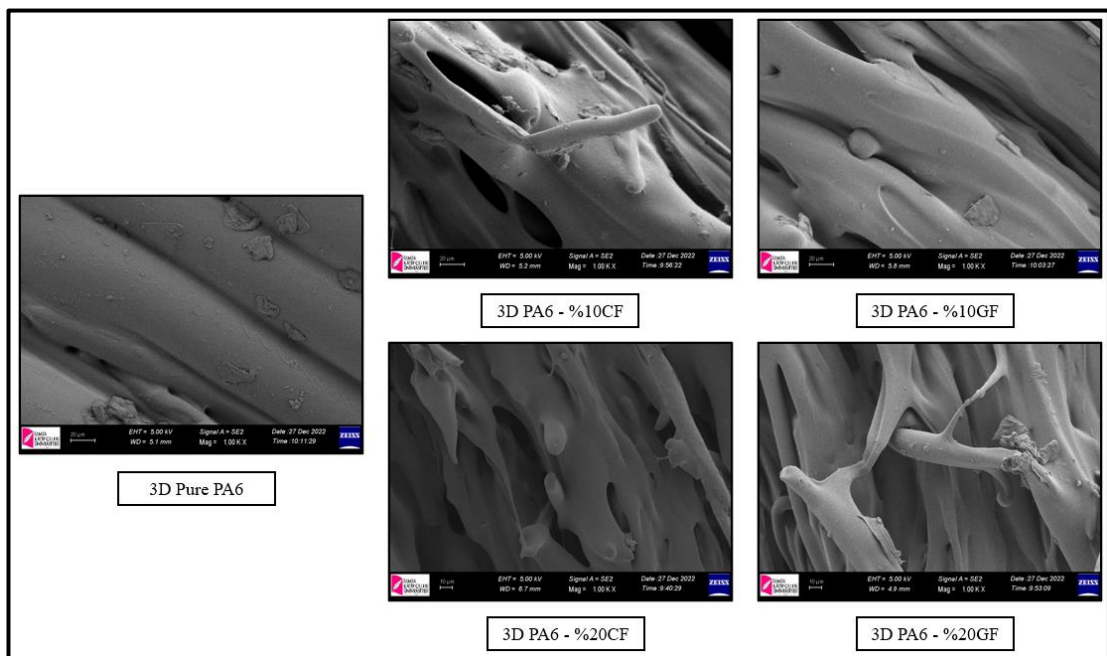
Figure 5.14: SEM images of the 3D printed specimens

The extrusion process has been performed at between 200-220°C in order to produce filaments. As far as shown in SEM images this heat could not be helpful for good integration of fiber. 3D printer's nozzle was raised up to 275°C and the extruder at 225-235°C during the 3D printing process. With the help of the heat increment, a better material structure has been procured. Moreover, material orientation could be set by taking the applied force into account with 3D printing. It is foreseen that the mentioned effects of the 3D printing process have provided to have material closer mechanical behavior to the metal counterpart.

5.6. True Scale Prototypes Production and Assembling Process

The mechanical tests showed that the PA6 - %20 CF was the most suitable material for both fulcrum rings due to its smallest strain values among the other combinations. For this reason, the true scale prototypes were produced by using the FFF method and used in the assembling process (Figure 5.15). The effects of alternative material on the clutch cover assembly metrics were examined, and compared with the analysis and theoretical calculations.

Figure 5.15: PA6-%20CF fulcrum ring prototype

The assembling process starts with the riveting of both fulcrum rings with the diaphragm spring and cover parts (Figure 5.16).
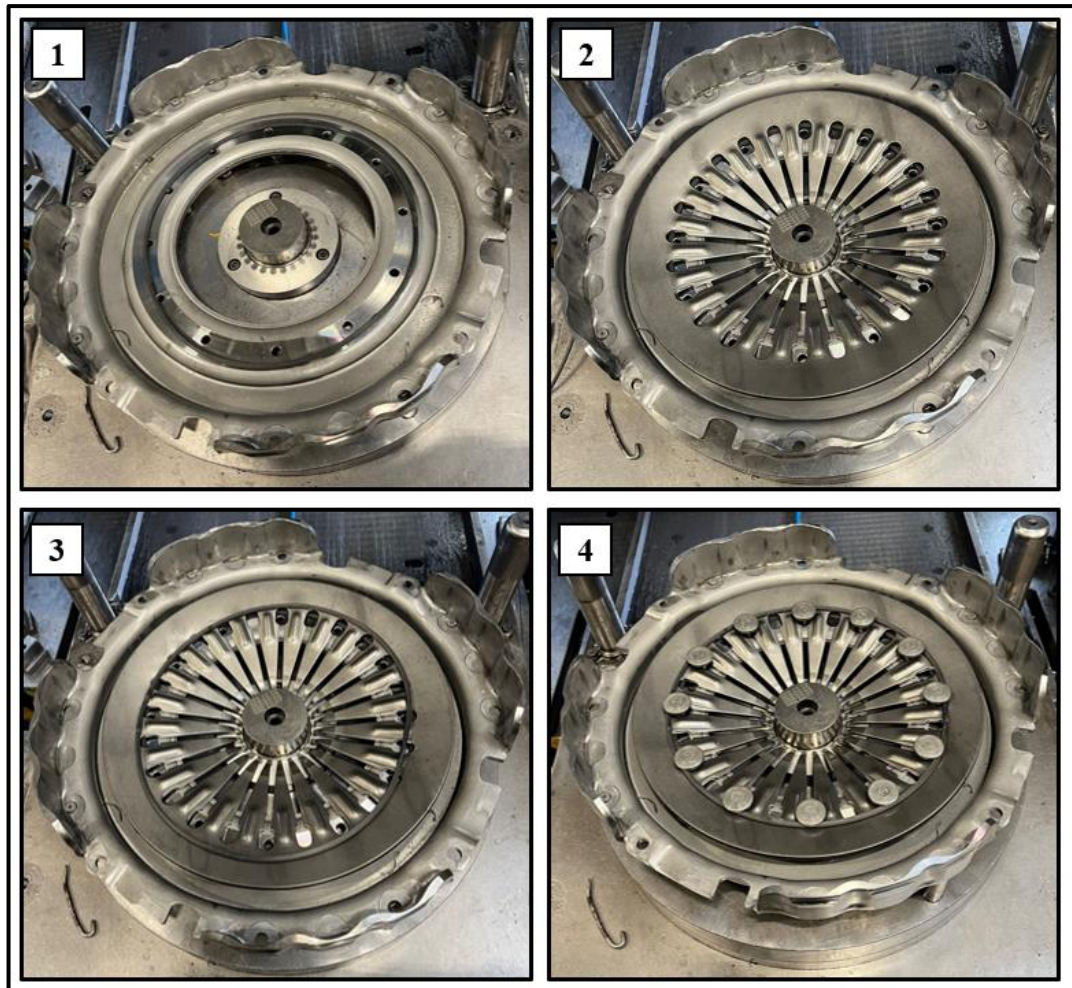
Figure 5.16: Assembling fulcrum rings with diaphragm and cover.

A compressive pressure is applied on both of the rings through stepped rivets at this stage. PA6 - %20 CF fulcrum rings could be deformed under this big pressure. In order to avoid this situation, Stepped rivet lengths were reduced by considering deformations observed in mechanical tests (Figure 5.17).
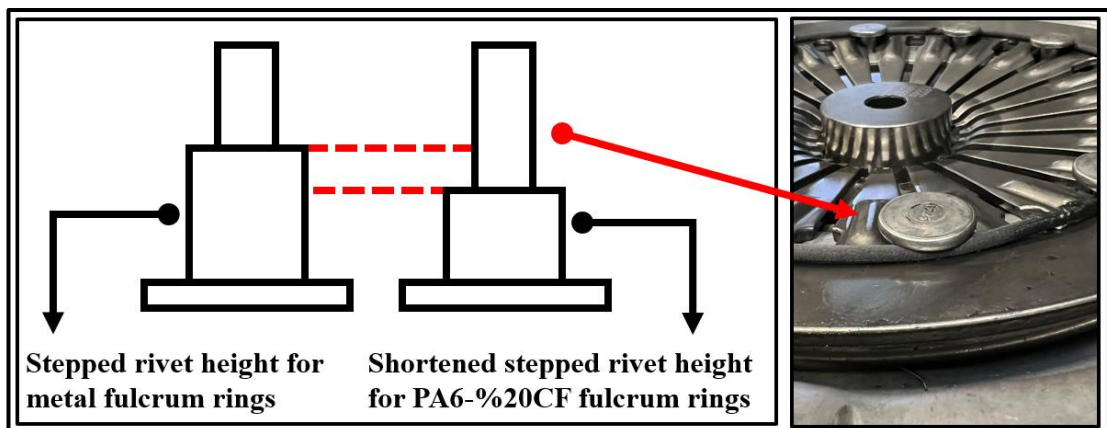
Figure 5.17: Shortened stepped rivet for assembling PA6 - %20CF fulcrum rings

The pressure plate and strap plates are inserted into the cover and riveted to complete the mounting (Figure 5.18).
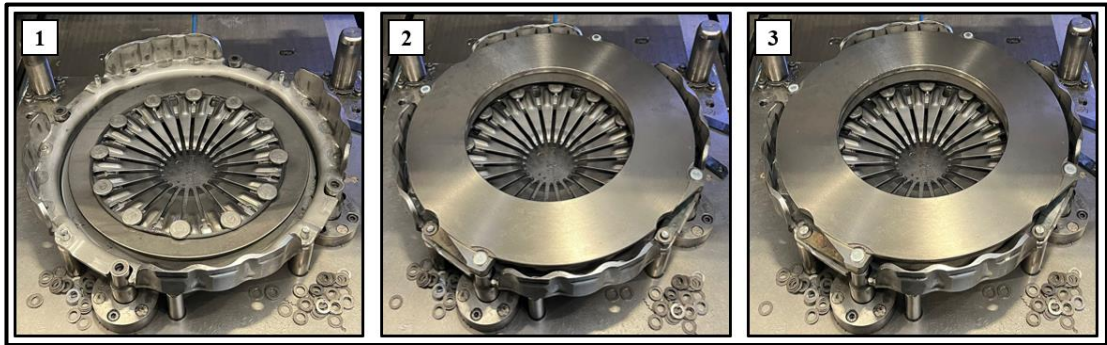
Figure 5.18: Completing the clutch cover assembly.

In Dönmez Clutch, each clutch cover assembly is tested in the cover assembly performance test device to be sure and trace each component before mounting on the vehicle. This test is very crucial to evaluate any kind of alternative material integration to the assembly. This test measures clamp load, release load, liftoff, and parallelism. The clutch cover assembly is then prepared for performance tests (Figure 5.19).

Figure 5.19: The clutch cover assembly performance test device.

5.7.   Product Performance Criteria Comparision

Several metrics define the clutch cover assembly performance which are clamp load (new), clamp load (worn), release load (new), release load (worn), maximum load, parallelism, lift-off, and fingertip height. The clamp load and release load are two of the most important metrics for the clutch mechanism. In this study, the push-type clutch cover assembly performance metrics were calculated, analyzed, and tested. These results can be shown in Figures 5.16 for clamp load and 5.17 for release load respectively. To clarify these results, the clamp load is the load that measured just after installation. In this context, the clamp load was read from the position of 6.693 which is installed position. When it comes to release load, it is needed to limit this load with a specific value due to release load can affect user confort directly. For this reason, this load always taken as maximum value.
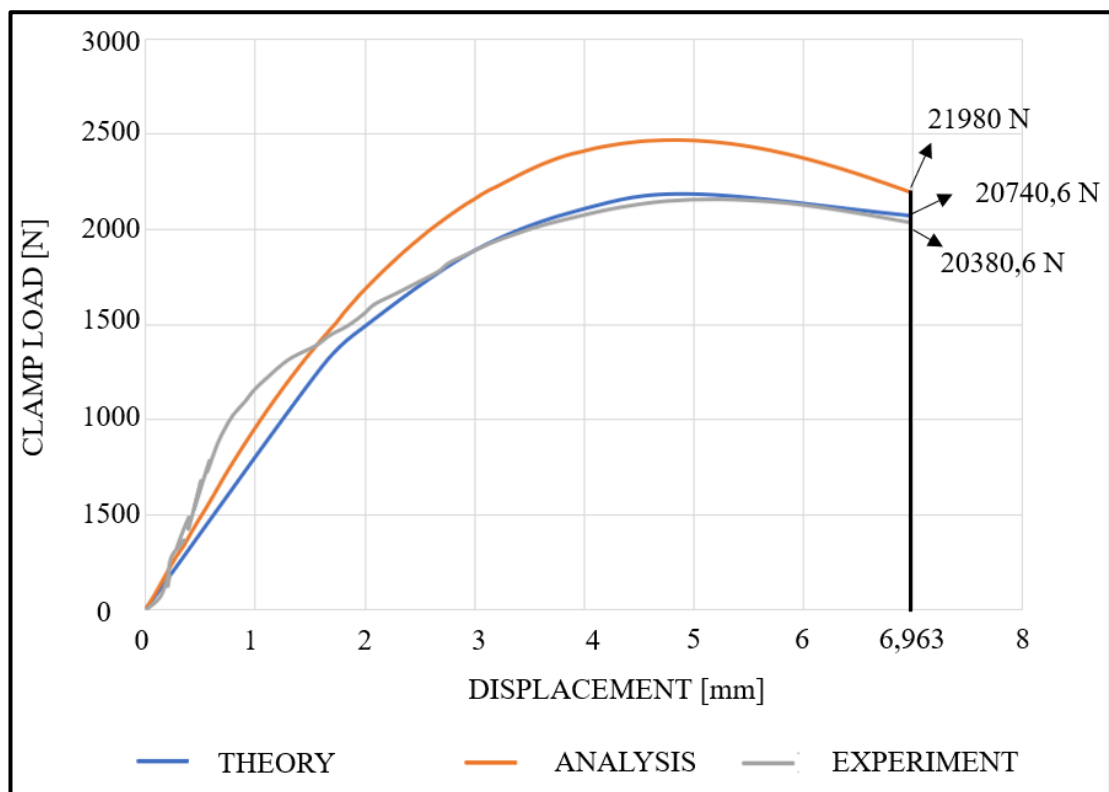
Figure 5.20: Clamp load Comparasion at operation point.
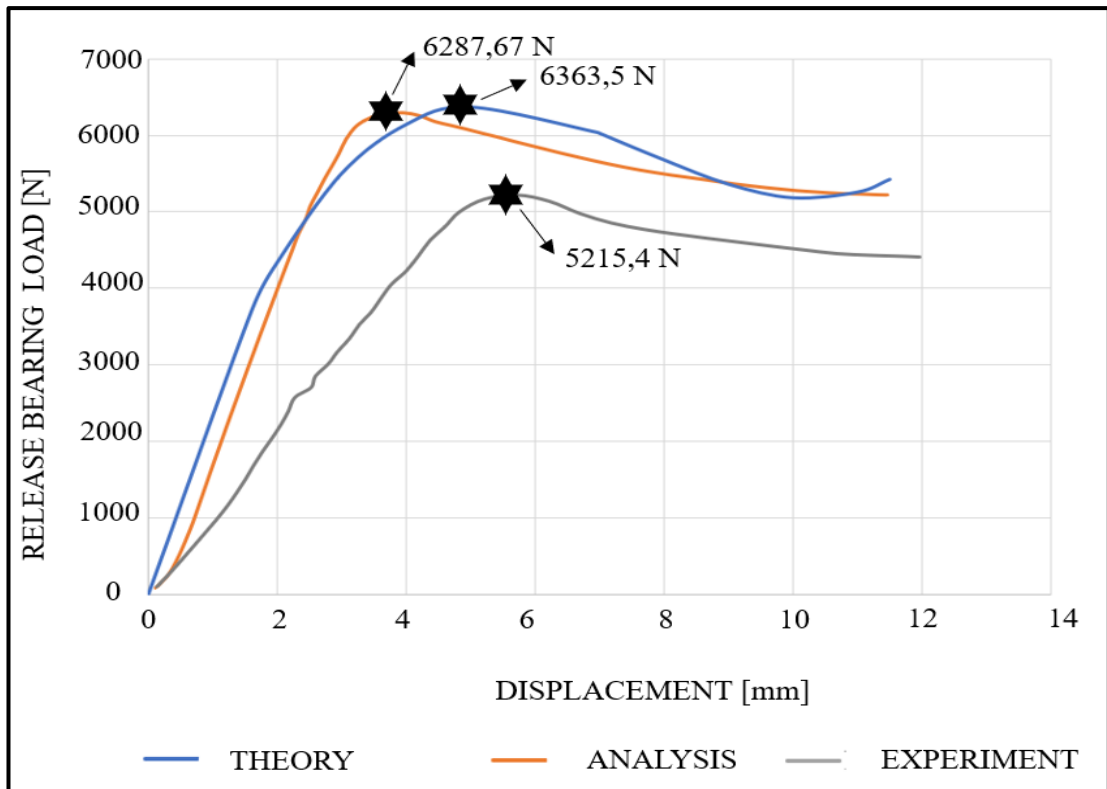
Figure 5.21: Maximum Release load Comparasion at operation point.

The PA6-%20CF was used as a replacement material, and the same experiments were performed to investigate how these two forces changed. Table 5.10 illustrates the findings for both clamp load and release load.

Table 5.10: The clamp and release load changes with the replacement

Material / Performance Metrics	Clamp Load [N]	Release Load [N]
Metal	20740	5215
PA6 - %20 CF	20320	5230

Chapter 6

6. Conclusion

This study aimed to create alternative materials to metal-based materials and successfully integrate them into the automotive industry. Thermoplastic composites are very promising materials due to their extraordinary properties. With developments in 3D printing technology, these materials have become possible to produce these materials with high quality and strength.

The comparison of the mechanical behavior of alternative material types under operating loads is the most significant part of the study. Finite element analysis was utilized to define operating loads. Several tests were conducted to determine the effects of fiber addition and the 3D printing method on mechanical behavior. It was noted that the behavior became closer to its metal counterpart relating to both fiber addition and 3D printing. The behavior of materials under various loading circumstances is the subject of numerous studies that aim to reduce the use of materials. The objectives of these investigations are to reduce the waste of materials and accurately replicate failure processes in simulations. Contrary to previous studies, we have found that 3D printed samples performed better compared to filament materials due to better bonding and fiber alignment. This status can be seen clearly in PA6 - %20CF filament and 3D printed specimen (Figure 6.1).

One of the objectives of this work was to estimate the behavior of the material under compressive loading circumstances by examining the compatibility of the experimental data with nine different macro-scale numerical models.
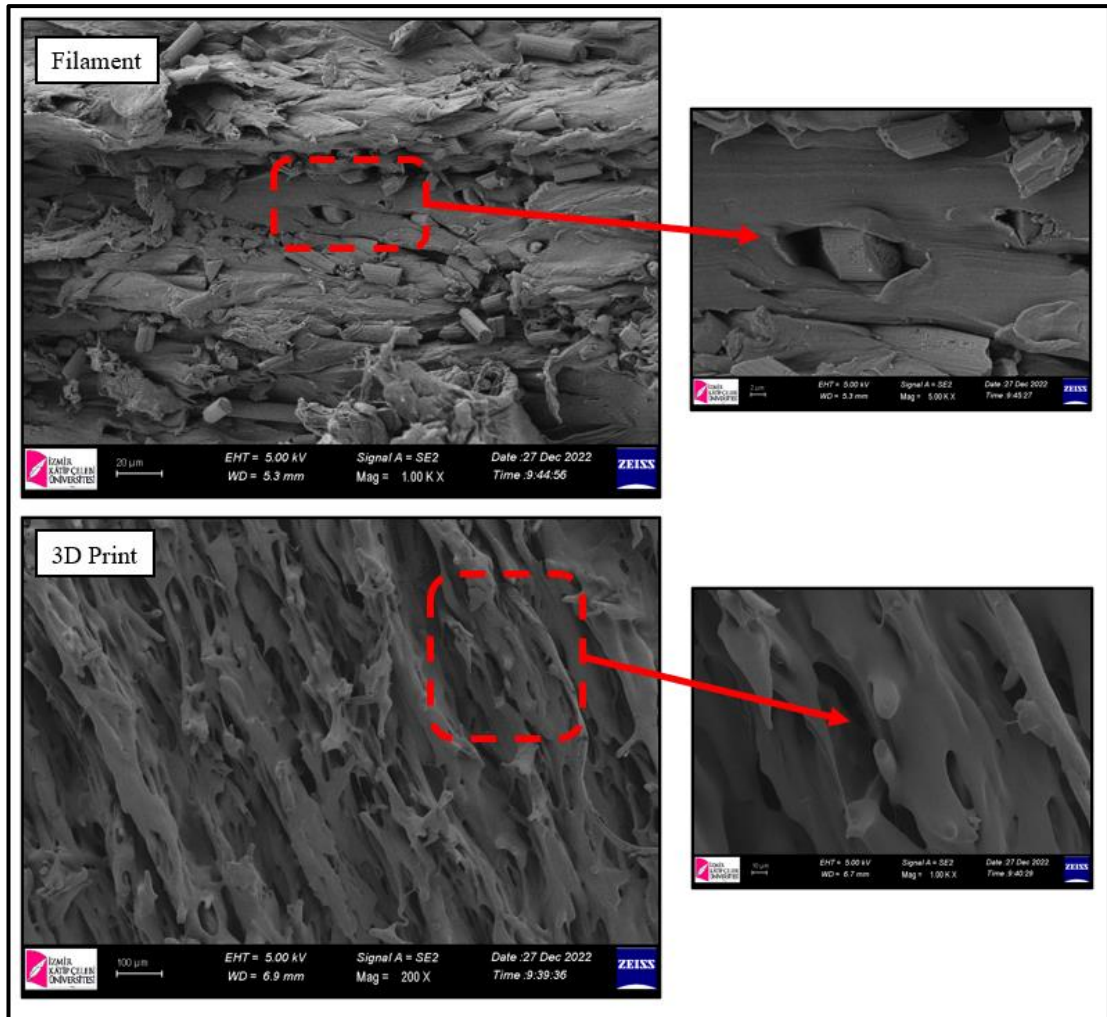
Figure 6.1: SEM images of PA6 - %20 CF

To conclude this comprehensive work on polymeric composites with 2 different reinforcing materials, and 2 different fiber percentages, the true scale prototypes were constructed and integrated into the clutch cover assembly to compare the performance results with the metal counterpart.

For further work, these findings can be applied to other metal replacement projects. In the case of automotive applications, compressive strength may be crucial in some product groups. These materials might alternate current ones with their compatible properties. Numerical modeling studies can be extended to handle various loads and suitability could be verified.

7. References

[1]   R. Waheed, S. Sarwar, and C. Wei, "The survey of economic growth, energy consumption and carbon emission," *Energy Reports*, Nov. 2019, vol. 5, pp. 1103–1115, doi: 10.1016/J.EGYR.2019.07.006.

[2]   "World Energy Outlook 2022 – Analysis - IEA." https://www.iea.org/reports/world-energy-outlook-2022 (accessed Nov. 03, 2022).

[3]   R. K. Sinha and N. D. Chaturvedi, "A review on carbon emission reduction in industries and planning emission limits," *Renew. Sustain. Energy Rev.*, Oct. 2019, vol. 114, p. 109304, doi: 10.1016/J.RSER.2019.109304.

[4]   "Energy Technology Perspectives 2020 – Analysis - IEA." https://www.iea.org/reports/energy-technology-perspectives-2020 (accessed Nov. 03, 2022).

[5]   J. M. Allwood, J. M. Cullen, and R. L. Milford, "Options for achieving a 50% cut in industrial carbon emissions by 2050," *Environ. Sci. Technol.*, Mar. 2010, vol. 44, no. 6, pp. 1888–1894, doi: 10.1021/ES902909K/SUPPL_FILE/ES902909K_SI_001.PDF.

[6]   J. Ongena and G. Van Oost, "Energy for Future Centuries: Will Fusion Be an Inexhaustible, Safe, and Clean Energy Source?," *https://doi.org/10.13182/FST04-A464*, Mar. 2017, vol. 45, no. 2T, pp. 3–14, doi: 10.13182/FST04-A464.

[7]   S. Wenlong, C. Xiaokai, and W. Lu, "Analysis of Energy Saving and Emission Reduction of Vehicles Using Light Weight Materials," *Energy Procedia*, Jun. 2016, vol. 88, pp. 889–893, doi: 10.1016/J.EGYPRO.2016.06.106.

[8]   T. Saraçyakupoğlu, "Usage of Additive Manufacturing and Topology Optimization Process for Weight Reduction Studies in the Aviation Industry," *Adv. Sci. Technol. Eng. Syst. J.*, Mar. 2021, vol. 6, no. 2, pp. 815–820, doi: 10.25046/AJ060294.

[9]   U. Kirsch, "Structural Optimization," 1993, doi: 10.1007/978-3-642-84845-2.

[10]   J. Liu *et al.*, "Current and future trends in topology optimization for additive manufacturing," *Struct. Multidiscip. Optim. 2018 576*, May 2018, vol. 57, no. 6, pp. 2457–2483, doi: 10.1007/S00158-018-1994-3.

[11]   N. S. Ermolaeva, K. G. Kaveline, and J. L. Spoormaker, "Materials selection combined with optimal structural design: concept and some results," *Mater. Des.*, Aug. 2002, vol. 23, no. 5, pp. 459–470, doi: 10.1016/S0261-3069(02)00019-5.

[12]   N. Sakundarini, Z. Taha, S. H. Abdul-Rashid, and R. A. R. Ghazila, "Optimal multi-material selection for lightweight design of automotive body assembly incorporating recyclability," *Mater. Des.*, Sep. 2013, vol. 50, pp. 846–857, doi: 10.1016/J.MATDES.2013.03.085.

[13]   G. May, I. Barletta, B. Stahl, and M. Taisch, "Energy management in production: A novel method to develop key performance indicators for improving energy efficiency," *Appl. Energy*, Jul. 2015, vol. 149, pp. 46–61, doi: 10.1016/J.APENERGY.2015.03.065.

[14]   H. Ritchie, M. Roser, and P. Rosado, "CO_2 and Greenhouse Gas Emissions," *Our World Data*, May 2020, Accessed: Nov. 06, 2022. [Online]. Available: https://ourworldindata.org/co2-and-other-greenhouse-gas-emissions

[15]   I. Energy Agency, "Energy Efficiency 2021," 2021, Accessed: Nov. 06, 2022. [Online]. Available: www.iea.org/t&c/

[16]   "Global Public Transportation Market Size Report, 2028." https://www.grandviewresearch.com/industry-analysis/public-transportation-market-report# (accessed Nov. 06, 2022).

[17]   K. D. Marshall, "The Economics of Automotive Weight Reduction," *SAE Tech. Pap.*, Feb. 1970, doi: 10.4271/700174.

[18]   S. K. Sah, M. A. Bawase, and M. R. Saraf, "Light-weight Materials and their Automotive Applications," *SAE Tech. Pap.*, Apr. 2014, vol. 4, doi:

10.4271/2014-28-0025.

[19] A. Hallal, A. Elmarakbi, A. Shaito, and H. El-Hage, "Overview of Composite Materials and their Automotive Applications," *Adv. Compos. Mater. Automot. Appl. Struct. Integr. Crashworthiness*, Oct. 2013, pp. 1–28, doi: 10.1002/9781118535288.CH1.

[20] R. Leal *et al.*, "Additive manufacturing tooling for the automotive industry," *Int. J. Adv. Manuf. Technol. 2017 925*, Mar. 2017, vol. 92, no. 5, pp. 1671–1676, doi: 10.1007/S00170-017-0239-8.

[21] G. M. Wood, "Lightweight Materials for Transportation," *http://dx.doi.org/10.1080/10667857.1993.11784987*, Sep. 2016, vol. 8, no. 9–10, pp. 221–223, doi: 10.1080/10667857.1993.11784987.

[22] K. S. Prakash, T. Nancharaih, and V. V. S. Rao, "Additive Manufacturing Techniques in Manufacturing -An Overview," *Mater. Today Proc.*, Jan. 2018, vol. 5, no. 2, pp. 3873–3882, doi: 10.1016/J.MATPR.2017.11.642.

[23] F. Stodolsky, A. Vyas, and R. Cuenca, "Lightweight materials in the light-duty passenger vehicle market: Their market penetration potential and impacts," *2. world car Conf. Riverside, CA (United States), 22-24 Jan 1995*, Jun. 1995, Accessed: Oct. 13, 2022. [Online]. Available: https://digital.library.unt.edu/ark:/67531/metadc712089/

[24] "LuK Clutch Course: An introduction to clutch technology for passenger cars".

[25] A. B. Hiziroglu, "The Car: A Brief History," *Auton. Veh. Law*, 2020, pp. 1–10, doi: 10.1007/978-3-031-01505-2_1.

[26] P. Dolcini, C. C. de Wit, and H. Bechart, "Dry Clutch Control for Automotive Applications," Oct. 2010, p. 114, Accessed: Nov. 20, 2022. [Online]. Available: https://hal.archives-ouvertes.fr/hal-00536612

[27] E. E. Wemp, "HISTORY OF AUTOMOTIVE-CLUTCH DEVELOPMENT," *SAE Tech. Pap.*, Jan. 1925, doi: 10.4271/250041.

[28] D. A. Hurter, P. G. Gott, C. A. Gottesman, and I. Arthur D. Little, "Study and

Test to Confirm Automobile Drivetrain Components to Improve Fuel Economy : Volume 1. History of the Automobile Transmission in the United States," May 1979, doi: 10.21949/1503647.

[29] C. Erbaş, "SIMULATION OF THE CLUTCH HILL START TEST FOR HEAVY COMMERCIAL VEHICLES," 2015.

[30] H. Chase, "PRACTICE AND THEORY IN CLUTCH DESIGN," *SAE Tech. Pap.*, Jan. 1921, pp. 357–396, doi: 10.4271/210052.

[31] H. S. Hele-Shaw, "A New Form of Friction Clutch," *Proc. Inst. Mech. Eng.*, Jun. 1903, vol. 65, no. 1, pp. 483–510, doi: 10.1243/PIME_PROC_1903_065_009_02/ASSET/PIME_PROC_1903_065_009_02.FP.PNG_V03.

[32] M. J. Nunney, "Light and Heavy Vehicle Technology," *Light Heavy Veh. Technol.*, Jan. 2007, doi: 10.4324/9780080465753.

[33] K.-L. Kimmig, D. P. Buehrle, D. R. Kolling, R. Daikeler, and M. Baumann, "Highest level of comfort - The dry double clutch faces the challenge." https://www.schaeffler.com/remotemedien/media/_shared_media/08_media_library/01_publications/schaeffler_2/symposia_1/downloads_11/Schaeffler_Kolloquium_2014_16_en.pdf (accessed Dec. 01, 2022).

[34] S. Kabacaoğlu, "Debriyaj sistemlerinde kullanilan diyafram yaylarda formun yorulma dayanimi ve mekanik karakteristiğe olan etkisinin teorik ve deneysel olarak iyileştirilmesi." Yüksek Lisans Tezi.

[35] "Troubleshooting: Common Clutch Issues and Causes | Haynes Manuals." https://haynes.com/en-us/tips-tutorials/troubleshooting-common-clutch-issues-and-causes (accessed Dec. 01, 2022).

[36] P. Guruparan, A. Sriraman, R. Iniyan, and K. Moses, "Analysis of Clutch Actuation System in Automobile to Reduce Pedal Vibration," Apr. 2015, vol. 12, pp. 46–54.

[37] M. Tirović, "Dry Clutch," *Encycl. Automot. Eng.*, Oct. 2014, pp. 1–30, doi:

10.1002/9781118354179.AUTO089.

[38] W. Schulz, "SACHS Tengelykapcsolo | PDF | Clutch | Automotive Industry."
https://www.scribd.com/document/108457556/SACHS-Tengelykapcsolo
(accessed Dec. 02, 2022).

[39] "Product | Dönmez Debriyaj."
https://www.donmezdebriyaj.com.tr/en/product/020_509 (accessed Oct. 13,
2022).

[40] "Release Forks for CV (Commercial Vehicles) - SACHS."
https://aftermarket.zf.com/go/en/sachs/products/commercial-vehicles/truck-
clutches/release-forks/ (accessed Dec. 04, 2022).

[41] S. Akbulut, "Motorlu taşıtlarda kullanılan kendinden ayarlı debriyajlar için ayar
mekanizmasının bilgisayar destekli tasarlanması, test edilmesi ve doğrulaması."
Fen Bilimleri Enstitüsü.

[42] M. Kilic, T. Cakmak, and G. Sevilgen, "Clutch pressure plate compactness
effect on the clutch system heat dissipation," 2016, Accessed: Dec. 04, 2022.
[Online]. Available: https://repository.up.ac.za/handle/2263/62035

[43] P. Maucher, "Optimized clutch design release load and operating comfort," in
Third LUK Clutch Symposium, April, 1986.

[44] J. O. Almen, "The uniform-section disk spring," *Trans. ASME*, 1936, vol. 58,
pp. 305–314.

[45] C. Schnorr, "Handbook for Disc Springs," *Schnorr Corp., Michigan, USA*,
2003.

[46] "MotorSports Clutch FlywheelCATALOG Vol.1." https://www.exedy-
racing.com/catalog/en/html5.html#page=9 (accessed Dec. 06, 2022).

[47] A. Ali, L. Ali, S. R. Shah, M. Khan, S. H. Imran, and S. I. Butt, "Dry friction
clutch disc of an automobile under transient thermal load: a comparison of
friction lining materials," in *MATEC Web of Conferences*, 2017, vol. 124, p.
7003.

[48] O. I. Abdullah, J. Schlattmann, and A. M. Al-Shabibi, "Stresses and deformations analysis of a dry friction clutch system," *Tribol. Ind.*, 2013, vol. 35, no. 2, pp. 155–162.

[49] K. Topczewska, J. Schlattmann, and O. I. Abdullah, "Temperature and thermal stresses distributions in a dry friction clutch," *J. Theor. Appl. Mech.*, 2020, vol. 58.

[50] M. Hoić, A. Miklik, M. Kostelac, J. Deur, and A. Tissot, "Analysis of the Accuracy of Mass Difference-Based Measurement of Dry Clutch Friction Material Wear," *Materials (Basel).*, 2021, vol. 14, no. 18, p. 5356.

[51] F. Huang, Y. Mo, and J. Lv, "Study on heat fading of phenolic resin friction material for micro-automobile clutch," in *2010 International Conference on Measuring Technology and Mechatronics Automation*, 2010, vol. 3, pp. 596–599.

[52] "CV Dual-Mass Flywheel (Truck DMF) for Reduced Vibration - SACHS." https://aftermarket.zf.com/go/en/sachs/products/commercial-vehicles/truck-clutches/dual-mass-flywheels/ (accessed Dec. 07, 2022).

[53] A. Yüceşan and S. Sezer, "Vibration isolation with clutch disk pre-damper mechanism for the idle rattle phenomenon," *J. Vib. Control*, 2018, vol. 24, no. 8, pp. 1518–1534.

[54] M. Zink and M. Hausner, "LuK clutch systems and torsional dampers," in *Schaeffler Symposium*, 2010, pp. 8–27.

[55] I. Minas, N. Morris, S. Theodossiades, M. O'Mahony, and J. Voveris, "Automotive dry clutch fully coupled transient tribodynamics," *Nonlinear Dyn.*, 2021, vol. 105, no. 2, pp. 1213–1235.

[56] M. Pisaturo, "Dry clutch for automated manual transmissions," *Struct. Anal. Control Strateg. PhD. Thesis Mech. Eng. cycle XII (2011-2013)(Accessed Dec. 16, 2016)*, 2013.

[57] G. L. Chen and X. Y. Chen, "Research on Commercial Vehicle Clutch Release

Bearing Fatigue Life Prediction Model," in *Applied Mechanics and Materials*, 2013, vol. 423, pp. 1853–1857.

[58] O. C. Bargun, A. Celik, U. O. Yazici, and A. Merdan, "IMPROVING THE SPINNING OPERATION OF VARIOUS CLUTCH RELEASE BEARINGS USED IN THE CLUTCH SYSTEMS OF HEAVY COMMERCIAL VEHICLES WITH A NEW SPINNING GEOMETRY".

[59] "Product | Dönmez Debriyaj." https://www.donmezdebriyaj.com.tr/en/product/050_844 (accessed Dec. 08, 2022).

[60] "Product | Dönmez Debriyaj." https://www.donmezdebriyaj.com.tr/en/product/000_034 (accessed Dec. 08, 2022).

[61] "Product | Dönmez Debriyaj." https://www.donmezdebriyaj.com.tr/en/product/029_049 (accessed Dec. 08, 2022).

[62] J. S. Patil, "Analysis for Optimum Design of Automotive Flywheel," *Int. Res. J. Eng. Technol.*, 2019, vol. 6, no. 6, pp. 708–715.

[63] A. Albers, "Advanced development of dual mass flywheel (DMFW) design-noise control for today's automobiles," in *Proceedings of the 5th LuK Symposium*, 1994, pp. 5–41.

[64] "Product | Dönmez Debriyaj." https://www.donmezdebriyaj.com.tr/en/product/029_403 (accessed Dec. 08, 2022).

[65] N. Kaya, I. Karen, and F. Öztürk, "Re-design of a failed clutch fork using topology and shape optimisation by the response surface method," *Mater. Des.*, 2010, vol. 31, no. 6, pp. 3008–3014.

[66] "Release Forks for CV (Commercial Vehicles) - SACHS." https://aftermarket.zf.com/go/en/sachs/products/commercial-vehicles/truck-

clutches/release-forks/ (accessed Dec. 09, 2022).

[67]   P. M. Subramanian, "Plastics recycling and waste management in the US," *Resour. Conserv. Recycl.*, 2000, vol. 28, no. 3–4, pp. 253–263.

[68]   S. R. Batten *et al.*, "Coordination polymers, metal–organic frameworks and the need for terminology guidelines," *CrystEngComm*, 2012, vol. 14, no. 9, pp. 3001–3004.

[69]   I. Gouzman, E. Grossman, R. Verker, N. Atar, A. Bolker, and N. Eliaz, "Advances in polyimide-based materials for space applications," *Adv. Mater.*, 2019, vol. 31, no. 18, p. 1807738.

[70]   J. T. Trotta, A. Watts, A. R. Wong, A. M. LaPointe, M. A. Hillmyer, and B. P. Fors, "Renewable thermosets and thermoplastics from itaconic acid," *ACS Sustain. Chem. Eng.*, 2018, vol. 7, no. 2, pp. 2691–2701.

[71]   W. D. Callister and D. G. Rethwisch, "Materials science and engineering : an introduction".

[72]   H. F. Brinson and L. C. Brinson, "Polymer engineering science and viscoelasticity," *An Introd.*, 2008, pp. 99–157.

[73]   M. Kazemi, S. F. Kabir, and E. H. Fini, "State of the art in recycling waste thermoplastics and thermosets and their applications in construction," *Resour. Conserv. Recycl.*, 2021, vol. 174, p. 105776.

[74]   S. D. A. Sharuddin, F. Abnisa, W. M. A. W. Daud, and M. K. Aroua, "A review on pyrolysis of plastic wastes," *Energy Convers. Manag.*, 2016, vol. 115, pp. 308–326.

[75]   R.-J. Müller, I. Kleeberg, and W.-D. Deckwer, "Biodegradation of polyesters containing aromatic constituents," *J. Biotechnol.*, 2001, vol. 86, no. 2, pp. 87–95.

[76]   M. Okan, H. M. Aydin, and M. Barsbay, "Current approaches to waste polymer utilization and minimization: a review," *J. Chem. Technol. Biotechnol.*, 2019, vol. 94, no. 1, pp. 8–21.

[77] J. Hopewell, R. Dvorak, and E. Kosior, "Plastics recycling: challenges and opportunities," *Philos. Trans. R. Soc. B Biol. Sci.*, 2009, vol. 364, no. 1526, pp. 2115–2126.

[78] S. M. Al-Salem, P. Lettieri, and J. Baeyens, "Recycling and recovery routes of plastic solid waste (PSW): A review," *Waste Manag.*, 2009, vol. 29, no. 10, pp. 2625–2643.

[79] Q. Liu and J. Paavola, "Lightweight design of composite laminated structures with frequency constraint," *Compos. Struct.*, 2016, vol. 156, pp. 356–360.

[80] G. Mittal, K. Y. Rhee, V. Mišković-Stanković, and D. Hui, "Reinforcements in multi-scale polymer composites: Processing, properties, and applications," *Compos. Part B Eng.*, 2018, vol. 138, pp. 122–139.

[81] M. Balasubramanian, *Composite materials and processing*. CRC press Boca Raton, 2014.

[82] V. Acanfora, R. Petillo, S. Incognito, G. M. Mirra, and A. Riccio, "Development of detailed FE numerical models for assessing the replacement of metal with composite materials applied to an executive aircraft wing," *Aerospace*, 2021, vol. 8, no. 7, p. 178.

[83] S. Prashanth, K. M. Subbaya, K. Nithin, and S. Sachhidananda, "Fiber reinforced composites-a review," *J. Mater. Sci. Eng*, 2017, vol. 6, no. 03, pp. 2–6.

[84] A. A. Baker, P. J. Callus, S. Georgiadis, P. J. Falzon, S. E. Dutton, and K. H. Leong, "An affordable methodology for replacing metallic aircraft panels with advanced composites," *Compos. Part A Appl. Sci. Manuf.*, 2002, vol. 33, no. 5, pp. 687–696.

[85] H. KAWABE, Y. AOKI, and T. NAKAMURA, "Design of optimum aircraft structure inspired by dragonfly wings," in *Proceedings of the American Society for Composites—Thirty-fifth Technical Conference*, 2020.

[86] A. Sellitto, A. Russo, A. Riccio, and M. Damiano, "Fibreglass wind turbine

blades: Damage tolerant design and verification," in *AIP Conference Proceedings*, 2020, vol. 2309, no. 1, p. 20032.

[87]   R. Stewart, "Automotive composites offer lighter solutions," *Reinf. Plast.*, 2010, vol. 54, no. 2, pp. 22–28.

[88]   S. D. Mancini, A. de O. Santos Neto, M. O. H. Cioffi, and E. C. Bianchi, "Replacement of metallic parts for polymer composite materials in motorcycle oil pumps," *J. Reinf. Plast. Compos.*, 2017, vol. 36, no. 2, pp. 149–160.

[89]   S. Ashley, "Rapid prototyping systems," *Mech. Eng.*, 1991, vol. 113, no. 4, p. 34.

[90]   I. Gibson *et al.*, *Additive manufacturing technologies*, vol. 17. Springer, 2021.

[91]   T. Campbell, C. Williams, O. Ivanova, and B. Garrett, "Could 3D printing change the world," *Technol. Potential, Implic. Addit. Manuf. Atl. Counc. Washington, DC*, 2011, vol. 3.

[92]   M. K. Thompson *et al.*, "Design for Additive Manufacturing: Trends, opportunities, considerations, and constraints," *CIRP Ann.*, 2016, vol. 65, no. 2, pp. 737–760.

[93]   "ISO - ISO/ASTM 52900:2021 - Additive manufacturing — General principles — Fundamentals and vocabulary." https://www.iso.org/standard/74514.html (accessed Dec. 11, 2022).

[94]   B. Brenken, E. Barocio, A. Favaloro, V. Kunc, and R. B. Pipes, "Fused filament fabrication of fiber-reinforced polymers: A review," *Addit. Manuf.*, 2018, vol. 21, pp. 1–16.

[95]   D. Fico, D. Rizzo, R. Casciaro, and C. Esposito Corcione, "A review of polymer-based materials for Fused Filament Fabrication (FFF): Focus on sustainability and recycled materials," *Polymers (Basel).*, 2022, vol. 14, no. 3, p. 465.

[96]   H. Bikas, P. Stavropoulos, and G. Chryssolouris, "Additive manufacturing methods and modelling approaches: a critical review," *Int. J. Adv. Manuf.*

Technol., 2016, vol. 83, no. 1, pp. 389–405.

[97] R. Melnikova, A. Ehrmann, and K. Finsterbusch, "3D printing of textile-based structures by Fused Deposition Modelling (FDM) with different polymer materials," in *IOP conference series: materials science and engineering*, 2014, vol. 62, no. 1, p. 12018.

[98] P. E. Romero, J. Arribas-Barrios, O. Rodriguez-Alabanda, R. González-Merino, and G. Guerrero-Vaca, "Manufacture of polyurethane foam parts for automotive industry using FDM 3D printed molds," *CIRP J. Manuf. Sci. Technol.*, 2021, vol. 32, pp. 396–404.

[99] M. M. Garmabi, P. Shahi, J. Tjong, and M. Sain, "3D printing of polyphenylene sulfide for functional lightweight automotive component manufacturing through enhancing interlayer bonding," *Addit. Manuf.*, 2022, vol. 56, p. 102780.

[100] C. Alexander, "Streamlining automotive production with additive manufacturing," *Quality*, 2018, vol. 57, no. 5, pp. 37–39.

[101] A. Riccio, M. Madonna, C. Palumbo, and A. Sellitto, "Additive manufactured polymeric shock absorbers for automotive applications," *Heliyon*, 2022, p. e11695.

[102] S. Cakmak, Ö. Yildiz, İ. Can Kaymaz, U. Kurt, and C. Eş, "Alternatif Polimer Esaslı Malzemelerin Debriyaj Diski Stoperine Entegrasyonu," 2022.

[103] A. Y. Dmitriev, R. S. Zagidulin, and T. A. Mitroshkina, "Special aspects of quality assurance in the design, manufacture, testing of aerospace engineering products," in *IOP Conference Series: Materials Science and Engineering*, 2020, vol. 714, no. 1, p. 12006.

[104] R. S. Zagidullin, N. I. Zezin, and N. V Rodionov, "Improving the quality of FDM 3D printing of UAV and aircraft parts and assemblies by parametric software changes," in *IOP Conference Series: Materials Science and Engineering*, 2021, vol. 1027, no. 1, p. 12031.

[105] Y. M. Deng and K. L. Edwards, "The role of materials identification and

selection in engineering design," *Mater. Des.*, Jan. 2007, vol. 28, no. 1, pp. 131–139, doi: 10.1016/J.MATDES.2005.05.003.

[106] "Materials and Design: The Art and Science of Material Selection in Product ... - Michael F. Ashby, Kara Johnson - Google Kitaplar." https://books.google.com.tr/books?hl=tr&lr=&id=lyDEACMTtUEC&oi=fnd &pg=PP2&dq=Ashby,+M.+F.,+%26+Johnson,+K.+(2013).+Materials+and+d esign:+the+art+and+science+of+material+selection+in+product+design.+Butt erworth-Heinemann.+&ots=MTw72dqNXq&sig=60DMOQ6GBfX2l5RST1Vw-atuSxw&redir_esc=y#v=onepage&q=Ashby%2C M. F.%2C %26 Johnson%2C K. (2013). Materials and design%3A the art and science of material selection in product design. Butterworth-Heinemann.&f=false (accessed Nov. 25, 2022).

[107] S. S. Kumar and G. Kanagaraj, "Evaluation of mechanical properties and characterization of silicon carbide–reinforced polyamide 6 polymer composites and their engineering applications," *Int. J. Polym. Anal. Charact.*, 2016, vol. 21, no. 5, pp. 378–386.

[108] S. C. Ligon, R. Liska, J. Stampfl, M. Gurr, and R. Mülhaupt, "Polymers for 3D printing and customized additive manufacturing," *Chem. Rev.*, 2017, vol. 117, no. 15, pp. 10212–10290.

[109] J. R. C. Dizon, A. H. Espera, Q. Chen, and R. C. Advincula, "Mechanical characterization of 3D-printed polymers. Addit Manuf 20: 44–67."

[110] S.-H. Wu *et al.*, "Mechanical, thermal and morphological properties of glass fiber and carbon fiber reinforced polyamide-6 and polyamide-6/clay nanocomposites," *Mater. Lett.*, 2001, vol. 49, no. 6, pp. 327–333.

[111] C. Hui, C. Qingyu, W. Jing, X. Xiaohong, L. Hongbo, and L. Zhanjun, "Interfacial enhancement of carbon fiber/nylon 12 composites by grafting nylon 6 to the surface of carbon fiber," *Appl. Surf. Sci.*, 2018, vol. 441, pp. 538–545.

[112] Y. Liu *et al.*, "An effective surface modification of carbon fiber for improving

the interfacial adhesion of polypropylene composites," *Mater. Des.*, 2015, vol. 88, pp. 810–819.

[113] J. U. Lee, B. Park, B.-S. Kim, D.-R. Bae, and W. Lee, "Electrophoretic deposition of aramid nanofibers on carbon fibers for highly enhanced interfacial adhesion at low content," *Compos. Part A Appl. Sci. Manuf.*, 2016, vol. 84, pp. 482–489.

[114] W. Chin, H. Liu, and Y. Lee, "Effects of fiber length and orientation distribution on the elastic modulus of short fiber reinforced thermoplastics," *Polym. Compos.*, 1988, vol. 9, no. 1, pp. 27–35.

[115] Y. M. A. Hashash, S. Jung, and J. Ghaboussi, "Numerical implementation of a neural network based material model in finite element analysis," *Int. J. Numer. Methods Eng.*, 2004, vol. 59, no. 7, pp. 989–1005.

[116] P. Steinmann, M. Hossain, and G. Possart, "Hyperelastic models for rubber-like materials: consistent tangent operators and suitability for Treloar's data," *Arch. Appl. Mech.*, 2012, vol. 82, no. 9, pp. 1183–1217.

[117] A. A. Tseng, J. Zou, H. P. Wang, and S. R. H. Hoole, "Numerical modeling of macro and micro behaviors of materials in processing: A review," *J. Comput. Phys.*, 1992, vol. 102, no. 1, pp. 1–17.

[118] R. W. Ogden, "Large deformation isotropic elasticity–on the correlation of theory and experiment for incompressible rubberlike solids," *Proc. R. Soc. London. A. Math. Phys. Sci.*, 1972, vol. 326, no. 1567, pp. 565–584.

[119] M. M. Attard and G. W. Hunt, "Hyperelastic constitutive modeling under finite strain," *Int. J. Solids Struct.*, 2004, vol. 41, no. 18–19, pp. 5327–5350.

[120] M. Mooney, "A theory of large elastic deformation," *J. Appl. Phys.*, 1940, vol. 11, no. 9, pp. 582–592.

[121] R. S. Rivlin, "Large elastic deformations of isotropic materials IV. Further developments of the general theory," *Philos. Trans. R. Soc. London. Ser. A, Math. Phys. Sci.*, 1948, vol. 241, no. 835, pp. 379–397.

[122] R. Rivlin, "Large elastic deformations of isotropic materials. V. The problem of flexure," *Proc. R. Soc. London. Ser. A. Math. Phys. Sci.*, 1949, vol. 195, no. 1043, pp. 463–473.

[123] R. S. Rivlin, "Large elastic deformations of isotropic materials VI. Further results in the theory of torsion, shear and flexure," *Philos. Trans. R. Soc. London. Ser. A, Math. Phys. Sci.*, 1949, vol. 242, no. 845, pp. 173–195.

[124] A. Isihara, N. Hashitsume, and M. Tatibana, "Statistical theory of rubber-like elasticity. IV.(two-dimensional stretching)," *J. Chem. Phys.*, 1951, vol. 19, no. 12, pp. 1508–1512.

[125] A. N. Gent and A. G. Thomas, "Forms for the stored (strain) energy function for vulcanized rubber," *J. Polym. Sci.*, 1958, vol. 28, no. 118, pp. 625–628.

[126] S. R. Swanson, "A constitutive model for high elongation elastic materials," 1985.

[127] S. R. Swanson, L. W. Christensen, and M. Ensign, "Large deformation finite element calculations for slightly compressible hyperelastic materials," *Comput. Struct.*, 1985, vol. 21, no. 1–2, pp. 81–88.

[128] O. H. Yeoh, "Some forms of the strain energy function for rubber," *Rubber Chem. Technol.*, 1993, vol. 66, no. 5, pp. 754–771.

[129] O. H. Yeoh, "Characterization of elastic properties of carbon-black-filled rubber vulcanizates," *Rubber Chem. Technol.*, 1990, vol. 63, no. 5, pp. 792–805.

[130] E. M. Arruda and M. C. Boyce, "A three-dimensional constitutive model for the large stretch behavior of rubber elastic materials," *J. Mech. Phys. Solids*, 1993, vol. 41, no. 2, pp. 389–412.

[131] A. N. Gent, "A new constitutive relation for rubber," *Rubber Chem. Technol.*, 1996, vol. 69, no. 1, pp. 59–61.

[132] E. C. Botelho, Figiel, M. C. Rezende, and B. Lauke, "Mechanical behavior of carbon fiber reinforced polyamide composites," *Compos. Sci. Technol.*, 2003,

vol. 63, no. 13, pp. 1843–1855, doi: 10.1016/S0266-3538(03)00119-2.

[133] M. A. Albadrani, "Failure Prediction in 3D Printed Kevlar/Glass Fiber-Reinforced Nylon Structures with a Hole and Different Fiber Orientations," *Polymers (Basel).*, 2022, vol. 14, no. 20, p. 4464.

[134] J. Pratama *et al.*, "A review on reinforcement methods for polymeric materials processed using Fused Filament Fabrication (FFF)," *Polymers (Basel).*, 2021, vol. 13, no. 22, p. 4022.

[135] J. Justo, L. Távara, L. García-Guzmán, and F. París, "Characterization of 3D printed long fibre reinforced composites," *Compos. Struct.*, 2018, vol. 185, pp. 537–548.

Curriculum Vitae

Name Surname   : İbrahim Can KAYMAZ

Education:

2017–2021   İzmir Dokuz Eylül University, Dept. of Mechanical Eng.

Work Experience:

2021 – 2023   Dönmez Debriyaj Sanayi ve Tic. A.Ş

Publications (if any):

1. Debriyaj Rulmani Taşiyicisi Ağirlik ve Maliyetinin İyileştirilmesi, Aralık 2021, 4. Ulusal Üniversite-Sanayi İş Birliği Ar-Ge ve İnovasyon Kongresi, Manisa, Türkiye

2.